Performance of steel open ended pile driveability prediction methods in dense sand

Evaluating pile driveability models and improving driveability predictions of a recent static axial capacity approach

K. ARGYROULIS

Port of Rotterdam SBE TU Delft Allnamics

Performance of steel open ended pile driveability prediction methods in dense sand

Evaluating pile driveability models and improving driveability predictions of a recent static axial capacity approach

by

K. ARGYROULIS

to obtain the degree of Master of Science at the Delft University of Technology, to be defended publicly on Monday September 19 2022 at 15:00 PM.

Student Number	5216516	
Project Supervisors		
	Prof. dr ir. K.G. Gavin,	TU Delft
	Dr. ir. M. Korff,	TU Delft
	Dr. Ir. A.A. Roubos,	Port of Rotterdam, TU Delft
	Ir. J. Putteman,	SBE
	Ir. R.F. van Dorp,	Allnamics BV
	Ing. M. Meeuwsen,	BV Ingenieursbureau M.U.C

Preface

This research concludes my studies for the degree of Master of Science in Geo-Engineering at Delft University of Technology. It was a combination of desk study and field observations, as I was very lucky to be able to participate in one of the largest projects of the Port of Rotterdam, the extension of the Amaliahaven terminals in the Maasvlakte area. During my Thesis, which focuses on pile driveability, I was able to witness the process of pile driving and also use the driving records in my study. Throughout the process of conducting my research, I had tremendous support from my supervisors who helped me tackle engineering difficulties and uncertainties that come with any research project. Their valuable feedback motivated and helped me develop critical thinking.

For that reason, I would like to thank my University's supervisors, Ken Gavin and Mandy Korff for sharing their knowledge and guiding me throughout the Thesis. Moreover, I would like to express my gratitude to Alfred Roubos and the Port of Rotterdam for giving me the chance to work on the Amaliahaven project and meet and communicate with experts at the site. Furthermore, I would like to thank SBE, specifically An-Sofie Lierman and Jan Putteman for providing me with everything I needed to accomplish this Thesis, alongside with their expert opinion and feedback during our meetings. In addition, I would like to show my appreciation to Allnamics, to Rob Van Dorp and Peter Middendorp, for providing me with the AllWave PDP software, without which I wouldn't be able to conduct my research, but I also want to thank them for sharing their knowledge and experience in pile driveability. Also, I would like to thank Mark Meeuwsen for his support, expert opinion and feedback throughout my Thesis.

Finally, I would like to thank everyone from the Amaliahaven project, who welcomed me at the site and specifically Arnold Van Der Werff, who devoted a lot of time guiding me through the different project phases.

Konstantinos Argyroulis

Delft, June

Abstract

Inefficient installation of pile foundations may lead to high risks of material damage, inadequate pile capacity, and time delays that can have significant financial implications to any kind of project, both onshore and offshore. Therefore, there is high demand for a comprehensive driveability analysis that considers key aspects of the installation process, such as the soil conditions, the pile-soil interaction and efficiency of the driving equipment used.

The total resistance during pile driving is usually estimated through numerical simulation techniques based on the wave equation, whereby the main inputs are the hammer, pile and soil properties. Commercially available driveability software, such as AllWave PDP, enable the modelling of the hammer-pile-soil system and simulate the stress wave phenomena during the installation process. Moreover, these programs have an integrated database of a variety of hammer models (hydraulic, diesel and more) that are used in practice, and also static and dynamic parameters for a variety of soils.

One of the key aspects in which this Thesis focuses on, is the static component of the driving resistance, referred to as SRD. Over the years, various SRD models have been developed, with the aim of estimating the static soil resistance during driving, while the dynamic components of the total resistance (increasing resistance due to inertial and viscous rate effects) are commonly being quantified in terms of damping factors.

This Thesis investigates the performance of frequently used traditional driveability models, such as the Alm & Hamre (2001), Toolan & Fox (1977) and Stevens et al (1982), in predicting the SRD in dense sand conditions. Furthermore, it examines the application of the Unified Method in SRD estimations. The Unified Method is a recently developed static capacity design approach for driven piles in silica sand. This design method will be included in the forthcoming 2022 edition of the ISO guidelines and will replace the four CPT based design methods (ICP, UWA, NGI, Fugro).

The performance of the aforementioned models has been evaluated through predictions of blow count profiles by utilizing pile driving records from five sites in the Netherlands, namely the Eemshaven (project known as Euripides) and APM, RWG, SIF and HHT terminals in the Port of Rotterdam. The diameter of the open-ended steel tubular piles examined in this study, is $0.762\ m$ for the Euripides project and $1.42\ m$ for the rest of the projects.

This research, will eventually highlight advantages and disadvantages of the commonly used SRD models, while it will further prove that by modifying the Unified Method, overall better driveability predictions can be made for a larger range of pile diameters than the current methods. The gain is that on one hand, with improved driveability predictions it is possible to minimize installation risks, optimize driving acceptance criteria, and select an appropriate hammering equipment. On the other hand, having a set of formulas that can be used both in estimating the SRD, as well as the static axial capacity, can reduce the engineering effort.

Table of Contents

APPENDIX D

List of Figures & Tables

APPENDIX A

APPENDIX B

APPENDIX D

TABLES

APPENDIX C

1. Introduction

1.1 Project Introduction

Although the Port of Rotterdam has a leading position as Europe's largest container port, the continuously rising container volumes has led the Port of Rotterdam Authority to make an investment for further expansion of the Prinses Amaliahaven located on Maasvlakte II.

Specifically, the two operational terminals, namely APM and RWG, in Prinses Amaliahaven of 1.5 and 1.7 km quay walls, respectively, are going to be expanded in a southerly direction as indicated in Figure 1.1-1. This expansion involves the construction of approximately 1 km and 821 m of deep-sea quay walls at the APM and RWG terminals, respectively. Figure 1.1-2 also depicts the planned expansion.

Figure 1.1-1: Map showing the already existing terminals APM and RWG in Prinses Amaliahaven, alongside with the planned expansion (photo taken from Google maps 2022).

A simplified drawing of the cross section of the new quay wall in the RWG and APM terminals is presented in Figure 1.1-3. As can be observed in Figure 1.1-3, there are also plans for a back-crane track founded on piles, over which the rear legs of the future container cranes will pass.

Figure 1.1-2: Expansion of Prinses Amaliahaven's quay walls (Port of Rotterdam website: Ongoing Projects: Quay Wall Construction Amaliahaven).

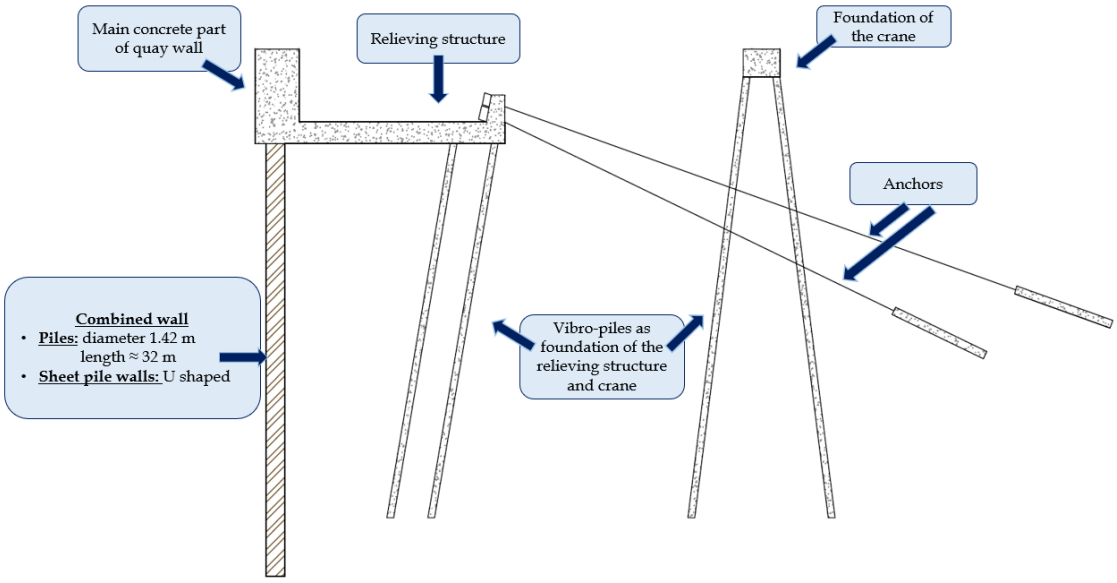

Figure 1.1-3: (New) Quay wall cross section sketch (the figure depicts just a simplified sketch of the actual cross. Created with AutoCAD 2021).

Moreover, the main part of the concrete wall is founded on a combined wall. The combined wall consists of steel open-ended tubular piles with a diameter of $1.42\,m$ and length of about $32\,m$, and of U-shaped sheet pile walls. The relieving structure is then founded on vibro-piles, while anchors for the stability of the whole structure will be used as well.

With respect to the soil profile encountered at Prinses Amaliahaven, this mainly consists of moderately fine silty sand with thin clay layers appearing locally and Pleistocene sand at deeper levels, where the foundations of the combined wall will be installed.

The quay walls in both terminals are to be connected with the already existing infrastructure, while construction works take place without imposing any hindrance to the operational terminals.

The Port of Rotterdam Authority awarded the project to the construction consortium of HOCHTIEF, Ballast Nedam and Van Oord, after going through a European tendering procedure.

1.2 Problem Description and Research Proposal

The expected port capacity increase with the planned expansion of the quay walls is approximately 4 million TEU (unit of measurement used to determine cargo capacity for container ships and terminals) corresponding to almost 25% of the annual total in 2020. The foundations of the new quay walls consist of combined walls with more than 500 steel open-ended tubular piles. Hence, pile driveability issues during construction works can have great consequences for the Port of Rotterdam.

However, inefficient installation of driven piles imposes risks regarding material damage, but also delays with possible great financial implications, not only to the Port of Rotterdam, but to any other construction project, onshore or offshore. Therefore, there is great demand for a comprehensive driveability analysis that considers all aspects of pile installation, such as soil conditions, soil-structure interaction, and efficiency of driving equipment, with the aim of minimizing the aforementioned risks.

Numerical simulation techniques that are based on the wave equation are utilized in order to assess the total driving resistance during pile installation. The total resistance consists of two components. A dynamic and a static. The dynamic component is related to increase in resistance due to inertial and viscous rate effects (Randolph (2000)), and is commonly

quantified using damping factors (Schneider et al (2010)). On the other hand, the static resistance component, referred to as SRD, which is also the focus of this research study, is estimated through various SRD models. Traditional SRD models are the Toolan & Fox (1977), Stevens et al (1982) and Alm & Hamre (2001). The Alm & Hamre (2001) model has been calibrated through back-calculated SRD profiles using a large database of driven open-ended tubular piles, making it one of the most reliable and most frequently used in practice.

Initially, this research study evaluates the performance of the aforementioned traditional driveability models, in predicting the SRD in dense sand conditions, by utilizing pile installation data collected from the Amaliahaven project, specifically from two sites, the APM and RWG terminals. Moreover, it highlights limitations and differences between these methods, by comparing recorded and predicted blow count profiles.

Limitations of the aforementioned approaches, usually appear as a lack of incorporation into their suggested formulas of important phenomena that affect the driving process, such as friction fatigue, degree of soil displacement during driving and modelling of plug resistance. For that reason, research studies have been made the last few years (e.g., Schneider et al (2010), Byrne et al (2018), Prendergast et al (2020)), to also evaluate the performance of CPT based static capacity approaches in estimating the SRD, in an effort to produce more reliable driveability predictions.

Therefore, this research also focuses on the applicability of a recently developed static axial capacity design method in estimating the static soil resistance during driving. This method is referred to as Unified Method. This new design approach has been calibrated using a 'Unified database' comprising of 71 high quality pile load tests in siliceous sand deposits (Lehane et al (2020)), and will be included in the forthcoming 2022 edition of the ISO guidelines replacing the four CPT based design methods (ICP, UWA, NGI, Fugro). Hence, an attempt is made to correlate the static axial (mid-term) capacity with the SRD, and modifications are suggested for this new method with the aim of utilizing it in future driveability analysis.

The performance of the *modified* Unified Method is evaluated by comparing predicted and measured blow count profiles from five sites in the Netherlands, namely the Eemshaven (project known as Euripides), APM, RWG (Amaliahaven project), SIF and HHT terminals, and compared to predictions made by the Alm & Hamre (2001) model.

Finally, this Thesis highlights some key features of the *modified* Unified Method that not only lead to improved SRD estimations, but also to an SRD model that is applicable to various driving conditions, (plugged - unplugged - partially plugged piles), and for a larger range of pile diameters than the examined traditional SRD approaches.

The overall gain, is that with improved driveability predictions, it is possible to minimize installation risks, such as excessive stresses on the pile during driving, decide or update driving acceptance criteria, such as pile capacity at the end of driving, optimize the driving process by choosing the most suitable hammering equipment, and avoid driving difficulties due to underestimation of the soil resistance. As mentioned earlier, a thorough driveability analysis based on high reliability SRD models, can minimize the costs of installation of steel open-ended piles for both onshore and offshore projects. Furthermore, having a reliable set of formulas that can be used both in driveability analysis and for estimating pile axial (mid-term) capacity, may reduce the engineering effort or confusion on which of the numerous available formulas - approaches to utilize in each case.

1.3 Research Objectives and Questions

This research evaluates the performance of traditional SRD models in dense sand deposits, utilizing driving records collected from the Amaliahaven and other projects. Moreover, modifications to the recently developed Unified Method are suggested, for predictions of the driving resistance of open-ended steel tubular piles, by considering aspects and factors that affect the driving process. An attempt is made to answer the following research questions:

- How reliable are the traditional SRD models in predicting the driveability of the steel open-ended tubular piles of the Amaliahaven project?

- How does the recently developed CPT based static capacity approach, namely the Unified Method, perform in SRD predictions (without modifications)?

- How can we utilize installation records of steel open-ended tubular piles in order to improve the SRD estimations of the Unified Method, and which key factors need to be considered in its *modified* form?

1.4 Method of Approach

The general steps to be followed in the driveability analysis of this Thesis in order to check the reliability of traditional driveability models or modify the Unified Method are depicted in Figure 1.4-1.

It should be noted that the traditional driveability models are not modified in this research due to the fact that they have already been calibrated by the corresponding authors. Moreover, with respect to the Unified Method, both the shaft and toe resistances need to be modified in order for this model to be appropriately used in driveability analysis.

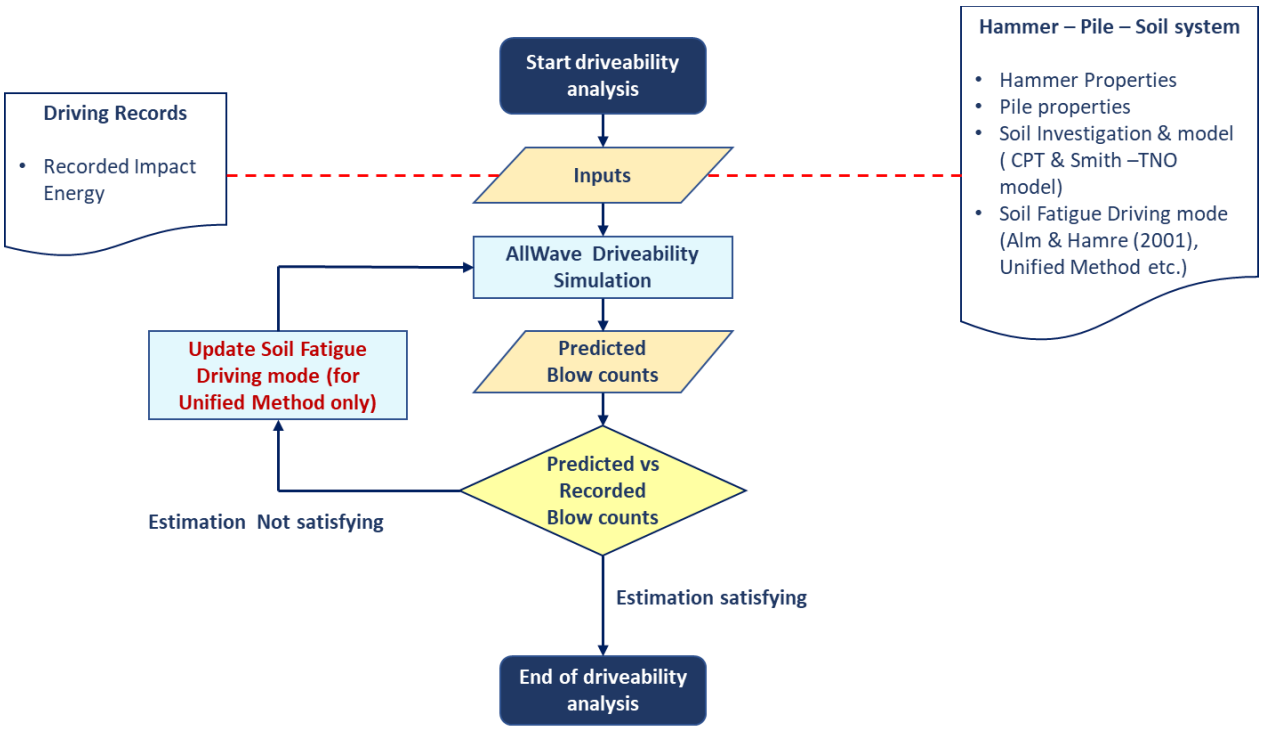

Figure 1.4-1: Working plan for evaluating the performance of traditional SRD models and modifying the Unified Method.

1.5 Limitations

The limitations of this research are listed below:

- The already available (traditional) driveability models examined in this Thesis are the Toolan & Fox (1977), Stevens et al (1982) and Alm & Hamre (2001). No other existing model has been used for comparison with the Unified Method.
- Reliability of the traditional driveability models of Toolan & Fox (1977), and Stevens et al (1982) is only investigated using two sites of dense sand deposits, namely the APM and RWG (Amaliahaven project).
- The modifications of the Unified Method are based only on back-analysis of data collected and previous research studies and conclusions.
- No signal matching has been used in this study, but only measured blow count profiles and driving energy have been utilized.
- A set up factor, and quake values have not been derived specifically from the driving records of the APM and RWG sites.
- Modifications suggested for the Unified Method are for soil profiles similar to the one encountered in the Amaliahaven project (dense sand).
- Only steel open-ended tubular piles have been examined in this study.

1.6 Chapter Organization

The main chapters to be presented in this study are listed below:

- Chapter 1: Introduction
- Chapter 2: Amaliahaven Project
- Chapter 3: Axial Capacity & Driveability
- Chapter 4: SRD Models
- Chapter 5: Reliability of SRD Models
- Chapter 6: Unified SRD Method
- Chapter 7: Application to other Case Studies
- Chapter 8: Discussion & Conclusions

2. Amaliahaven Project

This Chapter includes just a short presentation of relevant to this research background information regarding the expansion of the two terminals, APM and RWG, as well as the soil conditions encountered at the site.

2.1 Quay Wall Cross-Sections, APM & RWG

A simplified drawing of the cross-section of the new quay walls for the APM and RWG terminals has been presented in Figure 1.1-3.

This research will focus only on the piles of the combined wall by using the installation data collected in order to perform a driveability analysis. Thus, the rest of the parts of the wall will not be further discussed. The dimensions of the piles and the equipment used are presented in the following section.

Initially, prior to construction works, the ground level was at around $+6.50$ m from NAP. For the installation of the combi wall piles different stages of excavation took place in order to lower the ground level at around -2 m from NAP. Moreover, in order to have a dry working level, the water table had to be kept even lower, specifically at -2.50 m from NAP. Most of the (relevant) CPT data that are collected have been performed prior to the construction works, when the ground level was at around $+6.50$ m from NAP.

2.2 Pile and Equipment Properties

The pile properties of the combi wall are summarized in Table 2.2-1 for the APM and RWG terminals. All piles are steel open-ended, with a diameter of $1.42\,m$ and a wall thickness varying from $18\,mm$ for the APM piles to $19\,mm$ for the RWG site. The start of installation and the embedment depth are also summarized in the aforementioned table.

Table 2.2-1: Pile properties of the combi-wall of the APM and RWG terminals.

APM & RWG Combi Wall - Pile Properties			
	APM pile Properties	RWG pile Properties	Unit
Pile type	Steel Open-Ended	Steel Open-Ended	-
Pile material quality	X70	X70	-
Pile external diameter	1420	1420	mm
Wall thickness	18	19	mm
Start of installation (NAP)	-2.02	-2.02	m
Pile embedment depth (NAP)	[-32, -36]	[-32, -34]	m

The installation of the combi wall piles is done in two stages. In the first stage, after the area is excavated till around $-2\,m$ from NAP, the piles are installed through vibration up to around $-26\,m$ and $-23\,m$ from NAP at the APM and RWG terminals, respectively. Then, the final embedment depth is reached through impact driving using the hammers indicated in Table 2.2-2.

Table 2.2-2: Hammers used and specifications (these specifications can be found in any manufacturer's website).

APM & RWG Combi Wall Piles - Hammer Properties			
	Properties		Unit
Hammer type	IHC S-200	IHC SC-200	-
Max net energy/blow	200	200	kNm
Min net energy/blow	20	20	kNm
Blow rate (max energy)	45	45	blows/min
Ram weight	10	13.6	t
Hammer including Ram, in air	25.8	26.5	t

APPENDIX A includes photos personally taken from the two sites (Figure A 1, Figure A 2, Figure A 5, Figure A 3).

In these figures one can observe the stages and different equipment used in each case.

2.3 Amaliahaven Soil Profile

A combination of CPTs, boreholes and laboratory tests gave an insight to the soil encountered at the two sites, APM and RWG. Since a great number of CPTs were performed prior to the construction works, it was decided to summarize these findings that describe the soil for both sites in Table 2.3-1. It should be noted that the table contains just an indicative classification and description of the soil layers, as the level of appearance can vary within the project area. Thus, in this Thesis, when performing a driveability analysis for a specific pile, the nearest to that pile CPT is used. Moreover, it should be noted that although the soil profile consists primarily of silty sand, some clay layers [Code B.2, F, D] may appear locally, with the ranges of occurrence as seen in Table 2.3-1.

Table 2.3-1: Classification for the APM and RWG sites (soil description and parameters as indicated in geotechnical reports of the project).

Typical Soil Classification

APM terminal				RWG terminal			
Code	Typical q_c [MPa]	Occurrence [m NAP]	Classification	Code	Typical q_c [MPa]	Occurrence [m NAP]	Classification
A	15	[+6, -16]	Weak silty sand	A	15	[+6, -16]	Weak silty sand
B.1	5	[-16, -21 or -30]	Alternating layers of strong silty sand and sandy silt	B.1	4	[-16, -20 or -32]	Alternating layers of strong silty sand and sandy silt
B.2	1-2	[-21, -22]	Medium to strong clay and peat	B.2	1-1.5	[-20, -35]	Clay, highly silty, sometimes with peat.
C.1	15	[-22, -24]	Pleistocene sand	-	-	-	-
F	1-2	[-24, -25]	Medium to strong clay	-	-	-	-
C.2	>30	[-25, -45]	Pleistocene sand	C	>30	[-22, -40]	Pleistocene sand
D	4	[-38, -48]	Clayey with sand/silt	D	4	[-38, -45]	Clay with sand/silt
E	15	[-40, -45]	Clayey / Silty Sand	E	15	[-40, -64]	Clayey / Silty Sand

3. Axial Capacity & Driveability

In this Chapter factors that affect both the axial capacity of piles but also their driveability are briefly presented. Moreover, this Chapter includes the attempts of various researchers in correlating the Static Resistance during Driving and Static Axial Capacity of a pile based on the aforementioned influencing factors. Finally, the Smith (1960) model and the Method of Characteristics (Voitus van Hamme et al (1974), Saint-Venant (1867)) that are used to simulate the pile-soil-hammer system are presented.

3.1 Background Information on Piles, Hammers, Energy

Pile Types

Piles are mainly used as foundations of structures aiming at safely distributing loads throughout a soil mass. When speaking of pile axial capacity, what is meant is that the soil resists to loads applied to the vertical axis of an installed pile by means of friction along the skin or shaft of the pile and end bearing pressure at the tip or toe of the pile. This is illustrated in Figure 3.1-1.

With respect to the pile itself, it should be designed appropriately (e.g. choosing an appropriate steel grade, or concrete strength etc.), in order to avoid material damage due to loads applied, which could lead to structural failure. On the other hand, the soil properties and loads define how much friction and end bearing pressure will be mobilized. Therefore, the design of a pile foundation should consider soil-pile interaction as well. Thus, the ability of a soil – pile system to withstand loads after some time from the end of the installation process is then referred to as (midterm or ultimate) pile capacity. The terms midterm or ultimate capacity are used to distinguish the capacity developed after some time from the driving process and the capacity or soil resistance during driving, also referred to as SRD. As will be discussed in later chapters, the SRD is lower than the midterm or ultimate capacity due to time or set up effects, meaning increase of shaft capacity over time.

When using the term driveability of piles what is actually meant is how much the resistance of the soil is during pile installation using specific driving equipment and installation methods. The questions that need to be answered in a driveability analysis are

not only relevant with the resistance of the soil, but also with the efficiency of the equipment used, the driving time, and the possibility of material damage risks to the pile.

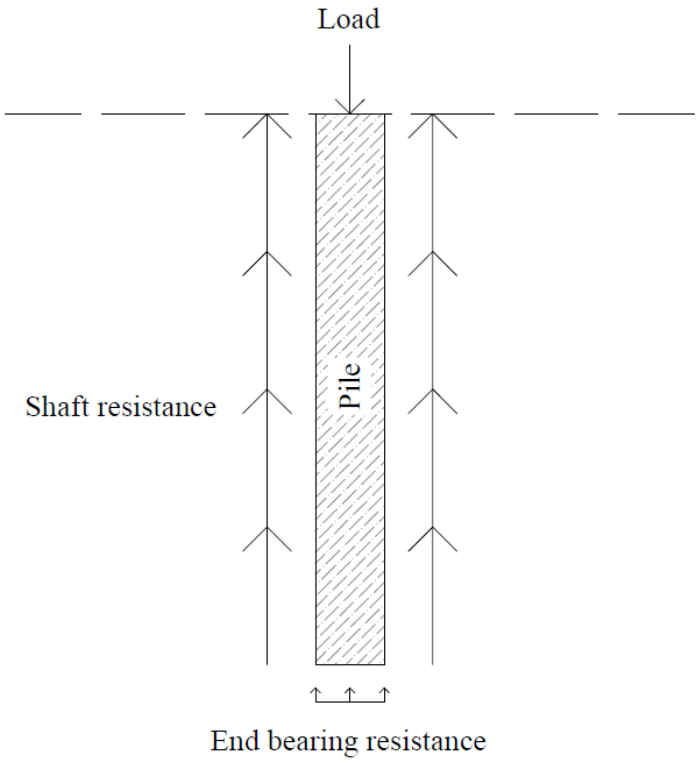

Figure 3.1-1: Axial Capacity of closed-ended piles (drawing created with AutoCAD 2021).

Both Fleming (2009) and Das (2011) describe the various types of piles and how they can be categorized. A short description is presented here, while the reader is referred to the aforementioned books for more details. In general, besides categorization according to material (steel, concrete, timber etc.), pile foundations can be classified according to their type and the type of construction. Specifically, two main types of piles, are the end bearing piles and the friction piles.

End bearing piles are usually embedded in a hard, relatively impenetrable material such as rock or very dense sand and gravel and they derive most of their capacity from the resistance of the rock or soil at the toe of the pile. On the other hand, friction piles obtain greater part of their carrying capacity by skin friction. This could be the case for a soft soil that becomes stiffer with depth. Thus, the pile does not reach an impenetrable rock or soil layer, but it is driven up to a specific depth into a penetrable soil. It should be noted though that in neither case the contribution of friction or toe resistance are

neglected. The aforementioned pile foundations just indicate what type of resistance has larger contribution to the total capacity. Of course, there are other types of piles that are not mentioned here, such as tension piles, laterally loaded piles, etc.

According to construction or installation process, piles can be classified into displacement piles or non-displacement piles. Displacement piles cause the soil to be displaced radially as well as vertically as the pile shaft is driven or jacked into the ground. With non-displacement piles (or replacement piles), soil is removed and the resulting hole is filled with concrete, or a precast concrete pile is dropped into the hole and grouted in. This Thesis will focus on displacement piles.

Hammer Types

There are various types of hammers that can be used to drive the pile into the soil. These can be classified by type, energy, speed, weight and source power. A short description of these hammers is presented below using as reference the Foundation Manual, and the IHC Hydrohammer brochure, which nicely describe the basic functions of each hammer type.

Drop hammer

This is the oldest and simplest type of hammer. The ram is lifted at a certain height (desired stroke height) by means of a rope or cable and then it is released. By its own weight the hammer falls and strikes the pile cap (Figure 3.1-2). The pile cap system is used to transfer the energy from the hammer to the pile. The potential energy is calculated as the weight of the ram times the stroke height.

An advantage of this type of hammer is actually its simple configuration. On the other hand, it is a very slow process, 5 to 10 blows per minute, and it is also difficult to maintain a certain dropping height during the installation process. Moreover, misalignment, which can be attributed for example due to not proper alignment of the leads, can lead to significant loses of energy. Typical drop heights are about $1.2\,m$.

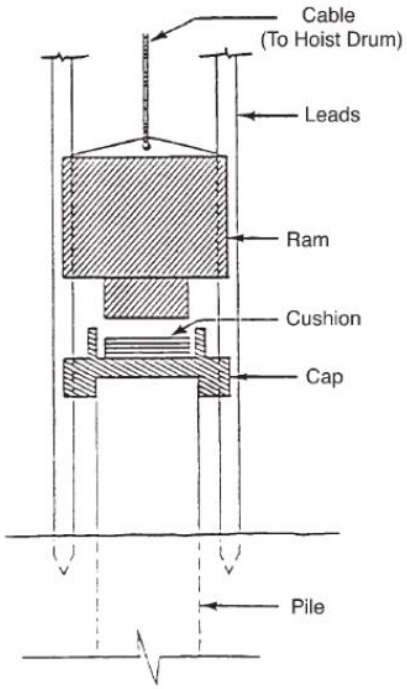

Figure 3.1-2: Basic components of a drop height (Foundation Manual).

Single or Double acting Steam/Air Hammer

A single or double acting steam/air hammer can be seen in Figure 3.1-3. The heavy ram in this case is connected to a piston enclosed in a chamber. Steam or air is supplied to lift the ram to a certain height. The lifting medium is then exhausted and the ram falls by its own weight (similar to the ram of the drop hammer). The difference between the single and double hammer is that the latter uses again steam or air to accelerate the piston's downward movement. In this case, due to additional energy during the downwards movement, the dropping height can be reduced. The single hammer has a stroke range of about $0.7\,m$ to $1\,m$ and operate at 60 to 70 strokes per minute. On the other hand, double hammers have a stroke range of about $0.25\,m$ to $0.5\,m$ and operate at 120 to 240 blows per minute. The rated energy can then be calculated as the total weight of the moving components (ram, piston etc.) times the stroke height and, for the case of double hammers, by adding the effective pressure acting on the piston's head during the downstroke.

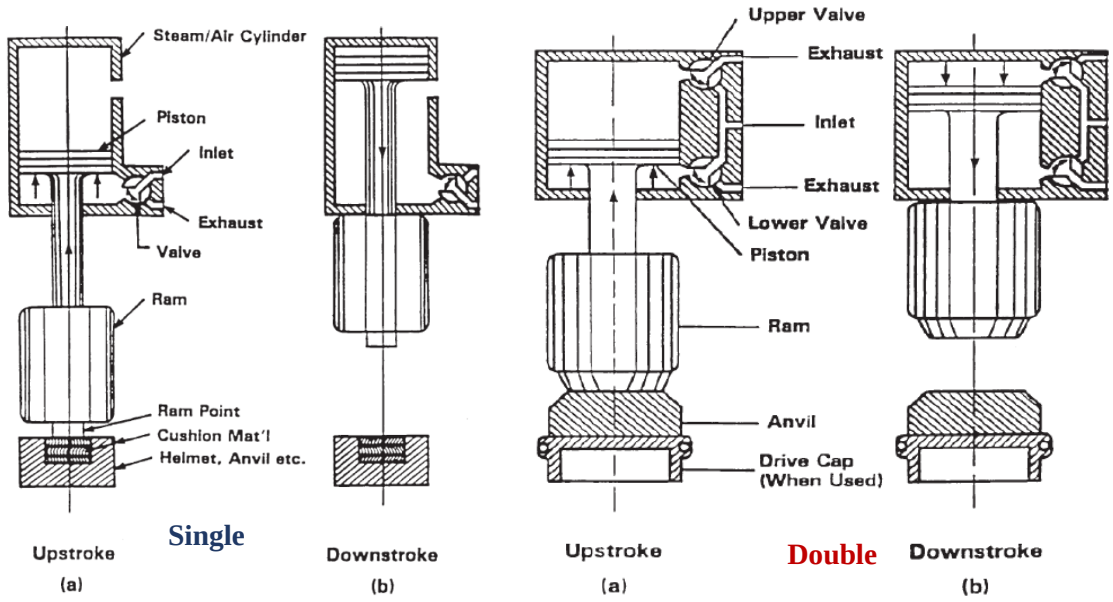

Figure 3.1-3: Basic components of a single or double acting steam/air hammer (Foundation Manual).

The advantage over drop hammers is the higher rate of blows per minute, which increases the speed of operation, and some hammers (double) can be entirely closed and operated submerged in the water. However, these hammers are heavy and require higher cranes and handling equipment capacities (higher cost), and they are sensitive to pressure and volume of the motive (steam or air) fluid.

Differential Acting Steam/Air Hammer

The differential acting steam/air hammer is very similar to a double acting hammer (Figure 3.1-4). Compressed air/steam is introduced between large and small piston heads to lift the ram to the top of its stroke. The valves are then switched so that the medium (motive fluid) used to lift the ram accelerates it in its down stroke. The rated striking energy is then calculated by adding the differential force due to the motive fluid pressure acting over the large piston head to the weight of the moving parts and by multiplying with the stroke height.

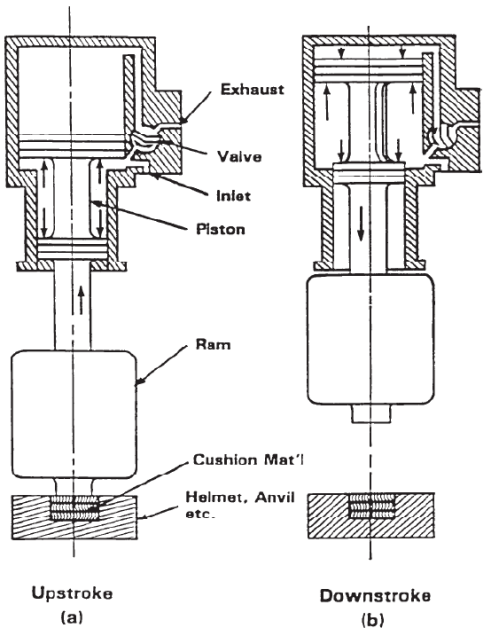

Figure 3.1-4: Basic components of differential acting steam/air hammers (Foundation Manual).

Single or double acting diesel hammers

The basic components of a diesel hammer can be seen in Figure 3.1-5. These are mainly a cylinder-encased ram, the impact block (anvil) that receives the impact of the ram and transmits the energy to the pile through the strike plate, followed by the hammer cushion to absorb part of the energy and avoid damaging the hammer, the pile helmet and pile cushion, which also absorbs energy to protect the pile from material damage. The operational cycle for a single acting diesel hammer can be seen in Figure 3.1-6.

The operation starts by lifting the ram with a cable from the cranes to a predetermined height and then is released. The ram falls under its own weight and activates a lever on the back of the fuel pump, which injects a measured amount of diesel fuel onto the top of the cup-shaped anvil (Figure 3.1-6 (A)).

Continuing its downward movement, the ram closes the intake/exhaust ports and compresses the air that is between the ram and the cup-shaped anvil (Figure 3.1-6 (B)), before impacting the anvil. The compression of the trapped air creates a preloading force upon the anvil, the helmet, and the pile (compression that “starts” the downward movement of the pile prior to blow).

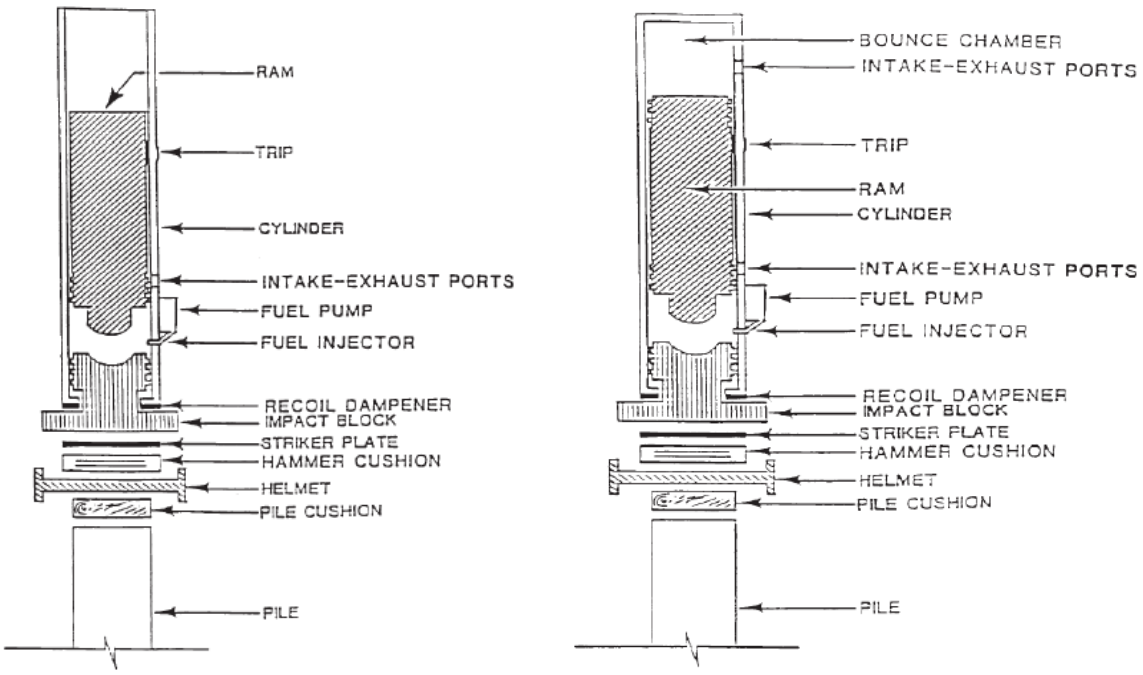

Figure 3.1-5: Basic components of a single (left) or double (right) acting diesel hammer (Foundation Manual).

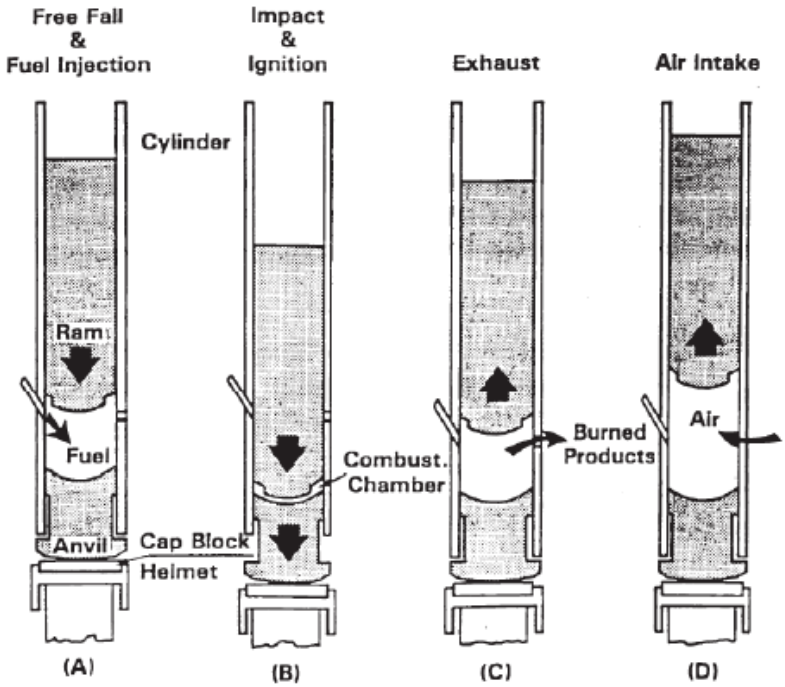

Figure 3.1-6: Operation cycle of a single acting diesel hammer (Foundation Manual).

When the ram strikes the anvil, the pile penetrates into the soil. At the same time the diesel fuel is atomized and splattered into the annular combustion chamber. The heat generated by the compression of air in the presence of atomized fuel, causes an explosion of the fuel (Figure 3.1-6 (C)). This explosion, not only recoils the ram (upward movement), but it further pushes the pile into the soil. On the upstroke, the ram opens the exhaust ports allowing the gas to escape and pressure equalization takes place in the cylinder. During the ram's upward movement, fresh air enters from the ports, cooling the cylinder (Figure 3.1-6 (D)), while at the same time the lever on the fuel injector pump returns to its original position for the next operation cycle.

The operation principles of the double acting diesel hammer, are the same as those mentioned earlier for the double action hammers. The top of the cylinder is capped in order for pressure to develop at the top of the ram (bounce chamber) during its downwards and upward movement. The downstroke energy now becomes a function of both the gravity and the internal pressure generated in the bounce chamber.

Operating diesel hammers in soft soils is a difficult process, because large displacements take place and most of the energy is absorbed, so little remains to lift the ram high enough to create sufficient compression in the next downstroke to ignite the fuel. To resume operation, the ram needs to be lifted again with the cable hoist.

For single action diesel hammers, typical blows per minute are around 40 to 60 and can have strokes in excess of $3\,m$. On the other hand, the double action diesel hammers can have a much higher blow rate, while having a low stroke, around $0.9\,m$ to $1.2\,m$.

Hydraulic Hammers

The basic components of a hydraulic hammer and its working principle are depicted in Figure 3.1-7. The basic components are again the piston and the ram, the valves P and R (pressure and returning lines) and accumulators, the anvil and the power pack that is used as external source to lift the hammer. Oil or water flows from the power pack through the supply - pressure valve to a cylinder chamber and returns through the returning valve. At rest (a) both valves remain open and oil circulates. The valves and accumulators are actually inside the hammer chamber but for this drawing are depicted outside of it for clarity of the working principle. The chamber above the piston is filled with compressed gas. When the hammer is set in operation (b), the return valve closes and the ram rises. At the end of the lifting phase, the pressure line closes and the return valve opens (c) in order for the ram to fall and impact the anvil. During this stage the ram receives additional

force from the gas pressure above the piston. In case of single acting hydraulic hammers, the energy induced to the pile comes only from the free-falling piston as described earlier for the rest of the single acting hammers.

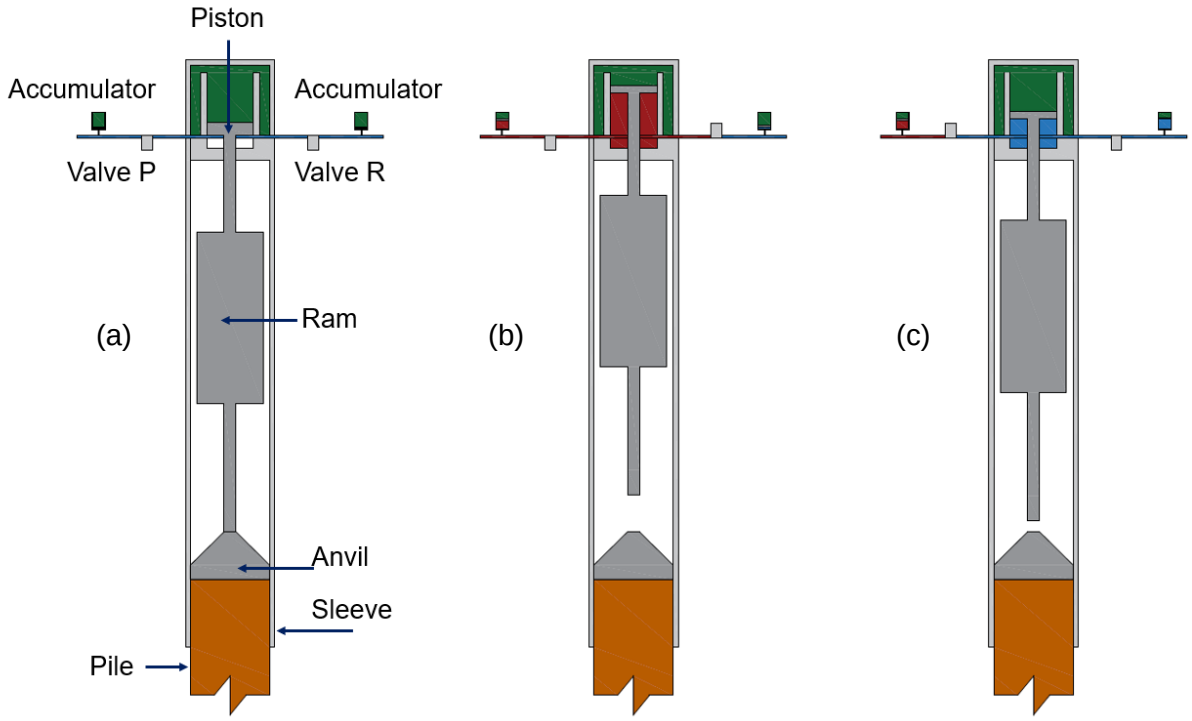

Figure 3.1-7: A simplified drawing of basic components of a hydraulic hammer and its working cycle (drawing created AutoCAD 2021).

Due to their working principle hydraulic hammers are more efficient, as it is much easier to control the stroke height in contrast to diesel hammers, which especially for soft soils, as described earlier might be difficult to operate. Additionally, the operation of a hydraulic hammer is claimed to be quitter than the typical diesel hammer, and more environmentally friendly, as the diesel hammers burn fuels during operation.

Energy Definitions

In this section, it is important to state the different hammer energy definitions that are used in pile driveability. Flynn et al (2019) explained the various definitions used starting with potential energy.

The potential energy immediately prior to the ram falling from a predetermined height can be given by [3.1.1], in which m is the mass of the ram, $g = 9.81\, m/s^2$, and h is the drop height.

$$E_{potential} = m * g * h \qquad 3.1.1$$

The maximum potential energy, or the potential energy corresponding to the maximum drop height is called rated energy. In this case, it is clear that [3.1.1] is used again with the only difference being the drop height which is replaced by the maximum drop height during driving. Since there are hammers (e.g. usually hydraulic hammers) that accelerate the ram's downwards movement, and thus increasing the amount of the potential energy, it is common for hammer manufacturers to provide directly the rated energy of the hammer instead of the potential.

As the ram moves through the gravity field, the potential energy from that field is progressively converted to kinetic energy. This conversion can be expressed by equation [3.1.2]. This energy is called impact energy and refers to the energy just before the impact of the ram to the anvil.

$$E_{impact} = \frac{1}{2} * m * v_{impact}^2 \qquad 3.1.2$$

If energy losses are not taken into account, then, the kinetic energy at impact would be equal to the potential and the impact velocity could be calculated with [3.1.3]:

$$v_{impact} = (2 * g * h)^{0.5} \qquad 3.1.3$$

However, losses in energy can occur due to various reasons such as friction, ram misalignment, inefficient combustion of fuel in diesel hammers, leading to pre-ignition and other problems, back pressure losses in the fluid ports (these can include valving, exhaust or relief ports, fluid hoses from the hammer to its power source) etc. The reduction in energy is typically quantified by the hammer efficiency [3.1.4]:

$$n = E_{impact}/E_{potential} \qquad 3.1.4$$

It is also important to state that impact energy is not the transferred to the pile energy. That is because, when for example cushions are used to protect the pile from material damage, again energy loses occur. The energy transmitted to the pile top is termed as ENTHRU energy and can be calculated by [3.1.5], in which F(t) and V(t) are the force and velocity magnitudes at time t after hammer impact, respectively. Transferred energy is usually measured using PDA (Pile Driving Analyzer) by placing a pair of strain gauges and accelerometers within 1 m of the pile head. EMX is the maximum transferred energy corresponding to one hammer blow.

$$E(t) = \int F(t) * V(t)dt \qquad 3.1.5$$

3.2 Stages of Stress History in Sands

As already mentioned, the axial capacity of a pile is a combination of soil resistances that apply at the pile shaft and tip. Thus, in order to have reliable estimations of the pile capacity or the soil resistances during pile driving, it is important to understand how the soil stresses change from the initial state – in situ conditions to the state in which the pile is already installed and the working load is applied. Therefore, in this section follows a brief presentation of the loading history and the associated stress paths of a soil element, which initially lies under the approaching pile (or CPT cone tip) and ends up adjacent to the pile shaft, as reported by White (2005) and can be observed in Figure 3.2-1. It should be mentioned that for stages A-C, when the soil lies beneath the pile or CPT cone tip, the loading is expressed in terms of spherical and deviatoric stresses, p' and q. Beyond stage

C, when the soil element is adjacent to the pile shaft, the loading is expressed as normal and shear stresses applied to the shaft, σ'_r and τ_s, respectively.

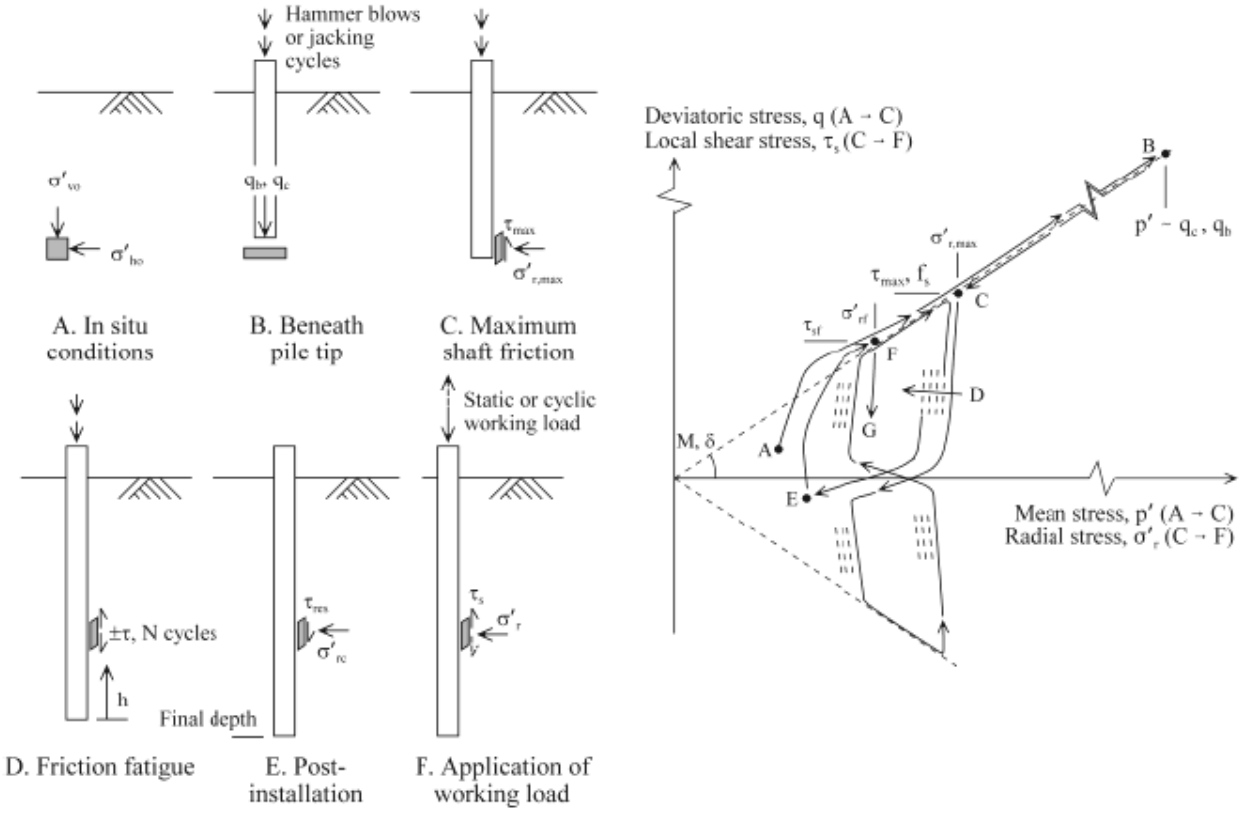

Figure 3.2-1: Loading history and stress paths of soil element adjacent to a displacement pile (White (2005)).

As the pile or CPT cone tip approaches the soil element, the local mean effective stress experiences a great increase, as can be seen in Figure 3.2-1 (Stage B). In case of driven piles, the highest stress mobilized during each blow is related to the base resistance q_b and in case of a CPT this stress is related to q_c (cone tip resistance). It should be mentioned that since q_b is typically two orders of magnitude greater than the in situ mean stress, suppressed axes have been utilized in Figure 3.2-1. Moreover, it is assumed that due to high strain levels close to the tip, the soil will move up the failure line in q - p' space.

As the soil element flows around the tip with further penetration the stress levels reduce (by two orders of magnitude). When it is adjacent to the pile shaft (but close to the tip, Stage C), the element exerts an upward shear resistance on the lower part of the pile shaft. In this stage the maximum unit shaft resistance, τ_{max} is mobilized. Additionally, the

author states that τ_{max} in case of open-ended piles might be lower than that of a closed-ended or plugged open-ended pile due to lower radial displacements (this is also discussed later, and was reported by White, Schneider et al (2007)).

Upon further penetration (Stage D), the soil element will be further away from the pile tip and cycles of shearing are applied. Research has shown that the horizontal stresses acting on the pile shaft at a given soil horizon tend to reduce with continued penetration. This phenomenon is termed as friction fatigue, (Heerema (1980)) and it is discussed later as well.

After installation, under no loading residual stresses remain both at the pile base and at the shaft close to the base. Due to decompression of the soil beneath the pile tip, the pile tends to rebound (move upwards) resulting in a counter-acting negative tension load (Stage E) being mobilized in the upper part of the shaft (Gavin, K., 2021, Soil Structure Interaction lecture notes).

Finally, (Stages F and G) application of static or cyclic working load will result in an increase of the radial stresses (from Stage E) as the shear stresses mobilized increase.

3.3 Plugged – Partially plugged – Unplugged Case

In the example presented in Figure 3.1-1, when a vertical load is applied on a pile, shaft and tip resistance will try to counter it. In this example though, the pile is considered closed-ended, meaning that only external friction is applied on the shaft and end bearing pressure at the toe.

Another example is presented in Figure 3.3-1. Now, an open-ended pile is considered, e.g., a steel hollow-pipe pile, in which a vertical load is applied as in the previous example. However, during driving of the hollow pile, the soil might fully or partially enter inside the pile.

In the extreme case in which the inner shaft friction becomes too high, a soil plug might be formed preventing any soil from entering inside the pile. Thus, during driving the soil beneath the tip is being pushed away – compacted. The capacity of the pile is then similar to the capacity of a closed-ended pile, as only external shaft friction and pressure at the gross base area of the toe will resist a vertically applied load (Figure 3.3-1 (a)). This might be the case for a pile with very small diameter and large wall thickness.

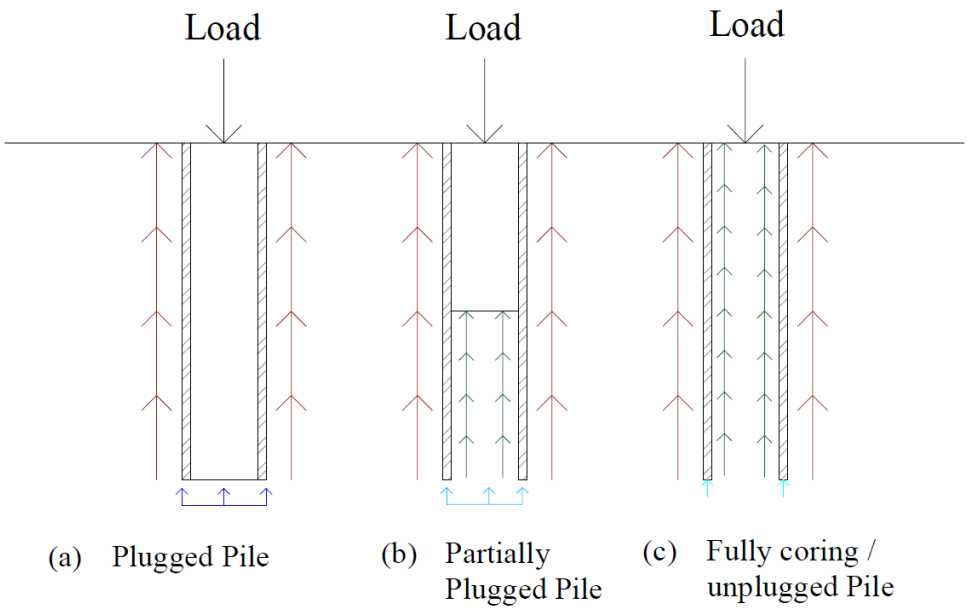

Figure 3.3-1: Axial capacity of open-ended piles during installation. (a) Plugged pile, (b) Partially plugged pile, (c) Fully coring - unplugged pile. For simplicity all piles presented in the figure have the same properties (drawing created with AutoCAD 2021).

Another scenario is the partially plugged pile. In this case, which is also illustrated in Figure 3.3-1 (b), during driving, the pile is partially filled with soil (partially plugged pile). This means that upon driving, the inner shaft friction increases with further penetration and eventually prevents any soil from entering the inside of the pile. The capacity then, is a combination of external shaft friction, internal friction between the soil and the pile, and pressure at the annulus of the pile tip and at the soil plug. It should be noted that the end bearing resistance in this case is lower than that of a fully plugged pile.

Finally, the third scenario that should be considered in case of open-ended piles is the unplugged pile, which is illustrated in Figure 3.3-1 (c). The fully coring case means that the soil fully enters inside the pile. This might be the case of large diameter piles. The capacity then consists of internal and external shaft friction and end bearing pressure at the annulus of the pile tip.

There are two ways to describe the degree of plugging. This is done by either calculating the IFR, which stands for incremental filling ratio and is defined as the incremental change of soil plug length relative to change in pile penetration, or by calculating the PLR, which stands for plug length ratio and is equivalent to the final plug length over the pile penetration depth. This is also illustrated in Figure 3.3-2. Moreover, Lehane et al (2005) suggested the use of FFR (final filling ratio), defined as a value of IFR averaged over a

distance of 3 pile diameters above the pile tip, to relate the unit end bearing value with the cone penetration resistance in sandy soil. It should be stated though that it is much easier to measure PLR than IFR in the field.

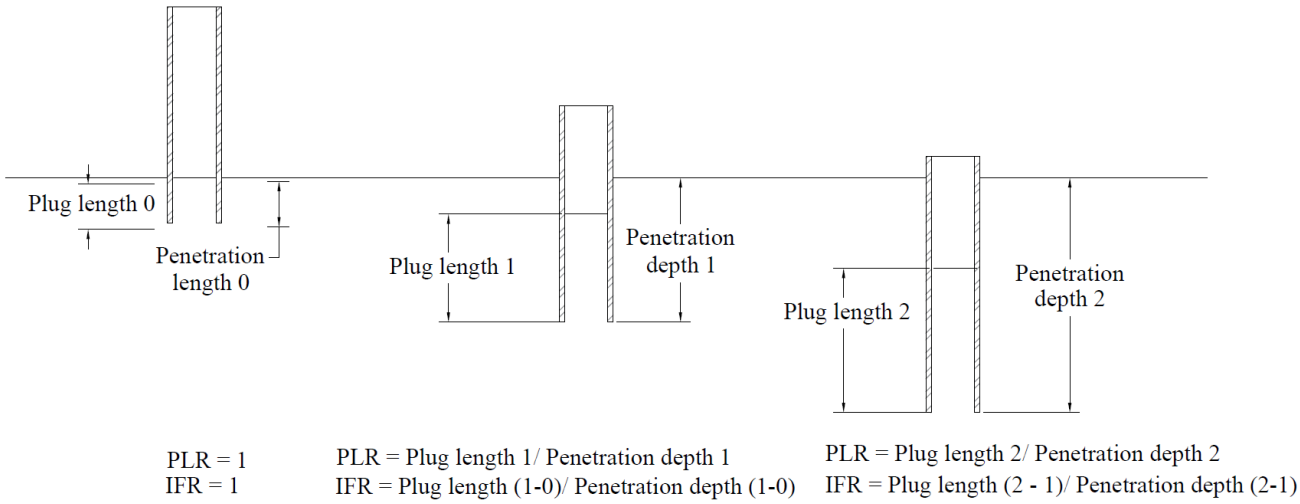

Figure 3.3-2: Incremental filling ratio (IFR) & plug length ratio (PLR) (drawing created with AutoCAD 2021).

The soil flow and radial stresses acting on a pile during installation are presented in Figure 3.3-3 by White, Schneider et al (2007). For closed-ended piles or plugged open-ended piles, the displacement or flow of soil around the pile tip is higher than in partially plugged open-ended piles or fully coring piles. That happens because part of the soil advances inside the pile and just part of it flows around the tip. The soil flow doesn't affect only the end bearing capacity of a pile but also the radial stresses developed along the pile outer shaft during driving. Hence, the radial stresses acting in closed ended piles are higher than in the other cases. It is reasonable then to expect higher radial stresses acting on a pile during installation in case of a partially plugged pile than a fully coring pile.

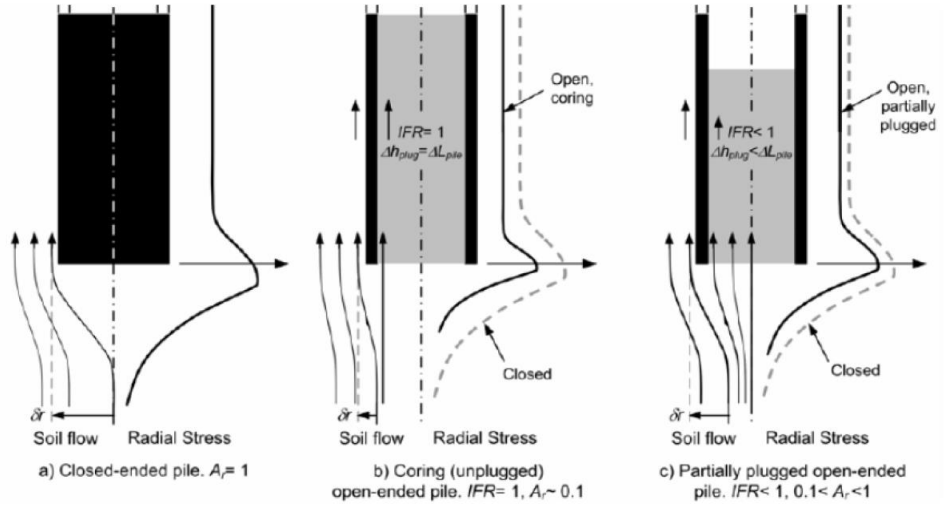

Figure 3.3-3: Schematic streamlines of soil flow and profiles of radial stresses in case of (a) close-ended piles, (b) coring (unplugged) open-ended piles, (c) partially plugged open-ended piles (White, Schneider et al (2007)).

3.4 Time Effects

It is suggested in various studies that the shaft capacity of piles driven in sand increases with time after installation. This phenomenon is known as pile ageing or set up effect (most commonly used term in driveability analysis), and it affects mainly the shaft capacity rather than the end bearing.

In one of these studies, Jardine et al (2006) interpreted the results of pile tests performed in dense sand at Dunkirk, France, by determining Intact Ageing Curves (IAC). These curves show how the ratio of shaft capacity at a given time over the shaft capacity calculated (after installation) with the ICP-05 design method (Jardine et al (2005)) develops with time. In this study it was observed that 1 day after installation the shaft capacities ratio was about 0.7.

This observation was consistent with the research of Karlsrud et al (2014) at Larvik silty sand and Gavin et al (2013) at Blessington dense sand. The aforementioned change of shaft capacity with time for the three locations, Dunkirk, Larvik and Blessington is

presented in Figure 3.4-1 as reported in the research paper of Gavin and Igoe (2021). It is clear in this figure that the measured capacities increase over time.

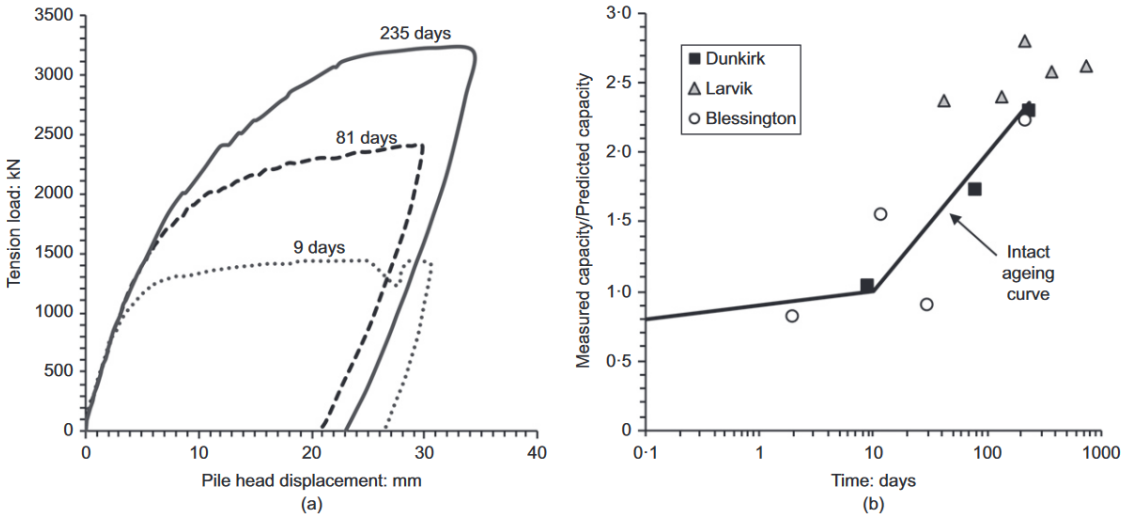

Figure 3.4-1: a) Ageing load test response at Dunkirk (after Jardine et al (2006)). (b) Variation of normalized capacity with time (Gavin and Igoe (2021)).

Moreover, Gavin et al (2015) concluded in their research that ageing does not depend on whether the piles are driven offshore or onshore, in dry, partially saturated deposits or sand saturated with salty or fresh groundwater, and that it appears to be independent of pile diameter. In addition, Lehane et al (2017) using a large database from previous research, derived equation [3.4.1] in order to estimate the variation of shaft capacity with time in sands:

$$F_{time} = \frac{1}{\exp(-0.1 * t^{0.68}) + 0.45} + d_{offset} \qquad 3.4.1$$

where, t represents the time after installation (thus, a value of 0 indicates the time factor exactly after the installation) and d_{offset} is a vertical offset to best fit the data, with suggested values of -0.1 and -0.2 when using ICP and UWA to calculate the shaft capacity, respectively. This factor when multiplied with the design shaft capacity based on the aforementioned methods, gives a continues shaft capacity increase with time.

Finally, Gavin and Igoe (2021) measured the radial effective stress and load distribution during installation, ageing and load testing for steel open-ended piles in Blessington's very dense sand. According to the measurements, during installation high radial stresses were observed that were significantly higher than the in situ horizontal stresses, especially near the pile tip (between $h/D = 1.5$ and $h/D = 5.5$). This was mainly attributed to the partially plugging that occurred during driving that led to a significant increase in vertical and horizontal stresses around the pile (greater than the pre-installation stresses). Continuous measurements of the radial stresses after installation showed (near the pile toe) a reduction over time, but they still remained above the in situ horizontal stresses (Figure 3.4-2).

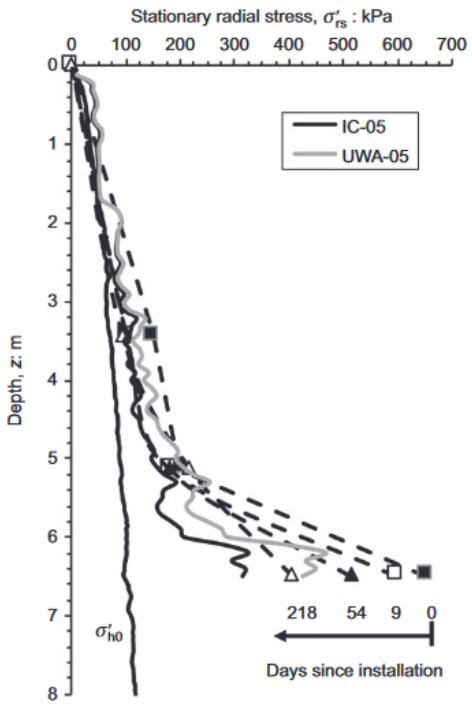

Figure 3.4-2: Changes in radial stresses over time, as observed at pile S5 (Gavin and Igoe (2021)).

This is in contrast with the observations, for example by Axelsson (2000), who indicated an increase of radial stresses with time. It should be noted though that in this report (Axelsson (2000)), the radial stresses after installation although increased with time, they were significantly lower than the in situ horizontal stresses, as can be seen in Figure 3.4-3. In any case, at all sites there is a tendency for radial stresses to approach the in-situ stresses (prior to installation), suggesting recovery of installation damage as reported by Lim et al (2014).

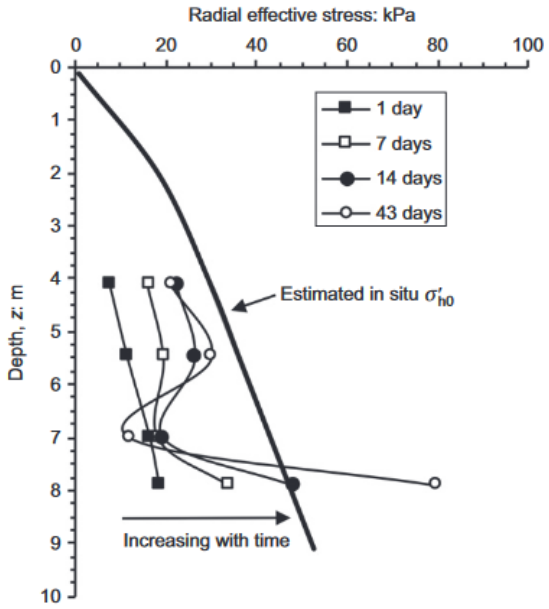

Figure 3.4-3: Change of radial stresses over time as reported by Axelsson (2000).

3.5 Friction Fatigue

The radial effective stresses and shear stresses that develop in any given soil horizon tend to reduce as the distance from the pile tip to that horizon increases (Heerema (1980)). This is termed as friction fatigue, and what is meant is that the shear stresses at a specific depth – soil horizon very close to the pile shaft tend to reduce with further penetration. This can be observed in Figure 3.5-1 by Lehane et al (1993). Figure 3.5-1 doesn't show only the effect of friction fatigue, but it also justifies the attempts to correlate the bearing and shaft resistance with the cone tip resistance from CPTs, as the resemblance between the shape of shear stresses around the shaft and the qc value is evident. It should be noted that in the CPT-based pile capacity design methods, friction fatigue is taken into account by a degradation factor that is in the form of $\left(\frac{h}{R}\right)^{-n}$, in which h is the distance of the soil horizon examined from the tip, R is the radius of the pile.

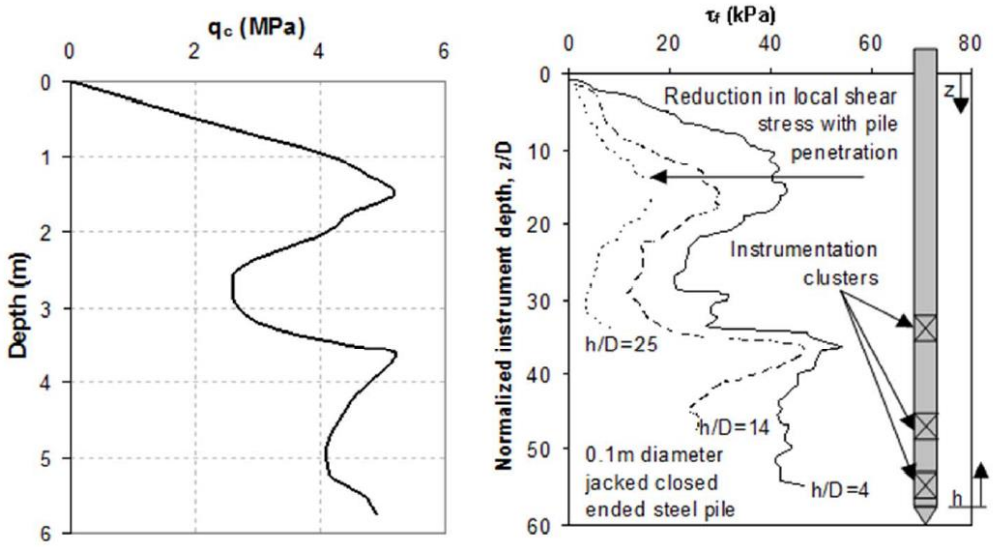

Figure 3.5-1: Instrumented test data indicating that shear stresses along the shaft are a function of the cone resistance from CPTs and the ratio (h/D) (Lehane et al (1993)).

Moreover, Jardine and Chow (2007) indicated some possible reasons for friction fatigue to occur (Figure 3.5-2). According to the authors friction fatigue can be caused by (a) free surface effects, meaning upward displacements of soil near the surface leading in reduction of radial stresses, (b) gapping caused by lateral movement, and most importantly by (c) the geometry of the steady flow system around the pile tip and (d) the number of cycling loading experienced by the soil element in a specific soil horizon during installation.

Additionally, it is important to mention the kinematics of friction fatigue near the pile tip, as reported by White and Bolton (2004) and illustrated in Figure 3.5-3. Initially, along the streamline XY high horizontal stresses develop as the soil is compressed laterally. As the soil continues along streamline YZ the interface zone immediately adjacent to the pile (Zone B) contracts with continued shearing at the pile soil interface. The unloading of the stiff soil, represented by a stiff spring, Zone A, due to contraction of Zone B leads to a reduction in shaft friction on the pile.

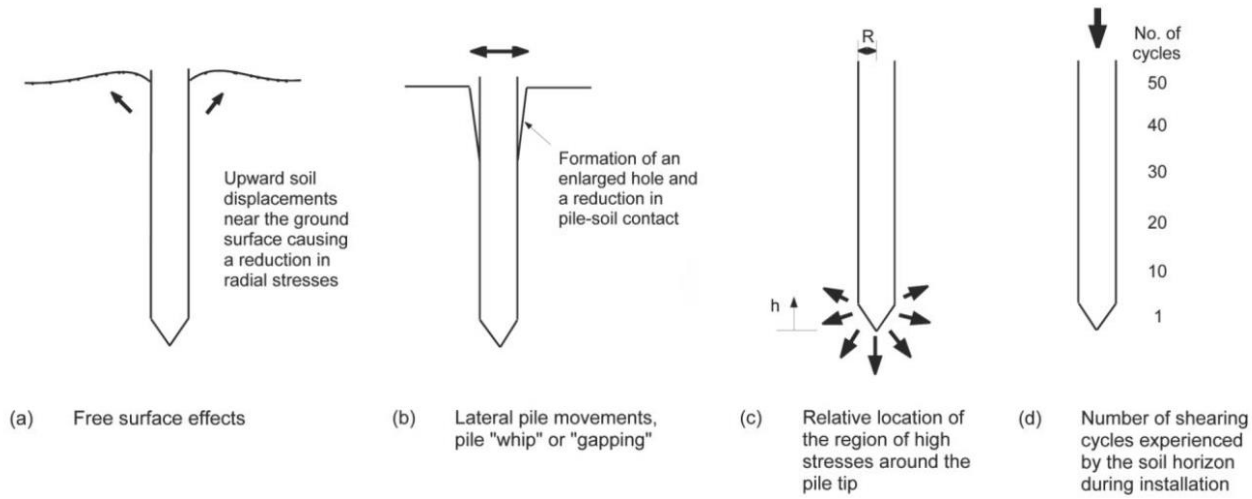

Figure 3.5-2: Friction fatigue possible causes (Jardine and Chow (2007)).

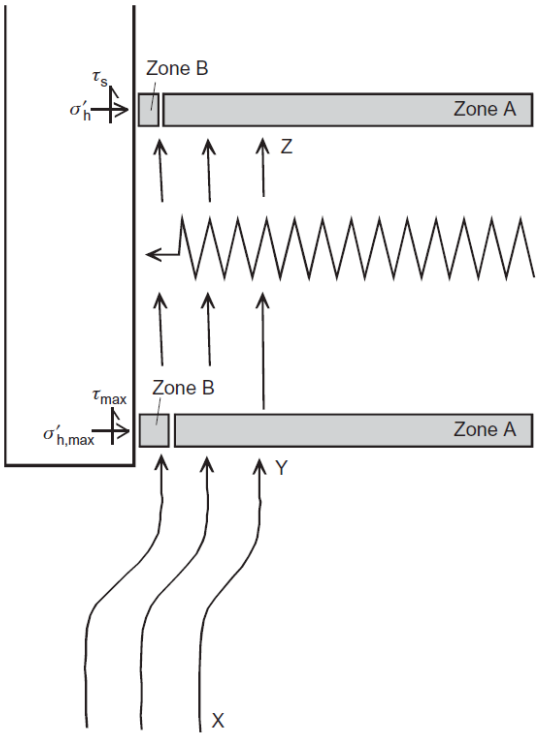

Figure 3.5-3: Kinematics of friction fatigue close to the pile tip as reported by White and Bolton (2004).

3.6 A Literature Review on Static Resistance during Driving

The soil resistance during pile driving consists of dynamic and static components. The dynamic components are related to increase of resistance due to inertial and viscous rate effects (Randolph (2000)), and they are usually quantified by using damping factors (Schneider et al (2010)). On the other hand, the static component of the resistance, also referred to as Static Resistance during Driving (SRD), is similar to the pile axial capacity. The differences between SRD and axial static capacity are due to consolidation, equalization, and pile ageing, as reported by Schneider et al (2010).

In a recent paper by Prendergast et al (2020) some major factors that influence the relation between the SRD and the axial static capacity calculated by CPT-based design methods are highlighted. First, as noted by other researchers as well (e.g., Schneider et al (2010), Byrne et al (2018)), the axial capacity CPT design methods were calibrated such that they could make good estimations of the axial capacity of piles 10-30 days after the end of installation process. Due to time effects, as explained in previous section, the shaft capacity has been observed to increase with time. Therefore, the soil resistance calculated with the CPT design methods (e.g., Unified Method) is expected to be higher than the SRD. Hence, a time factor should be applied in the shaft capacity of these design approaches, in order to estimate a skin resistance closer to the one experienced by the pile during driving.

Moreover, another important factor influencing the calculated SRD and should be taken into account in a driveability analysis, is the aforementioned phenomenon of friction fatigue (Prendergast et al (2020), Schneider et al (2010), Byrne et al (2018)). An example of this phenomenon was illustrated in Figure 3.5-1, as reported by Lehane et al (1993). During driving, with further pile penetration the shear stresses at a specific depth tend to reduce. Then, driveability analysis should be performed for each SRD calculated at each depth (Schneider et al (2010)). Another approach to take into account the friction fatigue effect was suggested by Schneider et al (2010). Specifically, the authors suggested a pseudo-average shear resistance to be calculated between the current and previous depth increments, and insert one SRD profile in the wave equation solver of the driveability analysis. In this simpler way, changes of the shape of shear resistance along the shaft during driving are taken into account.

Furthermore, Gavin and Lehane (2007) created a model in order to define the load-displacement response of a pile base in sand. During driving, the base resistance applied on the pile per hammer blow is significantly lower than the one estimated by the CPT

based axial capacity approaches, as it corresponds to the base capacity for displacements of the tip or head (depending on the method used) of $0.1 * D$. Byrne et al (2018) suggested to use this base-displacement model in order to approximate the base resistances encountered during driving, by estimating the actual settlements from each hammer blow from the driving records. By doing so, they showed that the UWA approach predicted $blows/0.25\,m$ closer to the measured ones, although in most cases it underpredicted the soil resistance. It should be noted though that the residual loads were completely ignored in this attempt.

Additionally, Paik et al (2003) and Byrne et al (2018) suggested different ranges of ratios of residual to CPT cone base resistances, for installation in medium to dense sand, for piles with $356\,mm$ diameter in the first research study and $4.2\,m$ in the latter case. Specifically, Paik et al (2003) suggested base residual stresses of 11-14% of the qc, while Byrne et al (2018) mentioned that a range of 1-10% of the qc value would be appropriate. On the contrary, Kirwan (2015) reported residual loads being 27% of the qc for a $340\,mm$ diameter open-ended pile installed in dense sand, when the IFR was measured to be 40%. Clearly, there is a lot of uncertainty, but Byrne et al (2018) and Prendergast et al (2020), by including residual loads of $1-10\%$ of the qc in the base displacement model of Gavin and Lehane (2007) reported that the predictions of blows/0.25 m were improved. Moreover, Gavin and Lehane (2007) stated in their paper that residual loads are expected to be higher in a fully plugged pile rather than in a fully coring pile. This might explain the higher residual loads on the smaller diameter pile examined in the paper of Paik et al (2003).

Finally, it should be noted that the hammer efficiency and stroke height assumed prior to the driveability analysis is a very important factor that affects the predictions. Prendergast et al (2020) showed that a slight change in the drop height or hammer efficiency (in the wave equation solver) could lead in great under or overpredictions when using the UWA for the static resistance calculation. In general, the higher the hammer efficiency or stroke height the lesser the blows required to drive the pile, with a greater risk for damaging the pile. Flynn et al (2019) measured the impact energy, which is the kinetic energy at impact with the pile and EMX, the maximum energy transmitted to the pile during penetration, in an attempt to define a varying hammer efficiency with depth in order to take into account more accurately the loses of energy (e.g. friction) during installation. By applying a varying hammer efficiency, the predicted blows required to drive the pile were in good agreement with the measured ones.

3.7 Wave equation models

This Chapter is concluded with a brief presentation of two wave equation models, the lumped model as used by Smith (1960) and the characteristic model (Voitus van Hamme et al (1974), Saint-Venant (1867)) as used by TNOWAVE and reported in the paper of Middendorp et al (2006), to simulate the hammer-pile-soil system during driving.

The propagation of driving energy along a pile may be analyzed with sufficient accuracy using a 'one-dimensional' idealization. In this idealization, only vertical (axial) pile displacement is considered, and the governing differential equation is given by [3.7.1] and [3.7.2], in which c is the velocity of the wave, E is the Young's modulus and ϱ is the density of the pile material:

$$\frac{\partial^2 u}{\partial t^2} - c^2 * \frac{\partial^2 u}{\partial x^2} = 0 \qquad 3.7.1$$

$$c = \sqrt{\frac{E}{\rho}} \qquad 3.7.2$$

Commercially available software, such as GRLWEAP or AllWave PDP are commonly used to simulate the pile driving process and predict the pile response by solving the aforementioned wave equation.

Smith (1960) based on one dimensional wave propagation theory developed a finite difference formulation for the general impact pile driving problem. The lumped model used by Smith (1960) is presented in Figure 3.7-1 below.

The hammer, pile and other parts involved in Smith's lumped model are represented by weights and springs. Time is also discretized into smaller time intervals and the action of each weight and spring is calculated for each and every time interval.

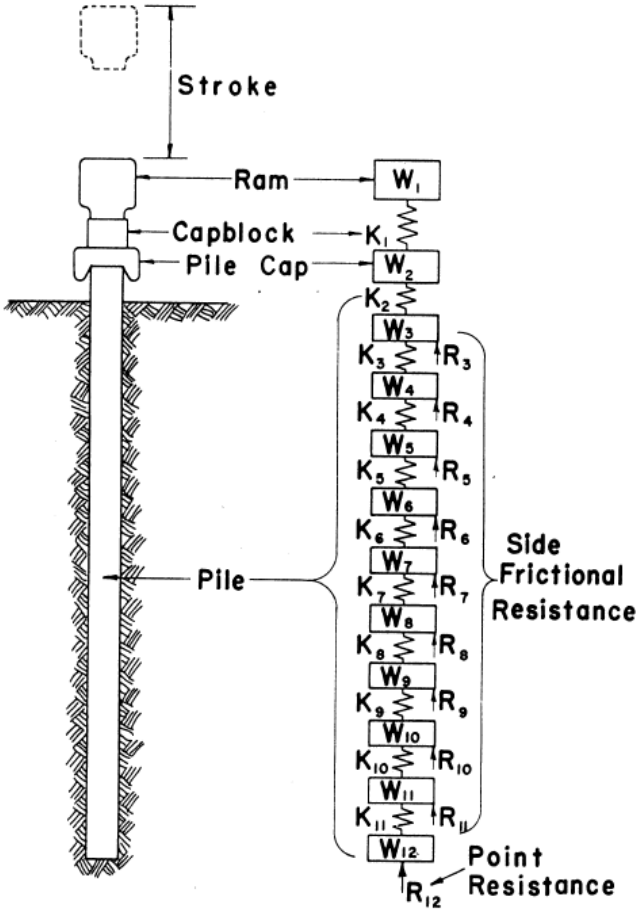

Figure 3.7-1: Hammer-pile-soil model (Smith (1960)).

In this way a mathematical determination can be made of stresses, pile penetration or permanent set per blow, against any amount or kind of soil resistance Smith (1960). The soil side resistance, Figure 3.7-2, acts on the masses, as can be seen in Figure 3.7-1, by an elasto-plastic spring representing the static resistance and a quasi linear dashpot to model the damping resistance (Rausche et al (1992)). Additionally, the pile tip resistance is modeled with a single spring at the point of the pile.

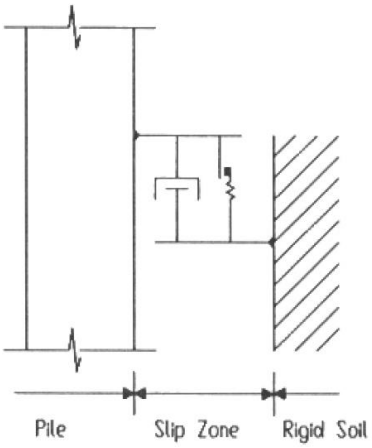

Figure 3.7-2: Smith (1960) pile-soil interface model (Rausche et al (1992)).

The load-deformation soil response can be seen in Figure 3.7-3 (Hirsch et al (1970)). The elasto-plastic behaviour, without taking into account damping effects, (Figure 3.7-3 (a)) is characterized by the ultimate soil resistance, R_u, and the quake value, Q, which is the deformation of the spring (or soil) below which, the soil is assumed to behave elastically. The modified load-deformation response to take into account damping is shown in Figure 3.7-3 (b), by introducing the Smith's damping constant $J\,(sec/m)$. This damping coefficient is assumed to be constant for a given soil under given conditions. The product of $J * V$, with V the pile velocity, is used to increase (or decrease) the soil resistance so as to produce damping (Hirsch et al (1970), Smith (1960)). The general expression to calculate the total soil resistance, R_t is given by [3.7.3]:

$$R_t = R_u * (1 + J * V) \qquad 3.7.3$$

Sometimes, R_u is defined as R_s, the ultimate static soil resistance (Rausche et al (1992)). It should be mentioned (Hirsch et al (1970)) that the soil at the tip of the pile is loaded in compression and it is believed that the damping coefficient at the tip is larger than that along the pile shaft.

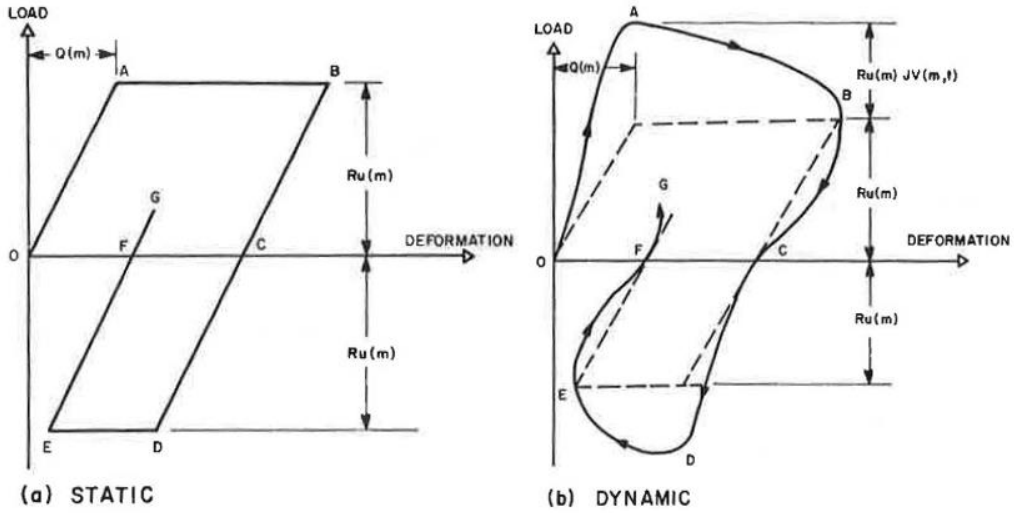

Figure 3.7-3: Load-deformation soil response in Smith's (1960) model (Hirsch et al (1970)).

The research institute TNO started the development of the wave equation program TNOWAVE in the late 1970's (Middendorp et al (2006)) based on HBG's (Hollandsche Beton Groep) friction model extension for the method of characteristics (Voitus van Hamme et al (1974), Saint-Venant (1867)). The wave equation model used is the characteristic model presented in Figure 3.7-4 below. The characteristic model, in contrast to the lumped model, which showed some disadvantages (Middendorp et al (2006)), doesn't assume a discrete but a continuous pile.

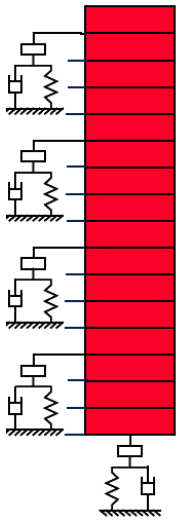

Figure 3.7-4: Characteristic -TNOWAVE wave equation model (Middendorp et al (2006)).

The pile is divided into equally spaced intersections. The spaces between the intersections are called elements, however they are not elements in the sense of finite element methods. The set of intersections common to each pair of spaces is to be considered as a co-ordinate system. The soil resistance is represented by elasto-plastic springs, dashpots and masses applied to the intersections between elements. The TNOWAVE algorithm based on the method of characteristics is presented in the following equations ([3.7.4] and [3.7.5]) and is depicted in Figure 3.7-5. The wave of forces arriving at the intersections are determined from the waves calculated at the former time-step (Figure 3.7-5). Between the intersections the pile is assumed frictionless and so the propagation of a wave will be undisturbed. Arriving at the intersection a part of the wave will be transmitted and another part reflected as depicted in Figure 3.7-6.

$$f_{n,i}^{\downarrow} = \frac{Z_N - Z_{N+1}}{Z_N + Z_{N+1}} * f^{\uparrow} + \frac{Z_{N+1}}{Z_N + Z_{N+1}} * (2f^{\downarrow} - W_{n,i}) \qquad 3.7.4$$

$$f_{n,i}^{\uparrow} = -\frac{Z_N - Z_{N+1}}{Z_N + Z_{N+1}} * f^{\downarrow} + \frac{Z_N}{Z_N + Z_{N+1}} * (2f^{\uparrow} + W_{n,i}) \qquad 3.7.5$$

where,

- N is the element number.
- n is the intersection (between elements) node number.
- i is the time step number.
- $f^{\downarrow}$ is the incident downward traveling wave at $n-1$ and $i-1$.
- $f^{\uparrow}$ is the incident upward traveling wave at $n+1$ and $i-1$.
- $f_{n,i}^{\downarrow}$ is the transmitted downward traveling force wave.
- $f_{n,i}^{\uparrow}$ is the transmitted upward traveling force wave.
- Z is the impedance (dynamic stiffness) of pile element N, or $N+1$.
- W is the total soil resistance ($W = Wa + Wv + Wu$, $mass + dashpot + spring$).

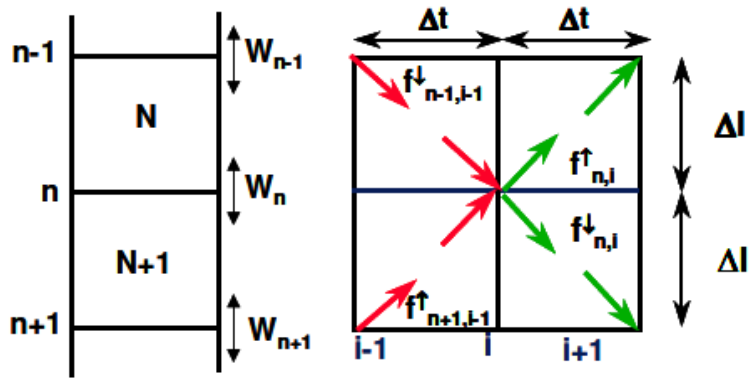

Figure 3.7-5: TNOWAVE algorithm (Middendorp et al (2006)).

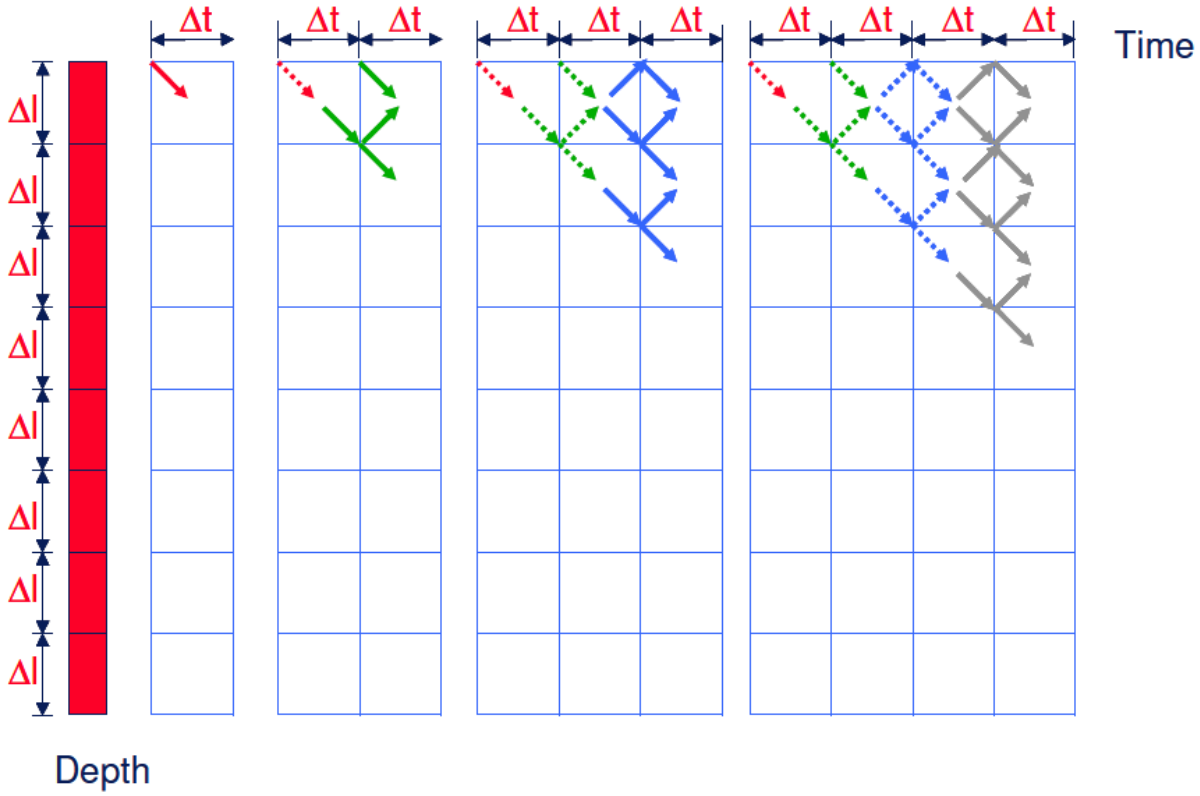

Figure 3.7-6 : Propagation of successive waves (Middendorp et al (2006)).

The magnitude of transmitted and reflected waves depends on the pile properties, (e.g., geometry) shaft friction and toe resistance. The equations for transmitted and reflected waves are derived from the fulfilment of equilibrium and continuity conditions at the intersections. Force, velocity, displacement and accelerations can be calculated from the waves and allow the calculation of energy and friction (Middendorp et al (2006)).

It should be noted that this Thesis utilizes the AllWave PDP software (Allnamics), which is based on the continuous pile model as presented in Figure 3.7-4 and on the method of characteristics. The static and dynamic soil resistances are simulated using Smith's soil model, as shown in Figure 3.7-3. More details will be presented in later Chapters.

4. SRD Models

In this section three traditional SRD driveability models are briefly described, alongside with a short introduction to the total resistance during driving. Specifically, these are the Toolan & Fox (1977), Stevens et al (1982), and the Alm & Hamre (2001) models. The most commonly used in practice though, is the Alm & Hamre (2001) model. Additionally, this Chapter includes the presentation of a new CPT based axial capacity design method, referred to as Unified Method. This method, is not intended for driveability studies but for estimating the static axial pile capacity in silica sand conditions.

4.1 Resistance During Driving

The static resistance during driving, SRD, for open-ended piles can be estimated by the general formulation presented below [4.1.1]. It should be noticed, that various components of the SRD are estimated differently by the aforementioned SRD models.

$$SRD = Q_{shaft} + Q_{toe} \tag{4.1.1}$$

where,

- SRD is the soil static resistance during driving, $[kN]$.
- Q_{shaft} is the total shaft resistance during driving (including the resistance both at the outer and the inner shaft area), $[kN]$.
- Q_{toe} is the resistance at the pile tip, $[kN]$.

The shaft and toe resistances, for open-ended piles, in their general form can be written as shown in [4.1.2] and [4.1.3], below.

$$Q_{shaft} = \pi * D * \int_0^L tf dz + \pi * D_i * \int_{L_{io}}^L tf_i dz_i \tag{4.1.2}$$

$$Q_{toe} = q_{an} * \pi * \frac{D^2 - D_i^2}{4} + q_{plug} * \pi * \frac{D_i^2}{4} \tag{4.1.3}$$

where,

- tf is the unit friction of the outer shaft during driving, $[kPa]$.
- D is the outer pile diameter, $[m]$.
- L is the pile penetration level, $[m]$.
- D_i is the inner pile diameter, $[m]$.
- tf_i is the unit friction of the inner shaft during driving, $[kPa]$.
- L_{i0} is the soil surface level inside the pile, $[m]$.
- q_{an} is the resistance of the soil applied in the annular area of the pile base, $[kPa]$.
- q_{plug} is the resistance of the soil plug, $[kPa]$.

For a close-ended pile, $D_i = q_{plug} = tf_i = 0$, and $q_{an} = q_b$, with qb the base resistance developed at the entire base area of the pile.

Figure 4.1-1 depicts the various SRD components discussed earlier.

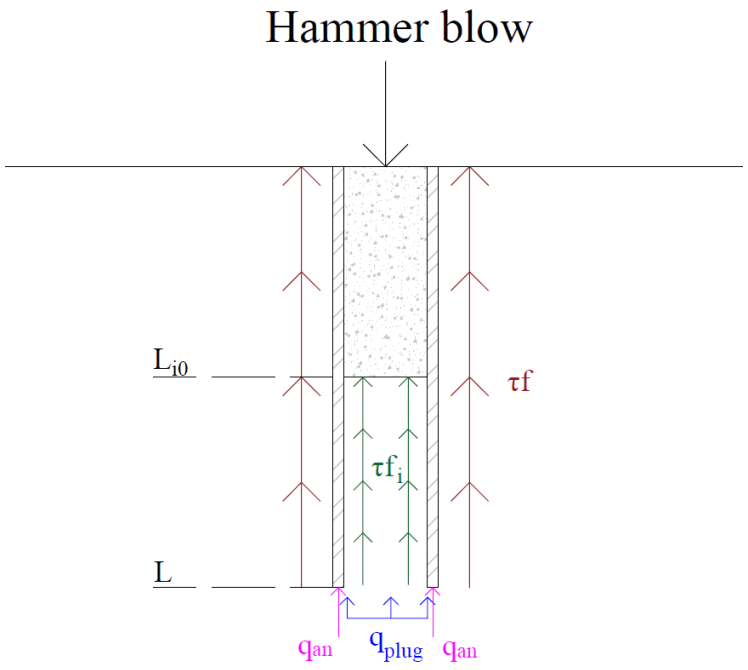

Figure 4.1-1: SRD components (drawing created with AutoCAD 2021).

As mentioned in Chapter 3, this Thesis utilizes the AllWave PDP software (Allnamics) to solve the wave equation [3.7.1], based on the method of characteristics that was discussed in Chapter 3.7 (Figure 3.7-5, Figure 3.7-6). Hence, this research uses a continues pile model (Figure 3.7-4) and Smith's (1960) discrete soil model represented by elasto-plastic springs and dashpots applied to the intersections between the pile elements and at the pile toe.

(Ignoring the inertia resistance), the total driving resistance can be written as [4.1.4]:

$$R_{total} = R_{static} + R_{dynamic}(R_{static}) = k * u + (J_S * v) * k * u \qquad 4.1.4$$

where,

- R_{static} is the static resistance during driving (shaft and toe), $[kN]$.
- $R_{dynamic}$ is the dynamic resistance as proposed by Smith (1960), $[kN]$.
- Js is Smith's damping constant, $[sec/m]$.
- v is the pile's element velocity $[m/sec]$.

In the next sections, traditional SRD models are presented, which basically aim at defining the maximum or yield stress (R_{static}) of the elastoplastic soil springs (Figure 3.7-3).

4.2 Toolan & Fox (1977)

One of the oldest methods proposed to estimate the static resistance during driving, is the Toolan & Fox (1977) SRD model.

The unit shaft friction in sands, according to Toolan & Fox (1977), can be calculated as a fraction of the qc value from the CPT. This is expressed in [4.2.1], below:

$$\tau f = qc/300 \qquad 4.2.1$$

It should be noted that the authors suggest an upper limit for the unit friction, equal to $120\ kPa$. Moreover, for an open-ended pile, unit friction is applied both in the external and internal shaft area.

As for the pile tip resistance during driving, this is calculated as a weighted average of the cone resistance qc, a number of diameters above and below the pile tip, and applied on the steel annulus for fully coring piles. For plugged piles it is mentioned that the toe resistance should be applied on the gross base area, while only external friction is applied at the outer shaft area.

4.3 Stevens et al (1982)

Stevens et al (1982) SRD model has produced satisfying driveability predictions for piles with diameter in the range of about 0.9 to $1\ m$ driven in the Arabian gulf. An advantage of both Stevens et al (1982) and Toolan & Fox (1977) SRD models is that the formulas suggested are easy to use. However, there are also disadvantages that come with the simplifications incorporated in these models that will be discussed in later chapters.

For cohesionless soils (e.g., sand) the unit shaft friction during driving is calculated with [4.3.1]:

$$\tau f = K * \sigma'_{vo} * tan\delta \qquad 4.3.1$$

where,

- K is the coefficient of lateral earth pressure, $[-]$.
- σ'_{vo} is the effective overburden pressure, [kPa].
- δ is the angle of friction between soil and pile, [°].

The value of K is taken as 0.7. The authors, suggest limitations to be applied on both δ and τf, which can be found in API (2000) guidelines. More recent versions of the API exist, but the 2000 version includes the same limits (for τf and δ) with those suggested

in the authors' paper. These are presented in Figure 4.3-1. Additionally, Table 4.3-1 summarizes the sand consistency based on relative density by Lambe and Whitman (1969).

The toe resistance for granular soils is calculated by [4.3.2], where Nq is a dimensionless bearing capacity factor, while the limits suggested can be seen in Figure 4.3-1.

$$qb = Nq * \sigma'_{vo} \qquad 4.3.2$$

The dimensionless bearing capacity factor can also be obtained from API (2000) guidelines.

For fully coring piles, the Lower Bound of this method assumes that unit skin friction is applied both on the outer and internal shaft area, but the internal is reduced by half (50% of equation [4.3.1]). The toe resistance is applied on the steel annulus. On the other hand, the Upper Bound of this method, assumes the internal shaft friction equal to the external (equation [4.3.1] is applied both inside and outside), while the toe resistance is calculated again by [4.3.2] and applied on the steel annulus.

In case of plugged piles, the Lower Bound of this method suggests that unit friction is applied only at the outer shaft area, while the end bearing pressure (calculated by [4.3.2]) is applied on the gross pile base area (full area below the tip), as the plug moves together with the pile. The Upper Bound for a plugged pile of this method suggests an increase of the external shaft friction by 30%, and 50% increase of the toe resistance. A corresponding increase is also applied on the limiting values of the unit shaft friction and toe resistance.

Table 4.3-1: Relative density by Lambe and Whitman (1969).

Consistency	Relative Density D_r (%)
Very Loose	0–15
Loose	15–35
Medium Dense	35–65
Dense	65–85
Very Dense	85–100

Density	Soil Description	Soil-Pile Friction Angle, δ Degrees	Limiting Skin Friction Values kips/ft^2 (kPa)	N_q	Limiting Unit End Bearing Values kips/ft^2 (MPa)
Very Loose	Sand	15	1.0 (47.8)	8	40 (1.9)
Loose	Sand-Silt**				
Medium	Silt				
Loose	Sand	20	1.4 (67.0)	12	60 (2.9)
Medium	Sand-Silt**				
Dense	Silt				
Medium	Sand	25	1.7 (81.3)	20	100 (4.8)
Dense	Sand-Silt**				
Dense	Sand	30	2.0 (95.7)	40	200 (9.6)
Very Dense	Sand-Silt**				
Dense	Gravel	35	2.4 (114.8)	50	250 (12.0)
Very Dense	Sand				

Figure 4.3-1: API (2000) guidelines for limiting unit shaft friction and end bearing capacity.

4.4 Alm & Hamre (2001)

The 2001 model is an updated version of the one originally proposed in 1998. The authors have been involved with pile driveability predictions for large, open-ended piles (diameters in the range of 0.762 to $2.74\,m$) installed in different soil conditions in the North Sea. Since 1998, the database has been continuously updated, and in particular, information from installations of long piles in normally consolidated clays has been gathered. Based on this complete database, a new and improved soil driveability model was then suggested (Alm & Hamre (2001)). The advantage of this soil model is that it directly utilizes CPT measurements, and hence avoids uncertainty that follows from individual interpretation of measured data.

The basic principles and formulas of this SRD model are presented briefly in this section. For more information the reader is referred to Alm and Hamre (2001).

Since a major contribution to the Static Resistance during Driving (SRD) is provided by friction along the shaft, this model incorporates the concept of friction fatigue by reducing

the shear stresses with increasing pile penetration. The general formulation of the side friction along a pile during the driving phase is given by [4.4.1] below:

$$f_s = f_{sres} + (f_{si} - f_{sres}) * e^{k(d-p)} \qquad 4.4.1$$

where,

- f_s is the side friction during driving, $[kN/m^2]$.
- f_{si} is the initial pile side friction $[kN/m^2]$.
- f_{sres} is the residual side friction $[kN/m^2]$.
- k is a shape factor for degradation, $[-]$.
- d is the depth of the soil layer considered, $[m]$.
- p is the penetration depth, $[m]$.

The concept behind [4.4.1] is that the side friction along the pile will reduce exponentially with increasing penetration depth (friction fatigue) up to a residual value skin friction. Hence, at the pile tip depth the side friction will be undegraded and degraded at shallower parts (away from the tip) of the pile.

As for the residual side friction, when dealing with non-cohesive soils it can be calculated by [4.4.2]:

$$f_{sres} = 0.2 * f_{si} \quad \text{non-cohesive} \qquad 4.4.2$$

Moreover, the initial side friction can be calculated using formula [4.4.3], below.

$$f_{si} = K * \sigma'_{vo} * \tan(\delta) \quad \text{non-cohesive} \qquad 4.4.3$$

where,

- K is the horizontal stress ratio after driving $[-]$.
- σ'_{vo} is the effective overburden pressure $[kN/m^2]$.
- δ is the constant volume friction angle $[degrees]$. Alm & Hamre (1998) model suggests $\delta = \varphi - 5^o$, with φ the soil friction angle.

The authors suggest that the term $K * \sigma'_{vo}$ in [4.4.3] can be directly linked to the cone resistance using equation [4.4.4], in which Pa is the atmospheric pressure.

$$K * \sigma'_{vo} = 0.0132 * q_c * (\sigma'_{vo}/Pa)^{0.13} \quad 4.4.4$$

Specifically, for [4.4.4], the authors mention that this formula was established based on the assumption that the friction (in an open-ended pile) occurs only on the outside wall of the pile. This means that when establishing the sand friction [4.4.3], only the outside shaft friction should be included in the calculations. Otherwise, one could apply both outer and inner shaft friction by reducing both by 50%. In other words, the internal shaft friction is already incorporated in the external formulation, indicated in [4.4.3].

As for the shape factor for degradation of the side friction with increasing penetration, the authors suggest that formula [4.4.5] can be used. By using this formula, a rapid degradation will be observed in case of dense sands.

$$k = (q_c/\sigma'_{vo})^{0.5}/80 \quad 4.4.5$$

Furthermore, formula [4.4.6] is used for the tip resistance for non-cohesive soils applied on the steel annulus. It should be mentioned that [4.4.6] leads in tip resistances increasing with soil density and will be in the range of 0.35 to 0.55 times the CPT cone resistance for loose to very dense non-cohesive soils. It should be mentioned that the Alm & Hamre (2001) SRD model assumes fully coring conditions.

$$q_{tip} = 0.15 * q_c * \left(\frac{qc}{\sigma'_{vo}}\right)^{0.2} \quad 4.4.6$$

Finally, Alm & Hamre (2001) mention that the formulas presented above can be seen as a Best estimate (or Lower Bound), while for the Upper Bound, the authors suggest a factor of 1.25 to be multiplied with the (total) SRD calculated with the aforementioned formulas.

4.5 Unified Method (2020)

The Unified Method is a recent development for estimating the axial capacity of driven piles in sand (Lehane et al (2020)). This method adapts key features of four CPT-based methods, namely ICP, UWA, NGI, and Fugro, which are currently included in both API and ISO guidelines. This method was calibrated using 71 static pile load tests in siliceous sand deposits, with pile diameters range from $300\,mm$ to $800\,mm$. Below, the formulas for estimating shaft and toe capacities are presented.

Field experiments with the Imperial College instrumented piles, reported by Lehane et al (1993), Chow et al (1998) and Lim and Lehane (2014), have confirmed that the local ultimate shaft friction developed on the shaft of a displacement pile obeys Coulomb's law [4.5.1]:

$$\tau f = \sigma'_{rf} * tan\delta_f = \left(\frac{ft}{fc}\right) * (\sigma'_{rc} + \Delta\sigma'_{rd}) * tan\delta_f \qquad 4.5.1$$

where,

- σ'_{rf} is the radial effective stress at peak friction, $[kPa]$.
- δ_f is the ultimate constant volume interface friction angle, $[degrees]$.
- σ'_{rc} is the radial effective stress after installation and equalization, $[kPa]$.
- $\Delta\sigma'_{rd}$ is the increase in radial stresses during loading (dilation), $[kPa]$.
- f_t/f_c is a ratio equal to 1 in case of compression loading and 0.75 in case of tension, $[-]$.

The radial effective stresses after installation and equalization are given by equation [4.5.2], (Lehane et al (2020)), below:

$$\sigma'_{rc} = (q_c/44) * A_{re}^{0.3} * \left[\max\left(1, \frac{h}{D}\right)\right]^{-0.4} \qquad 4.5.2$$

where,

- $A_{re} = 1 - PLR * \left(\frac{D_i}{D}\right)^2$ is the effective area ratio, $[-]$.
- $PLR = L_p/L$ is the plug length divided by embedded length, $[-]$.

- q_c is the local cone tip resistance from CPT, $[kPa]$.
- D_i is the internal pile diameter, $[m]$.
- D is the external pile diameter, $[m]$.
- h is the distance of a soil horizon from the pile tip, $[m]$.

Initially, it can be observed from [4.5.2] that the radial effective stresses are a function of the penetration depth and the external diameter. The dependence of σ'_{rc} on h arises due to:

- ❖ the reduction in stresses with increased distance from the pile tip.
- ❖ the contraction of sand around the shaft area, due the increasing number of shearing cycles with further pile penetration (Figure 3.5-2, Figure 3.5-3).

Moreover, the Unified Method indicates a variation of σ'_{rc} at any soil horizon with the distance from the pile tip normalized by the pile diameter (h/D). According to the authors, with this normalization, geometrical effects are taken into account, while it has been observed (White et al (2004)) that the rate of reduction of radial stresses (of the soil mass surrounding the pile) due to contraction of the pile-soil interface zone, at a given soil horizon h, is greater at higher levels of (normal) radial stiffness $(kn = 4G/D)$, which varies inversely with the pile diameter. Additionally, the authors examined variations of σ'_{rc} with h and h/D and showed that the bias of calculated to measured capacities is removed when h/D is taken into account instead of h, as proposed by Alm & Hamre (2001).

Furthermore, equation [4.5.2] implies variation of σ'_{rc} with the effective area ratio, A_{re}. As the authors mention, Gavin and Lehane (2003) have confirmed that τf varies with the degree of soil displacement during installation and that it is lowest for fully coring piles and largest for closed-ended piles. The average degree of soil displacements can be quantified by the term A_{re}, which is actually the ratio of the volume of soil displaced to the total pile volume. By incorporating the PLR factor, soil displacements from partially plugged piles can be taken into account. Lehane et al (2020), suggest the following formula [4.5.3] for estimation of PLR if there are no measurements, with $D_{CPT} = 35.7\,mm$.

$$PLR = \tanh\left[0.3 * \left(\frac{D_i}{D_{CPT}}\right)^{0.5}\right] \qquad 4.5.3$$

Equation [4.5.1] also incorporates the term $\Delta\sigma'_{rd}$, which is used to estimate the increase of radial effective stresses upon loading. During loading, the thin interface zone between

pile and shaft that contracts with increasing number of cyclic loading, will tend to dilate upon further shearing (e.g., re-orientation of the soil grains). The restrain to dilation by the surrounding soil mass leads to an increase in the radial effective stresses on the pile shaft. Using cavity expansion theory, Lehane et al (1993), assessed this increase [4.5.4], where G is the operational shear modulus of the sand mass, y is the dilation of the sand at the shaft interface, $y/2D$ is the cavity strain and kn is the normal stiffness:

$$\Delta\sigma'_{rd} = 4 * G * \frac{y}{D} = kn * y \qquad 4.5.4$$

As can be observed, $\Delta\sigma'_{rd}$ is inversely proportional to D, and thus for large offshore piles, its contribution to τf becomes insignificant. Lehane et al (2020) proposed the following formula [4.5.5] to calculate $\Delta\sigma'_{rd}$, in which all terms have been previously defined.

$$\Delta\sigma'_{rd} = \left(\frac{q_c}{10}\right) * \left(\frac{q_c}{\sigma'_v}\right)^{-0.33} * \left(\frac{D_{CPT}}{D}\right) \qquad 4.5.5$$

As for the constant volume friction angle, it was shown by Jardine et al (1992) and Shell UK Ltd that it can be estimated through correlation with the mean particle size of the sand, d_{50}. Specifically, it was shown (Figure 4.5-1) that δf reduces with increasing mean effective particle size d_{50} as the relative roughness increases. However, during installation, crushing of sand at the pile tip and extensive shearing reduces the grading of all sands to that of a fine sand, as was shown by Yang et al (2010). Other researchers, as stated by the authors, have confirmed the relatively low sensitivity of δf to d_{50} and adoption of a mean $\delta f = 29^0$ was used for the calibration of the Unified Method.

It is important to mention that the Unified Method models the peak external shaft friction when using [4.5.1]. For that reason, in driveability analysis the shaft resistance is calculated through [4.1.2] without taking explicitly into account the inner shaft friction. The inner shaft friction (plug resistance) is incorporated into the toe resistance formulation that is described below.

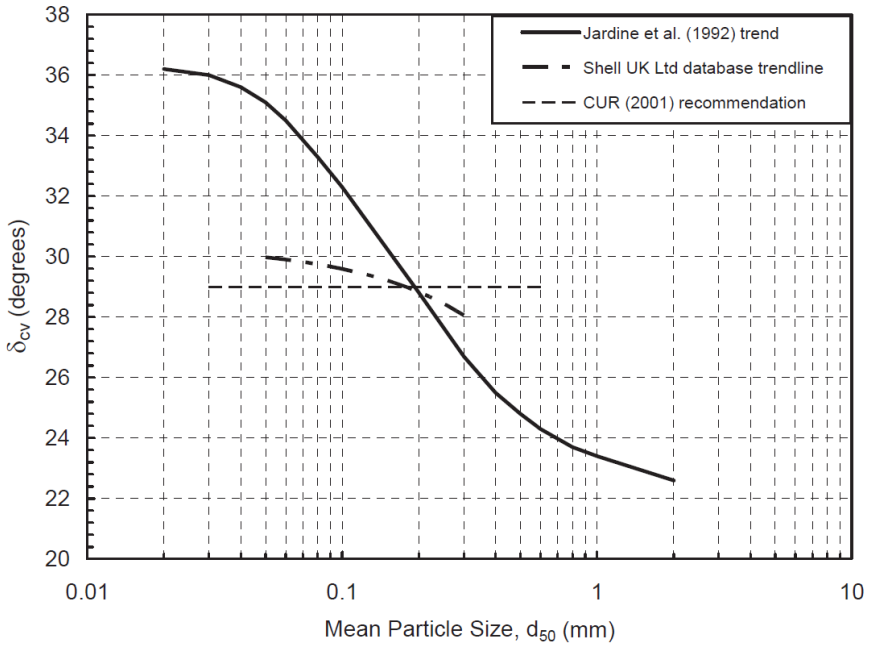

Figure 4.5-1: Interface friction angle in sand. Illustrative trends from direct shear interface tests (Jardine et al (1992) and Shell UK Ltd).

In other words, for both closed or open-ended piles [4.5.1] is applied on the outer shaft area only. In addition, it is important to state that the Unified Method has been calibrated to predict shaft capacity developed approximately 2 weeks after driving.

For both open and closed-ended piles, equation [4.5.6] can be used to determine $q_{b0.1}$, which is the resistance mobilized at the pile base at displacements of the tip $0.1 * D$, (Lehane et al (2020), Figure 4.5-2).

$$q_{b0.1} = [0.12 + 0.38 * A_{re}] * q_p, \ for \frac{L}{D} > 5, \ and \quad q_{b0.1} = A_{re} * q_p, \ for \frac{L}{D} \leq 5 \qquad 4.5.6$$

$A_{re} = 1$ in case of closed-ended piles leading to $q_{b0.1} = 0.5 * q_p$.

The term q_p is an average value of qc in the vicinity of the pile tip and, more specifically, is defined as the end bearing resistance expected for an 'imaginary cone' that has the same diameter as the pile being considered or equivalent diameter for a pipe pile ($D_{eq} = D * A_{re}^{0.5}$). In relatively homogeneous sands, q_p can be taken as the average q_c value in a zone $\pm 1.5D$, above and below the pile tip. In more variable strata, designers can assume q_p =

$1.2q_{c,Dutch}$ (Schmertmann 1978) or adopt the technique proposed by Boulanger and DeJong (2018).

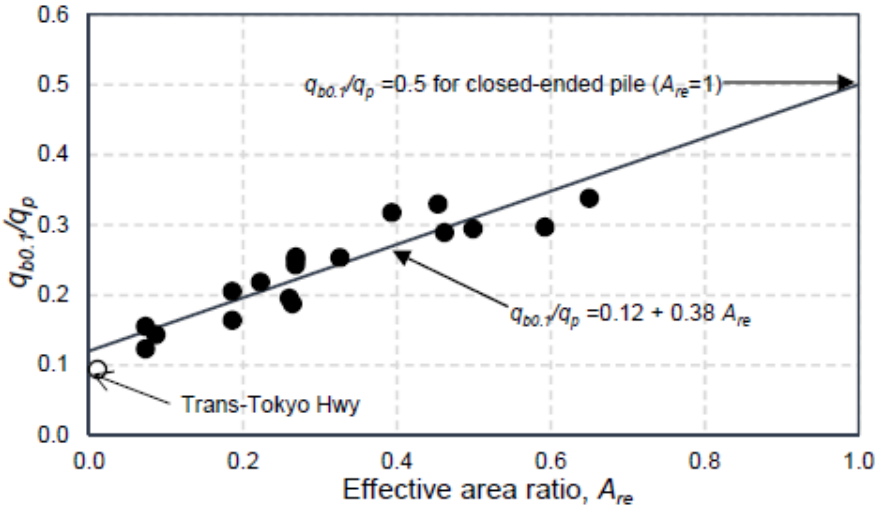

Figure 4.5-2: $q_{b0.1}/q_p$ as function of the effective area ratio (Lehane et al (2020)).

It should be clarified that the Unified Method applies formula [4.5.6] at the entire base area of the pile, for both open and closed-ended piles, as it assumes an equivalent closed-ended pile including the inner plug resistance.

5. Reliability of SRD Models

This Chapter examines the SRD estimations of the traditional SRD models. Specifically, these are the Toolan & Fox (1977), Stevens et al (1982), and the Alm & Hamre (2001) models. The performance of these models is examined through comparisons of measured and predicted blow count profiles. This comparison is most commonly used in driveability studies, because measuring the blow counts is much easier, and requires no costs in contrast with signal matching, which on the other hand offers greater information on, for example, the energy transferred to the pile and the soil resistances. The performance of these models will be investigated by utilizing the installation records from the Amaliahaven project, specifically, from the two sites, APM and RWG. In addition, the Unified Method is also used, in its 'raw' format, to predict the SRD of the combi-wall piles of the APM terminal.

5.1 CPTs Selection for Driveability Study

As mentioned in Chapter 2, CPTs were performed prior to installation of the steel open-ended tubular piles, when the ground level was at around $+6\,m$ from NAP. The ground level was then excavated till around $-2\,m$ from NAP (working level), while the groundwater table was kept at $-2.5\,m$ from NAP.

Initially, the soil variability is investigated, by comparing CPTs that were performed in the vicinity of the piles examined in this Thesis. In this way, it is examined, whether averaging of the qc values of the CPTs around the piles is needed to account for soil variability. For each and every pile of the Amaliahaven project, the nearest CPTs around the piles examined, are depicted in Figure 5.1-1.

It can be observed from Figure 5.1-1 that there aren't significant changes in the soil conditions, for both the APM and RWG sites, even when comparing CPTs that were performed at a distance of $30\,m$ from the pile, with CPTs performed $0.5\,m$ from the pile (e.g., Pile BP-02, or Pile BP-64). Therefore, since the soil variation is insignificant, it was decided to use only the CPTs (Figure 5.1-1) nearest to the piles examined and not average them. Moreover, by examining the blow counts required to drive the steel open-ended piles from various locations at both sites, it was observed (for the cases in which the driving from the hammer energy was almost the same) that more or less, the same number of blows/0.25 m was required to drive the piles.

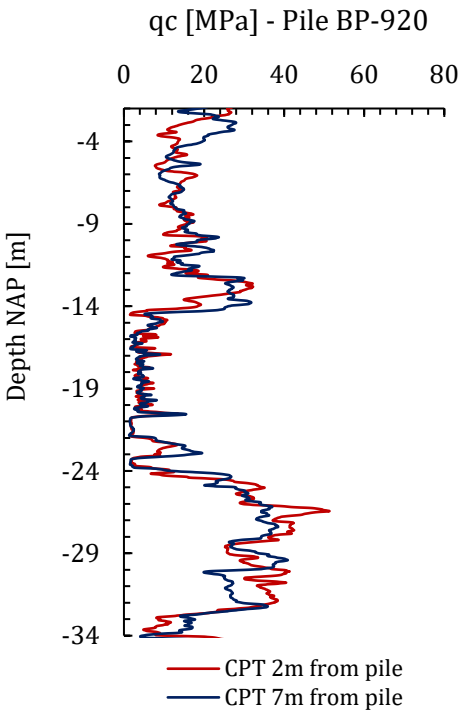
qc [MPa] - Pile BP-920
0
20
40
60
80
-4
-9
-14
-19
-24
-29
-34
Depth NAP [m]
CPT 2m from pile
CPT 7m from pile

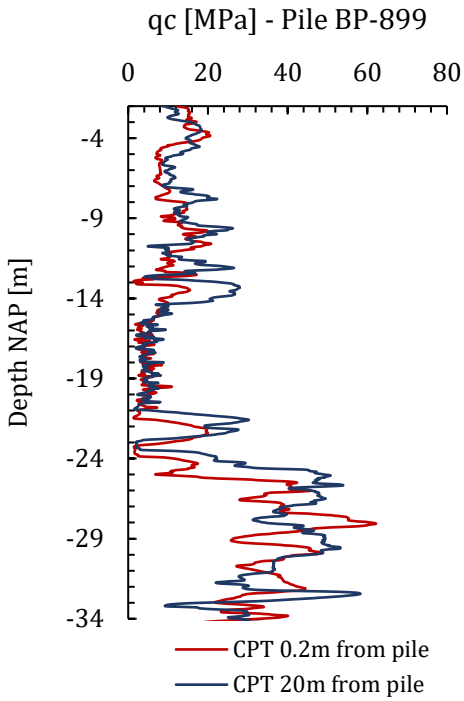
qc [MPa] - Pile BP-899
0
20
40
60
80
-4
-9
-14
-19
-24
-29
-34
Depth NAP [m]
CPT 0.2m from pile
CPT 20m from pile

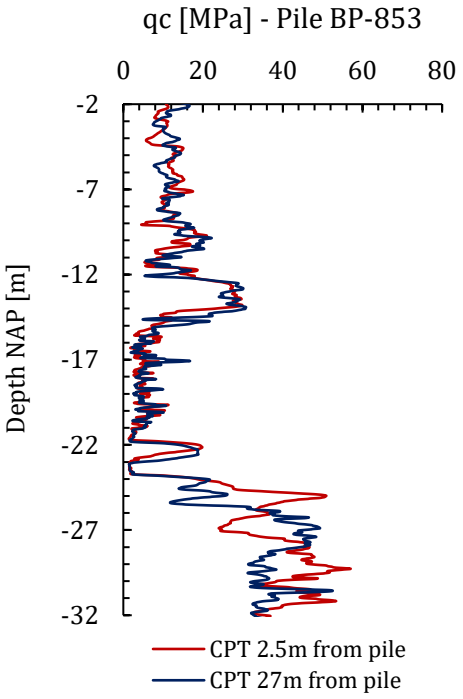
qc [MPa] - Pile BP-853
0
20
40
60
80
-2
-7
-12
-17
-22
-27
-32
Depth NAP [m]
CPT 2.5m from pile
CPT 27m from pile

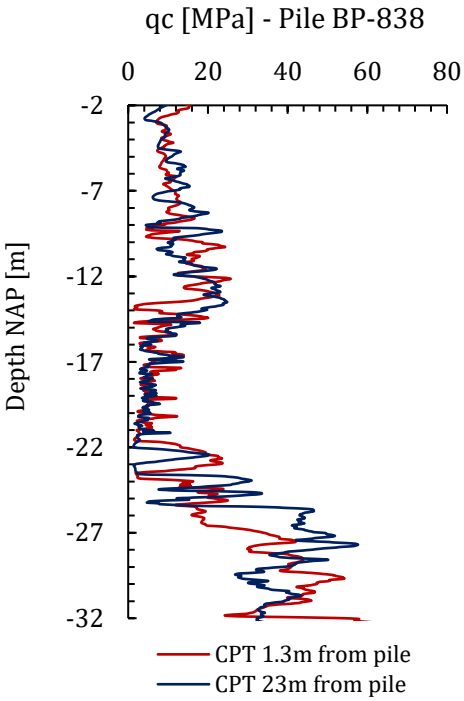
qc [MPa] - Pile BP-838
0
20
40
60
80
-2
-7
-12
-17
-22
-27
-32
Depth NAP [m]
CPT 1.3m from pile
CPT 23m from pile

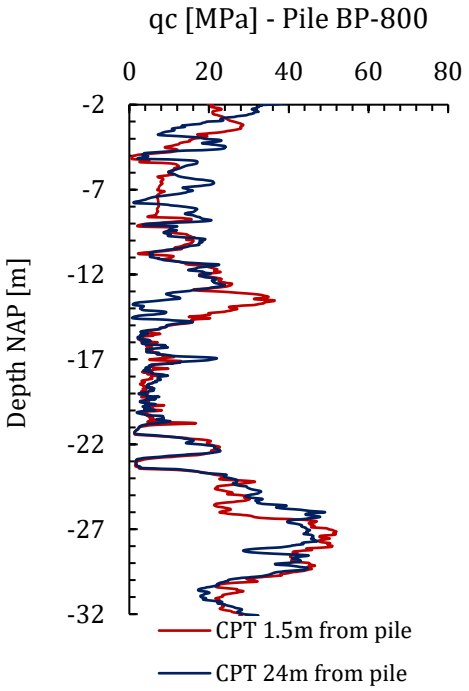
qc [MPa] - Pile BP-800
0
20
40
60
80
-2
-7
-12
-17
-22
-27
-32
Depth NAP [m]
CPT 1.5m from pile
CPT 24m from pile

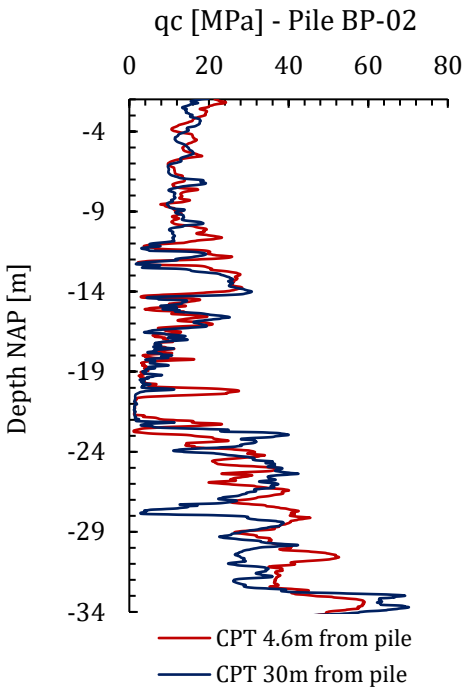
qc [MPa] - Pile BP-02
0
20
40
60
80
-4
-9
-14
-19
-24
-29
-34
Depth NAP [m]
CPT 4.6m from pile
CPT 30m from pile

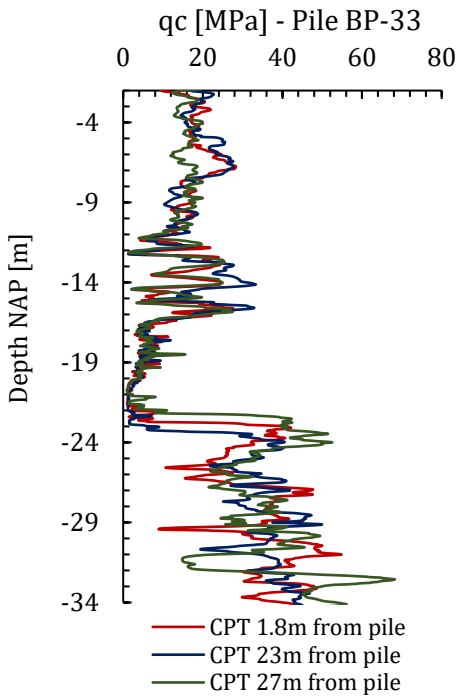
qc [MPa] - Pile BP-33
0
20
40
60
80
-4
-9
-14
-19
-24
-29
-34
Depth NAP [m]
CPT 1.8m from pile
CPT 23m from pile
CPT 27m from pile

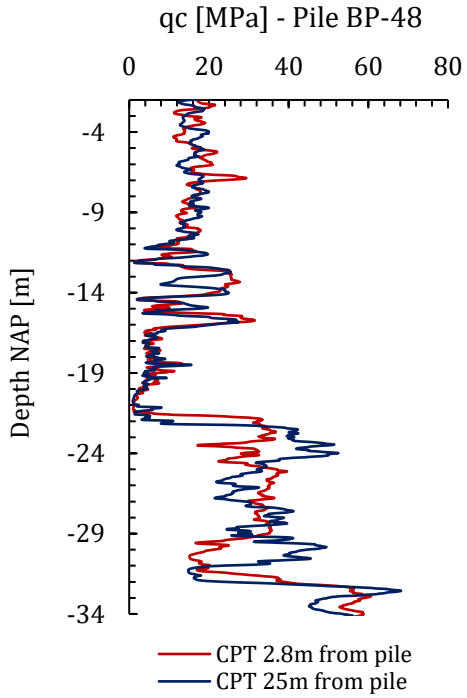
qc [MPa] - Pile BP-48
0
20
40
60
80
-4
-9
-14
-19
-24
-29
-34
Depth NAP [m]
CPT 2.8m from pile
CPT 25m from pile

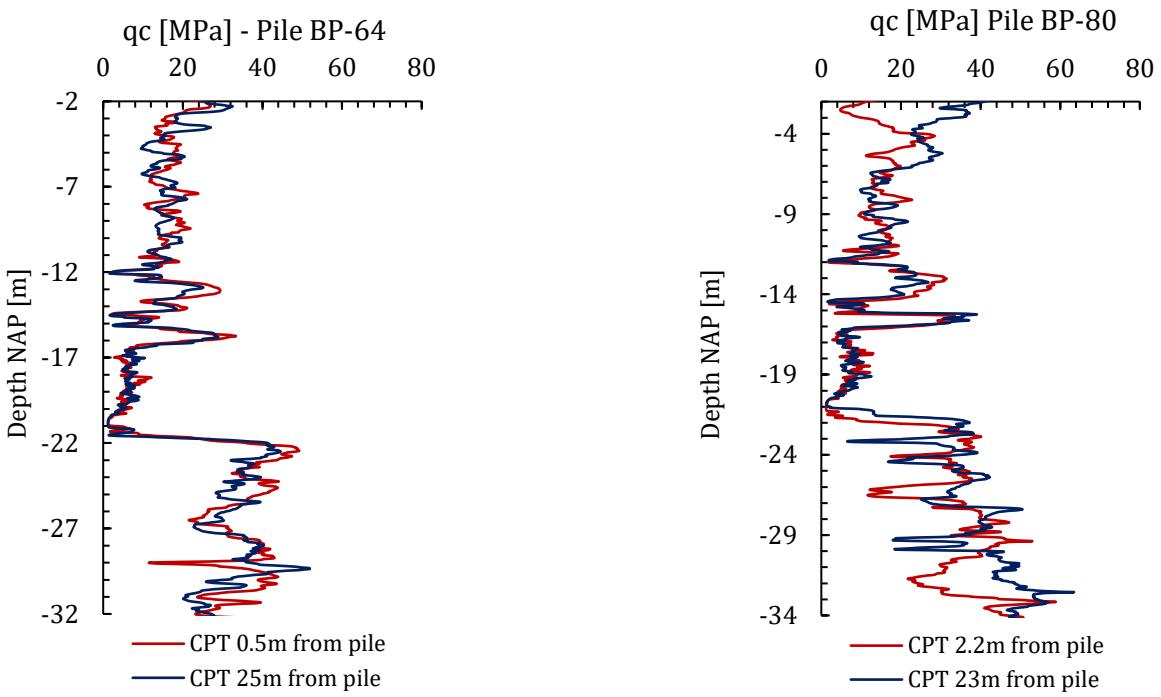

Figure 5.1-1: Comparison of CPTs nearest to the piles examined in this Thesis, from both the APM and RWG sites.

Secondly, before creating the hammer-pile-soil model in AllWave PDP, it was examined whether a reduction to the initial CPTs, the CPTs prior to excavation, should be employed in order to take into account the overburden pressure reduction. For that reason, a comparison is made first with CPTs that were performed after the excavation and installation of piles. However, it should be mentioned, there are only a few available, and in most cases have been performed in greater distance from the piles, compared to the initial CPTs prior to excavation. A comparison of CPTs prior to and after the excavation is presented in Figure 5.1-2.

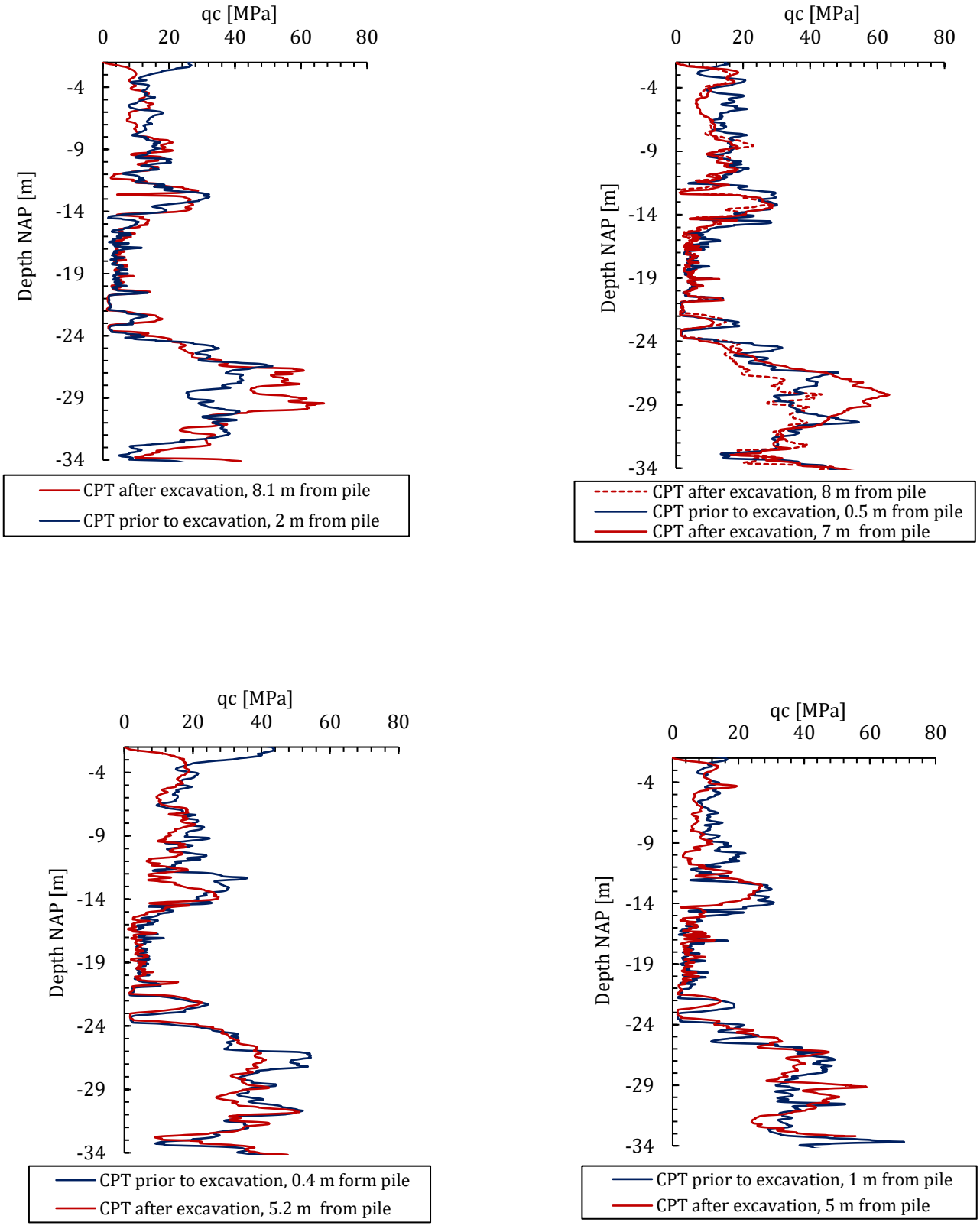

Figure 5.1-2: Comparison of CPTs prior to and after excavation for four different piles at four different locations (APM site, Amaliahaven project).

By comparing CPTs prior to and after the excavation and installation of the combi-wall piles, in four different locations for four different piles, it can be observed that the qc value in some cases might be higher after the excavation and installation of piles, but not significantly reduced. Both CPTs prior to and after excavation are very similar in shape and magnitude, so a reduction to the qc value to take into account the reduction of the overburden pressure due to excavation might be too unconservative.

It should be highlighted that the difference between a driveability study and pile design is that in the latter case, it is desirable to be (slightly) on the conservative side in order to avoid overestimating pile capacities. However, in driveability studies the aim is to define the maximum soil resistance, so that suitable hammering equipment can be selected. For that reason, an example in Figure 5.1-3 is presented, in which equation [5.1.1] (also incorporated into the software) has been utilized to reduce the cone resistance, qc of the CPT.

$$q_{c,after\ excavation} = \sigma'_v/\sigma'_{v0} * q_{c,prior\ to\ excavation} \qquad 5.1.1$$

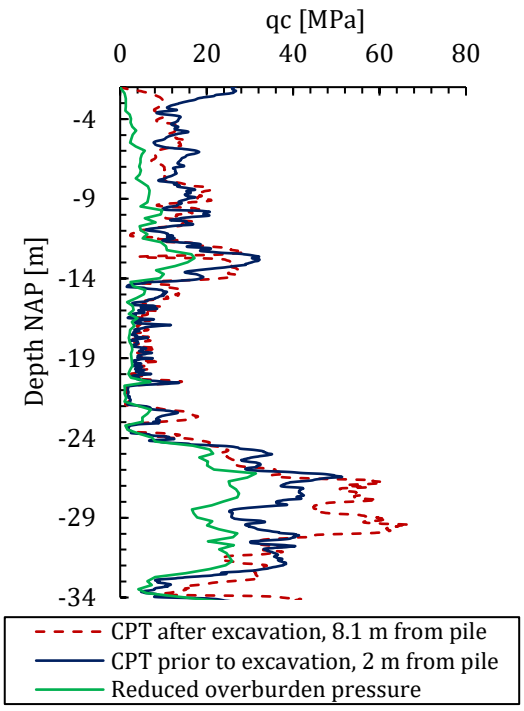

Figure 5.1-3: CPTs prior to, after excavation and modified CPT to account for overburden pressure reduction (APM site, Amaliahaven project).

It can be observed from Figure 5.1-3 that indeed equation [5.1.1] is unconservative for a driveability analysis, as the qc value, specifically around $-24\,m$ from NAP till $-34\,m$ NAP, is on average about 52% of the qc value after the excavation, and 67% of the qc value prior to excavation and installation. Two more piles and their corresponding CPTs prior to and after excavation were examined as in Figure 5.1-2, and the same trend was observed (both CPTs are very similar in shape and magnitude).

Based on the aforementioned observations, CPTs before the excavation (those nearest to the piles that have been installed) are chosen for the driveability analysis that follows, without reducing the qc value to account for overburden pressure reduction. The reasons for selecting the CPTs prior to excavation and installation are summarized below:

- There is a great number of available CPTs prior to excavation and installation of the combi-wall piles that were performed very close to the piles. From Figure 5.1-1 it can be observed that there isn't a significant soil variation in both sites, and for that reason, no averaging between the CPTs is performed.

- Being performed very close to the piles, uncertainty of soil variability is minimized.

- There are only a few CPTs after excavation and installation of the combi-wall piles available, and not as closely performed as the CPTs prior to installation.

- CPTs performed prior to and after excavation are very similar, both in shape and magnitude (Figure 5.1-2).

- Reduction of the qc value to account for reduced overburden pressure is not applied to the CPTs prior to excavation. It has been shown that equation [5.1.1], which is also incorporated into the AllWave PDP software (optional), is unconservative for driveability analysis, in which the aim is defining maximum resistances for suitable hammering equipment selection.

5.2 Performance of Traditional SRD models

This section evaluates the performance of the traditional SRD models, Toolan & Fox (1977), Stevens et al (1982), and the Alm & Hamre (2001) using the Amaliahaven installation data for the two sites APM and RWG. It should be mentioned that although these three models are included to every commercially available driveability software, the Alm & Hamre (2001) model is most frequently used in practice.

Initially the hammer-pile-soil model as created in AllWave PDP is presented in Figure 5.2-1.

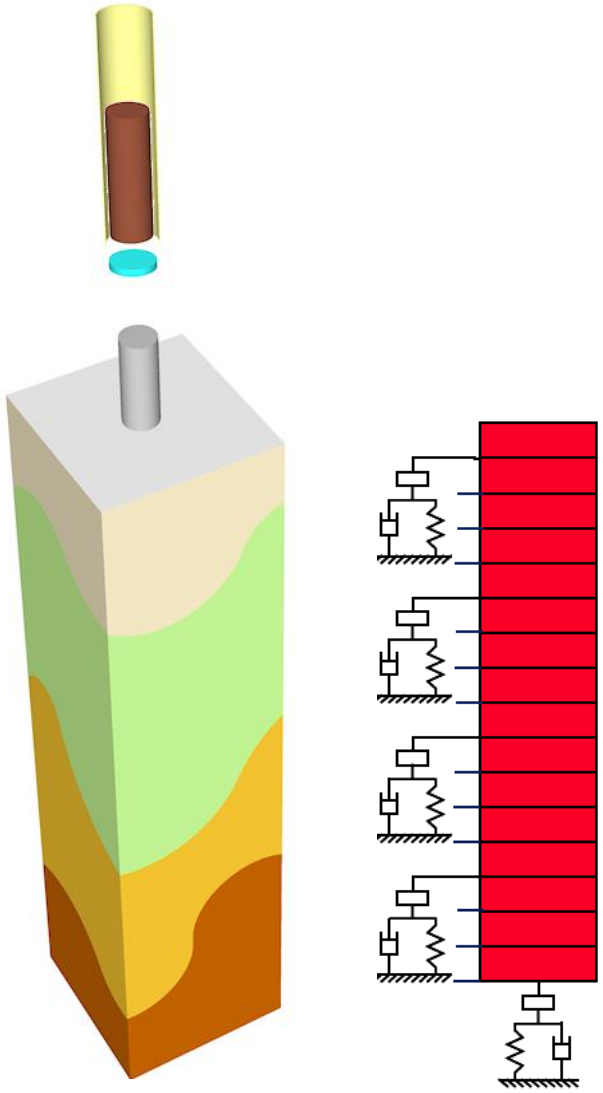

Figure 5.2-1: Hammer – Pile – Soil model used for driveability analysis (AllWave PDP).

Pile and hammer properties have already been presented in detail in Chapter 2. It should be mentioned that commercially available driveability software, such as AllWave PDP that is used in this Thesis, or GRLWEAP, have an integrated database of a variety of hammer models (hydraulic, diesel and more) that are used in practice, and so the user, who can always modify the hammer properties, is mainly asked to choose the right components of the hammer (e.g., anvil, cushion, etc.).

The main components used to model the hydraulic hammers IHC S-200 and IHC SC-200 are the ram and the anvil. For open-ended steel tubular piles, cushion to protect the piles from damage is usually not required (steel to steel), which also increases the hammer's efficiency as the energy transferred from the anvil to the pile is not being further reduced besides the typical loses coming, e.g. from heat, noise, friction, etc. Both ram's and anvil's properties, e.g. weight, length, etc., (for both hammers) are already integrated in the hammer database of the software.

The piles are modeled using the properties indicated in Table 2.2-1.

The properties of the asymmetric elasto-plastic springs (Figure 5.2-2) used to model the pile soil interface are summarized in the following Tables (Table 5.2-1, Table 5.2-2, Table 5.2-3).

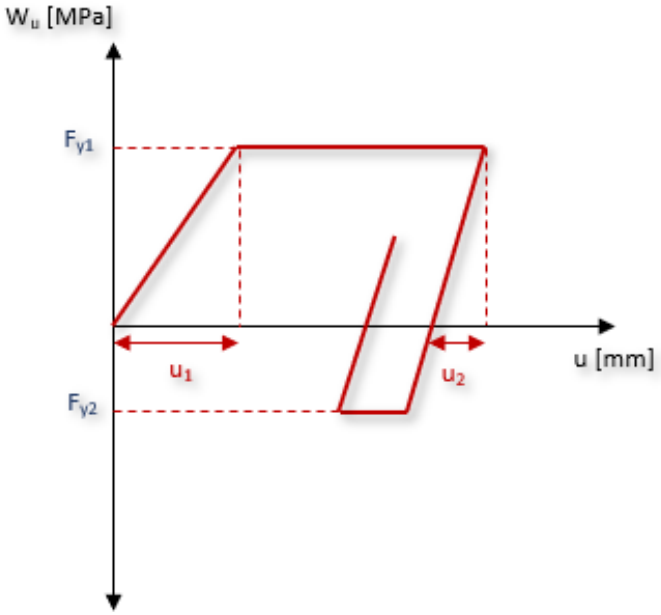

Figure 5.2-2: Asymmetric elasto plastic spring used to model the pile-soil interface (shaft & toe models).

Table 5.2-1: Alm & Hamre (2001) soil spring parameters.

	F_{y1} [MPa]	F_{y2} [MPa]	u_1 [mm]	u_2 [mm]	Smith Damping factor [s/m]
Toe model	$q_{tip} = 0.15 * q_c * \left(\frac{qc}{\sigma'_{vo}}\right)^{0.2}$	0.1*F_{y1}	2.5	2	0.5
Shaft model	$f_{sres} + (f_{si} - f_{sres}) * e^{k(d-p)}$	F_{y1}	2.5	2	0.25
Fatigue factor	f_s/f_{si}	-	-	-	-

Table 5.2-2: Toolan & Fox (1977) soil spring parameters.

	F_{y1} [MPa]	F_{y2} [MPa]	u_1 [mm]	u_2 [mm]	Smith Damping factor [s/m]
Toe model	$qc\ (averaged +/-1.5D)$	0.1*F_{y1}	2.5	2	0.5
Shaft model	$qc/300$	F_{y1}	2.5	2	0.17
Fatigue factor	-	-	-	-	-

Table 5.2-3: Stevens et al (1982) soil spring parameters.

	F_{y1} [MPa]	F_{y2} [MPa]	u_1 [mm]	u_2 [mm]	Smith Damping factor [s/m]
Toe model	$Nq * \sigma'_{vo}$	0.1*F_{y1}	2.5	2	0.5
Shaft model	$K * \sigma'_{vo} * tan\delta$	F_{y1}	2.5	2	0.27
Fatigue factor	-	-	-	-	-

Typical values for the quake have been chosen for the shaft and toe spring models. These values are also the ones suggested by the authors of these models (Toolan & Fox (1977), Stevens et al (1982), and Alm & Hamre (2001)). It should be clarified though, that the value of u_2 is taken deliberately slightly smaller than u_1 to indicate the stiffer response of the soil during unloading. Moreover, Allnamics suggests that the yield stress during tension for the toe model is typically 10% the yield stress during compression, while for the shaft model it remains the same. As for the Smith (1960) damping factor, values suggested by the authors of the models are used, and for the Toolan & Fox (1977) model values suggested by Hirsch et al (1976), and also reported by Byrne et al (2012) and (2018) have been utilized.

Before presenting the driveability post-predictions, it is important to state that the main variables of the hammer-pile-soil system, are the hammer, pile and soil properties. Modeling of the hammer and pile is fairly accurate, however in order to constraint the unknowns only to the soil model, it is crucial to define the transferred to the pile energy during installation. Sometimes, energy records are not available (especially if the pile has not been driven yet), and thus, the energy is usually assumed constant for the entire installation. In such cases, it is important to perform driveability analysis for different energy levels in order to define at least a Lower and Upper Bounds of the blow counts to be expected. In case of the Amaliahaven project, impact energy (energy just before the ram impacts the anvil) has been recorded from the two hydraulic hammers, which means that the actual transmitted energy to the pile will be estimated by the software using equation [3.1.5]. In such cases, it is also important to have measurements of the transferred energy to the pile, using for example PDA, in order to compare it with the one estimated by the software. However, transferred energy measurements weren't obtained for the purposes of this Thesis. Therefore, the post-predictions contain already some degree of uncertainty that can be considered as one of its limitations.

The pile driveability post-predictions for 10 piles of the Amaliahaven project, for two sites, namely APM and RWG, are presented in Figure 5.2-4, Figure 5.2-5, Figure 5.2-6, Figure 5.2-7, Figure B 1, Figure B 2, Figure B 3, Figure B 4, Figure B 5, and Figure B 6. Four piles, two from each site are presented here, while the results of the remaining 6 are included in APPENDIX B. Shaft and toe resistances presented in these figures, are the ones mobilized during driving. Figure 5.2-3 below, is a picture taken at the end (almost) of installation of one of the combi-wall piles at RWG site. A frame has also been used to avoid misalignment. Additionally, on the left part of Figure 5.2-3, a combi-wall pile that was installed partially with vibratory driving is presented.

Figure 5.2-3: Installation of steel open-ended combi-wall pile with the IHC-S 200 hydraulic hammer (photo personally taken).

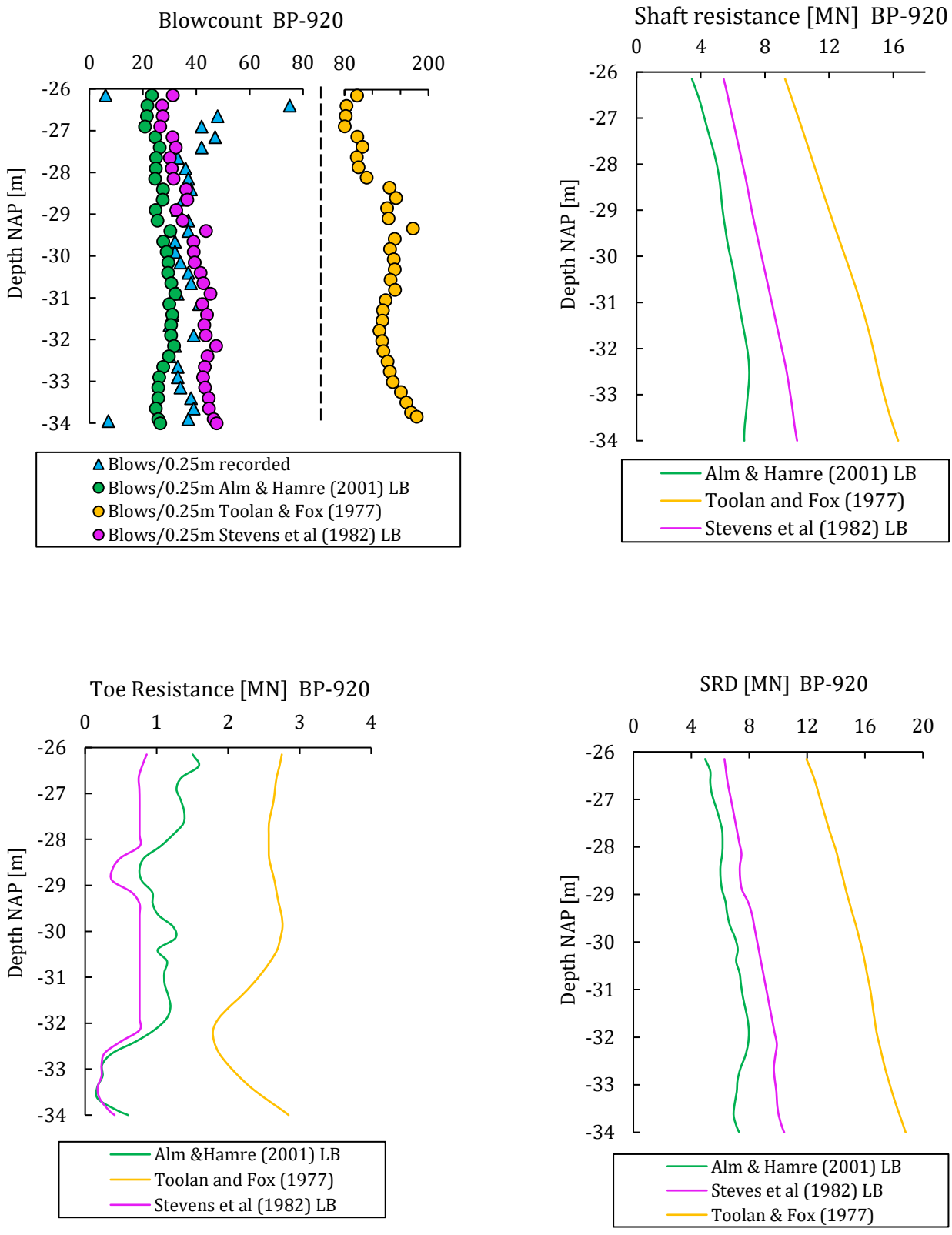

Figure 5.2-4: Driveability post-prediction for combi-wall pile BP-920, using Alm & Hamre (2001), Toolan & Fox (1977), and Stevens et al (1982) SRD models. APM terminal.

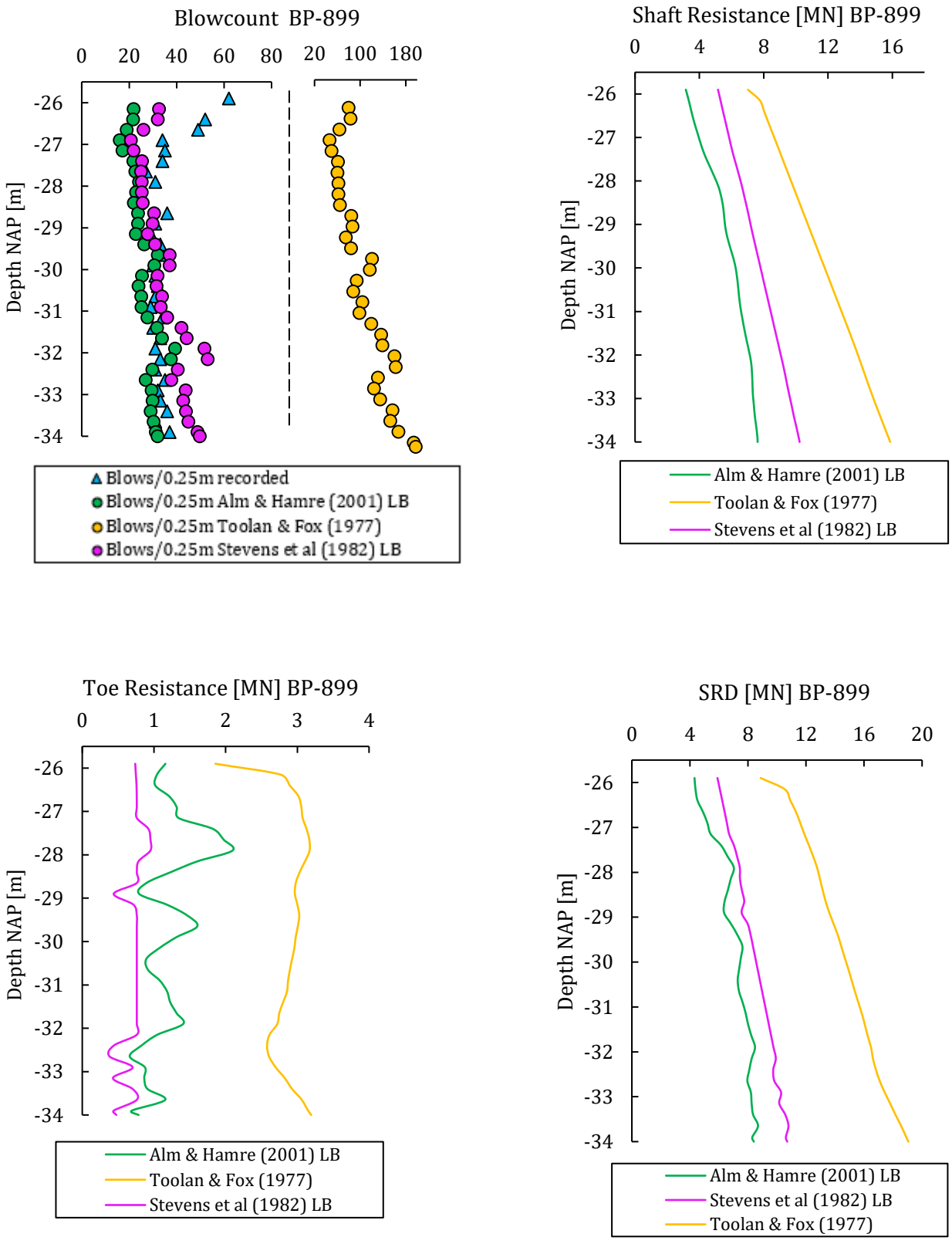

Figure 5.2-5: Driveability post-prediction for combi-wall pile BP-899, using Alm & Hamre (2001), Toolan & Fox (1977), and Stevens et al (1982) SRD models. APM terminal.

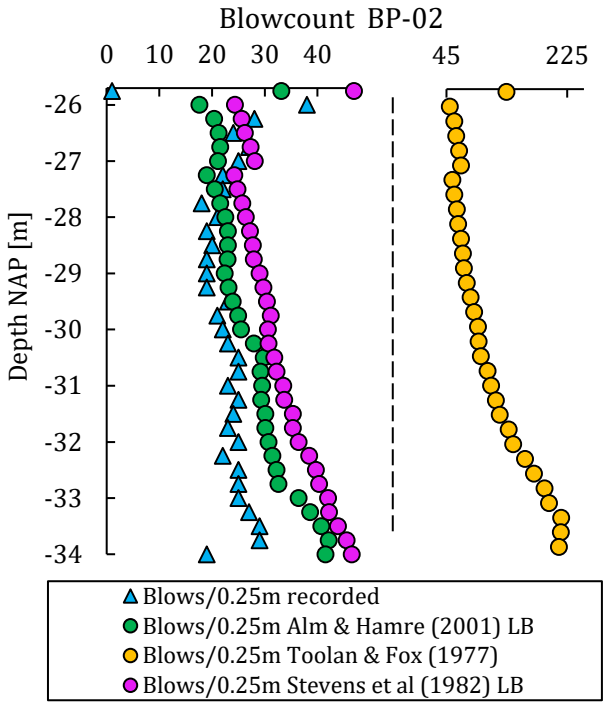

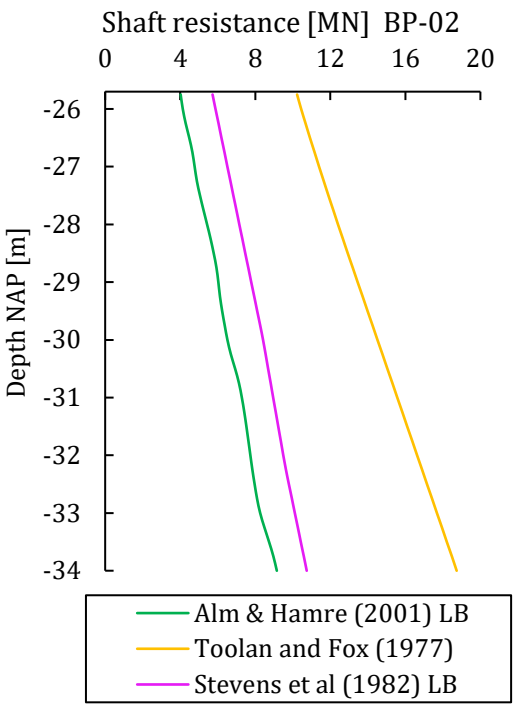

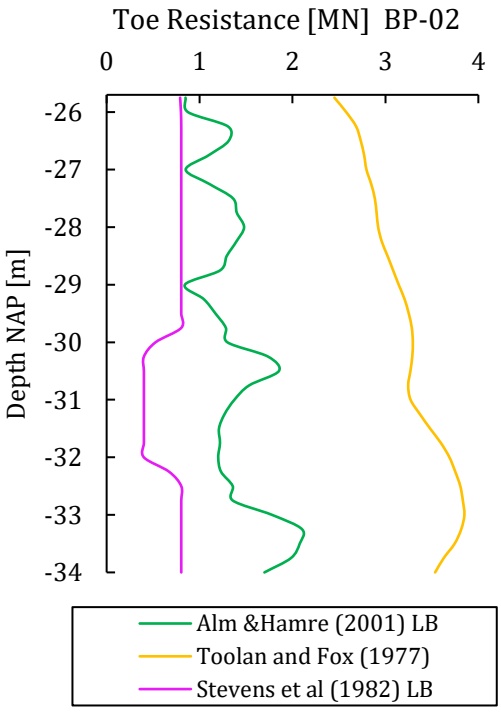

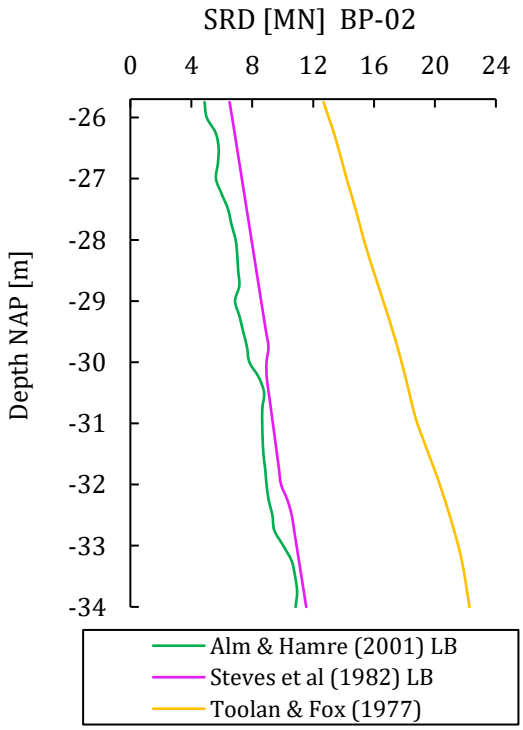

Figure 5.2-6: Driveability post-prediction for combi-wall pile BP-02, using Alm & Hamre (2001), Toolan & Fox (1977), and Stevens et al (1982) SRD models. RWG terminal.

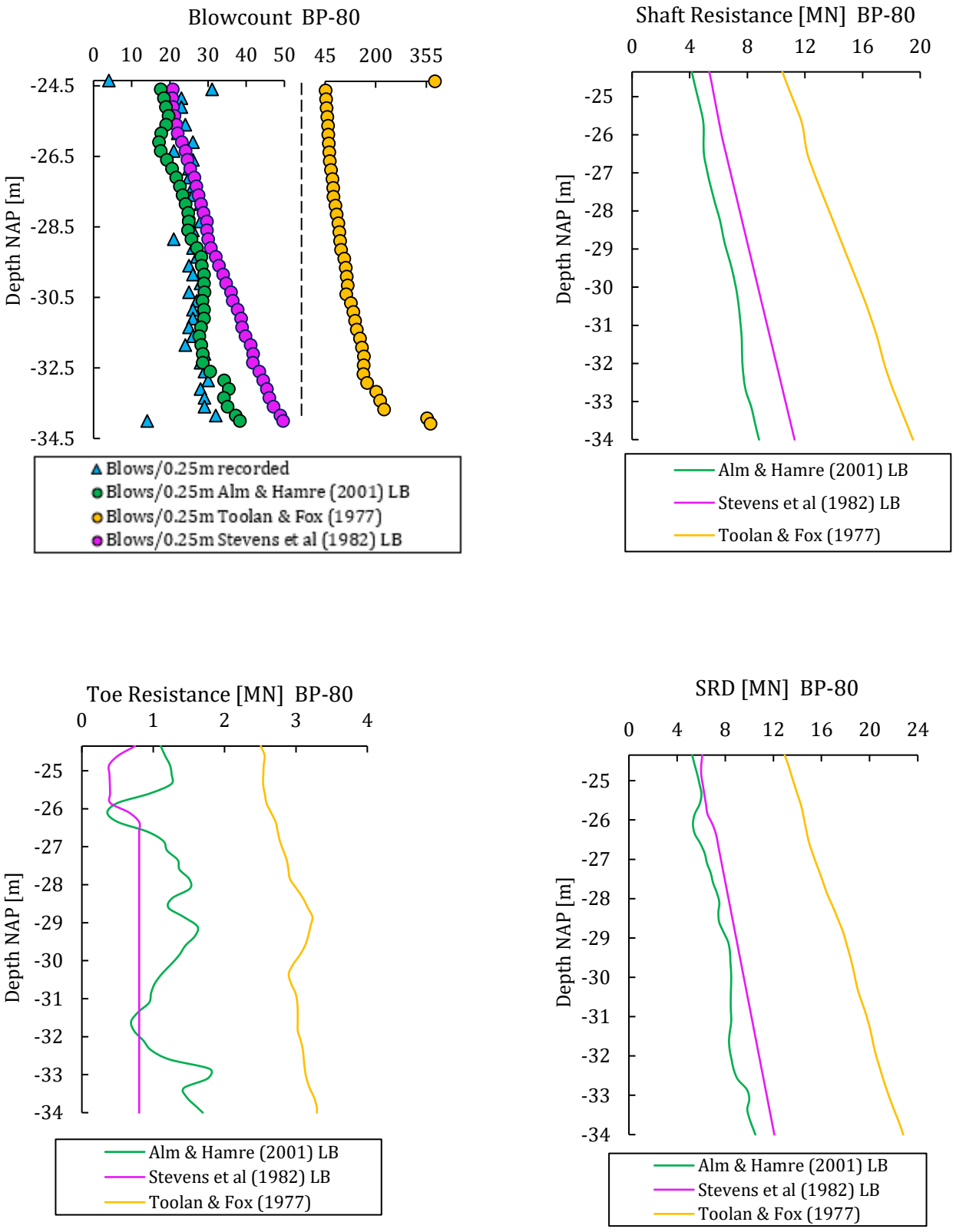

Figure 5.2-7: Driveability post-prediction for combi-wall pile BP-80, using Alm & Hamre (2001), Toolan & Fox (1977), and Stevens et al (1982) SRD models. RWG terminal.

APPENDIX B contains the rest of the driveability post-predictions for the Amaliahaven project, specifically for the sites APM and RWG. It continues from the current Chapter and presents the results of the remaining 6 steel open-ended piles of the two sites. The results for all the post-predictions are commented in this Chapter.

First, it is important to notice that both in the graphs presented here, and in APPENDIX B regarding the post-predictions of the traditional SRD models, the results of the Toolan & Fox (1977) model are presented separately in a different horizontal (blows/0.25 m) scale. That is because this model highly overpredicts the blow counts required to drive the pile, while in some cases it predicts refusal, e.g., blows/0.25 m approximately 500, whereas it should be stated that some projects set the refusal to 100 or 120 blows/0.25 m, since the driving time increases, as well as due to the risk of damaging the piles. In this research it was deliberately set to 500, in order to inspect the extent of the overprediction. Figure 5.2-8 below, depicts an example of the overpredicted blow counts for pile BP-48 of the RWG site, for which the shaft and toe resistances mobilized during driving are presented in Figure B 5.

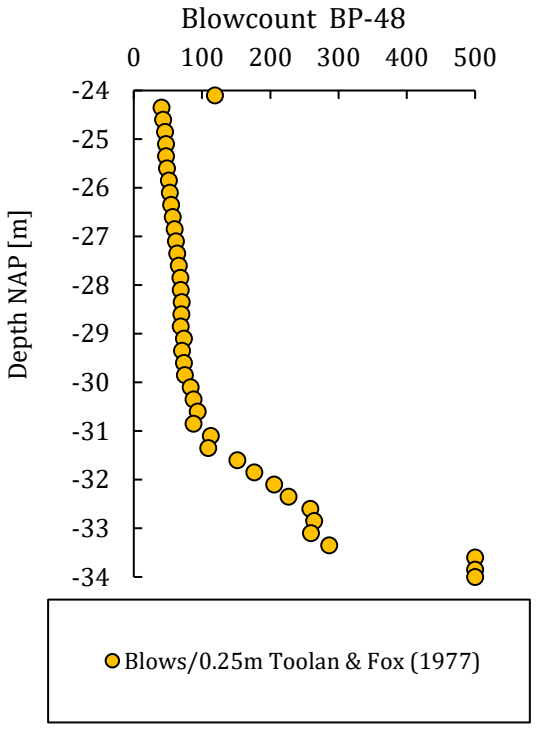

Figure 5.2-8: Driveability post-prediction for combi-wall pile BP-48, using Toolan & Fox (1977) SRD model. RWG terminal.

Toolan & Fox (1977) Evaluation

General Observations

Figure 5.2-8 shows clearly an overestimation of the static resistance during driving by this model. The blow count profiles produced when modelling the hammer-pile-soil system, specifically for pile BP-899, are on average 5 times larger than the recorded blow counts. This overestimation can be observed in all of the examined piles. The most important reasons for using Toolan & Fox (1977) SRD model are listed below:

- The SRD model is easy to use.
- Shaft friction and toe resistances are straightforward functions of the qc value of the CPT.

Unit shaft friction

The shaft friction mobilized during pile driving is estimated by dividing the qc value by a constant factor [4.2.1]. In other words, this model suggests to simply use the qc value of the CPT and divide it with 300. However, this factor is probably project specific, and keeping it constant might not be ideal for various soil conditions, e.g., silty sand, medium sand, dense sand etc. Moreover, this model does not take into account that the shaft friction does not remain constant during the pile installation process. On the contrary, it has been observed (Chapter 3.5) that the radial effective stresses and shear stresses that develop in any given soil horizon tend to reduce as the distance from the pile tip to that horizon increases (friction fatigue). This means that the shaft friction applied, for example at a level $-5\,m$ from the ground surface, will tend to reduce as the tip of the pile moves from $-6\,m$ to $-7\,m$. Therefore, shaft friction (at each pile-soil interface level) does not remain constant during installation. Reasons on why friction fatigue occurs have been mentioned in Chapter 3.5.

In addition, this method also suggests a limit of $120\,kPa$ for the unit shaft friction in sands, but this might also be an unconservative approach for a driveability study, in which the goal is to establish maximum resistances.

Furthermore, Gavin and Lehane (2003) have confirmed that τf varies with the degree of soil displacement during installation and that it is lowest for fully coring piles and largest for closed-ended piles (Chapter 4.5). However, partially plugging conditions (usually for $D < 0.76\,m$) are not taken into account in [4.2.1]. Therefore, the formula suggested by

Toolan & Fox (1977) will probably not be suitable for smaller diameter piles that (partially) plug during driving.

When inspecting the results of the post-predictions (for both APM and RWG sites), the component that leads to a high overestimation is the shaft resistance, as it has greater contribution than the toe resistance. By comparing the shaft and toe resistances of the traditional SRD models, it can be observed that the toe resistance, although being higher than the other two methods, is in a reasonable range, while shaft friction is also almost twice than the other two methods. Probably, this occurs due to incorporation of the outer and inner shaft friction in the calculations.

In Figure 5.2-9 an example is presented for pile BP-80 of the RWG site (see also Figure 5.2-7), which shows the influence of shaft friction in the results, and specifically what would be the outcome of the post-prediction if [4.2.1] is assumed to be the total friction applied on the pile, meaning that [5.2.1]:

$$qc/300 = Fr_{inner\ shaft\ area} + Fr_{outer\ shaft\ area} < 120\ kPa \qquad 5.2.1$$

Interestingly, when applying [5.2.1] as the total shaft resistance including both internal and external friction, the predicted blow counts are very similar to those calculated by Stevens et al (1982) SRD model for the Lower Bound case. It can be seen in Figure 5.2-9 that the shaft friction produced lies in between the one produced by Stevens et al (1982) SRD model and Alm & Hamre (2001) SRD model. Since this is not how the authors mention to use their model, the aforementioned formula [5.2.1], does not consist a suggestion on how shaft friction should be modeled when using this SRD model, but it is just a modification that was used for comparison with the other models. Additionally, it is not in the scope of this Thesis to adjust or modify the already existing (traditional) SRD models.

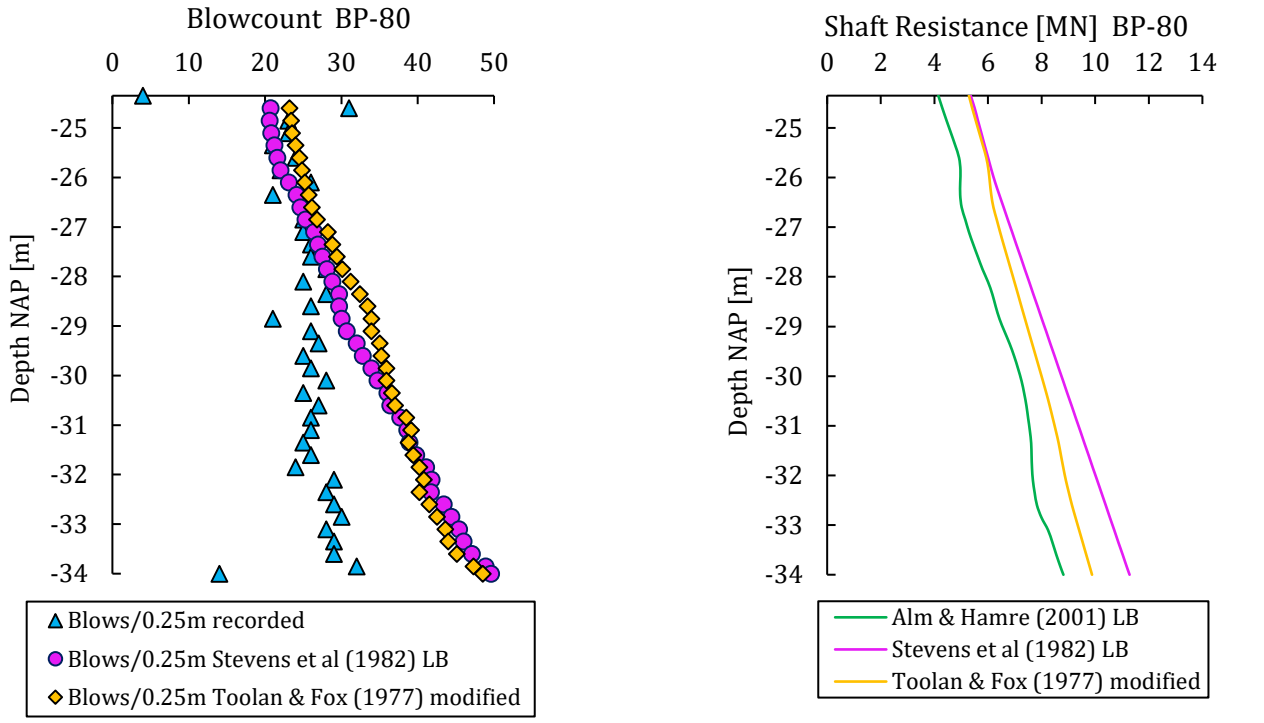

Figure 5.2-9: Modification applied to Toolan & Fox SRD model. Shaft friction is calculated by [5.2.1].

Toe Resistance

The toe resistance is calculated as a weighted average of the qc value over a number of pile diameters above and below the pile tip and is applied on the steel annulus. The results presented earlier have been produced by utilizing an average qc value of $+/-1.5D$ (above/below) from the pile tip. This average technique (often used in design) might not be appropriate for every driveability study as it might lead to an underestimation of the toe resistance. However, by examining the CPTs it was observed that the qc value doesn't vary a lot from -24 to $-34\,m$ from NAP. Moreover, Alm & Hamre (2001), and Schneider et al (2010), suggested using $30-50\%$ of the qc value (applied on the steel annulus). Despite the aforementioned observations, applying the qc value on the steel annulus to estimate the toe resistance during driving is a reasonable approach.

The issue with this toe model is that it can only be used in fully coring conditions. Moreover, Toolan & Fox (1977) model suggests that for plugging conditions the entire base area should be used in calculations. However, applying the qc value on the pile base gross area might lead to an overestimation of the blow counts. Additionally, as in the case

of the shaft model, this method doesn't take into account the resistance mobilized at the toe in partially plugged pile conditions.

Overall

- Overestimation of the blow counts is mainly produced due to overestimation of the shaft friction (shaft friction has greater contribution to the total SRD than toe resistance for all models).
- Shaft model doesn't take into account friction fatigue, and also the degree of soil displacements induced during driving (which affects the unit shaft friction).
- A reasonable approach is used to estimate the toe resistance during driving, although there are suggestions for using lower resistance values.
- Toe model can only be used for fully coring piles.
- Toe model doesn't consider partially plugging conditions, implying that it might lead to underestimation of the toe resistance of a smaller diameter partially plugged pile.

Stevens et al (1982) Evaluation

General Observations

In general, the post-predictions made for the APM and RWG sites, by utilizing the Stevens et al (1982) SRD model are satisfying. It should be mentioned that for the predictions the Lower Bound suggested by the authors has been used. The advantages of this SRD model are summarized below:

- As in the case of Toolan & Fox (1977) SRD model, Stevens et al (1982) method is easy to use.
- Both shaft and toe models are calculated by utilizing the effective overburden pressure [4.3.1], [4.3.2], which implies that knowledge of the qc value from the CPT is not required, assuming that the rest of the parameters, like relative density, interface friction angle, etc. are known.

Unit shaft friction

The unit shaft friction is calculated with equation [4.3.1]. As can be observed, this model uses the pre-installation vertical effective stresses in order to estimate the shaft friction during driving. However, as mentioned in Chapter 3.2, during installation, the stresses on a soil element are not constant, due to for example displacements or grain crushing. The same applies for the lateral earth pressure coefficient, which is also assumed constant and equal to 0.7 for the entire driving process. Moreover, this method doesn't take into account friction fatigue or the degree of soil displacements during driving, as stated earlier for Toolan & Fox (1977) SRD model.

From the post-predictions, it can be observed that Stevens et al (1982) SRD model, when using the Lower Bound, it tends to slightly overestimate the blow counts especially for the last meters of installation (see for example Figure 5.2-7). However, this overestimation doesn't lead in an unreasonable range of blow counts.

Also, it can be noticed that the overestimation is produced again, (as in the case of Toolan & Fox (1977) SRD model) by the estimation of the shaft friction. It was previously mentioned that the shaft friction has greater contribution to the SRD than the toe resistance. In case of Stevens et al (1982) SRD model, the shaft friction (Lower Bound) is generally higher than the one estimated by the Alm & Hamre (2001) SRD model (Lower Bound), while the toe models are more or less the same.

Figure 5.2-7 can be used as an example, to highlight the overestimation of the blow counts produced when using the Lower Bound of this model, but it can also be used to highlight the effect of shaft friction on the predicted blow counts, when using the Upper Bound that utilizes the full internal friction (the difference between the Lower and Upper Bounds is that the first applies as internal friction half of the external calculated by [4.3.1], while the latter assumes both internal and external friction to be equal). The comparison is provided in Figure 5.2-10.

It should also be noticed that this model utilizes limits for the shaft friction (based on the soil density, friction angle, etc.), according to the API (2000) guidelines. The interface friction angle is determined by the soil description and density (Figure 4.3-1). However, there are various formulas that can be used to determine the soil density (e.g., Lunne & Christoffersen (1983), Kulhawy et al (1990), Jamiolkowski et al (2001), Baldi et al (1986), Schmertmann (1978) etc.). Moreover, the sand consistency can be defined by Lambe and Whitman (1969) as can be seen in Table 4.3-1. Therefore, one can easily use different formulas or criteria to assess the relative density and define whether the sand is loose,

medium etc., which will lead to different values of friction angle, and different limits for the shaft friction according to the API table in Figure 4.3-1.

On the other hand, one could think that applying limiting values on the shaft friction might be unconservative for driveability analysis. However, these limitations seem necessary in order to have predictions in a reasonable range (Figure 5.2-10).

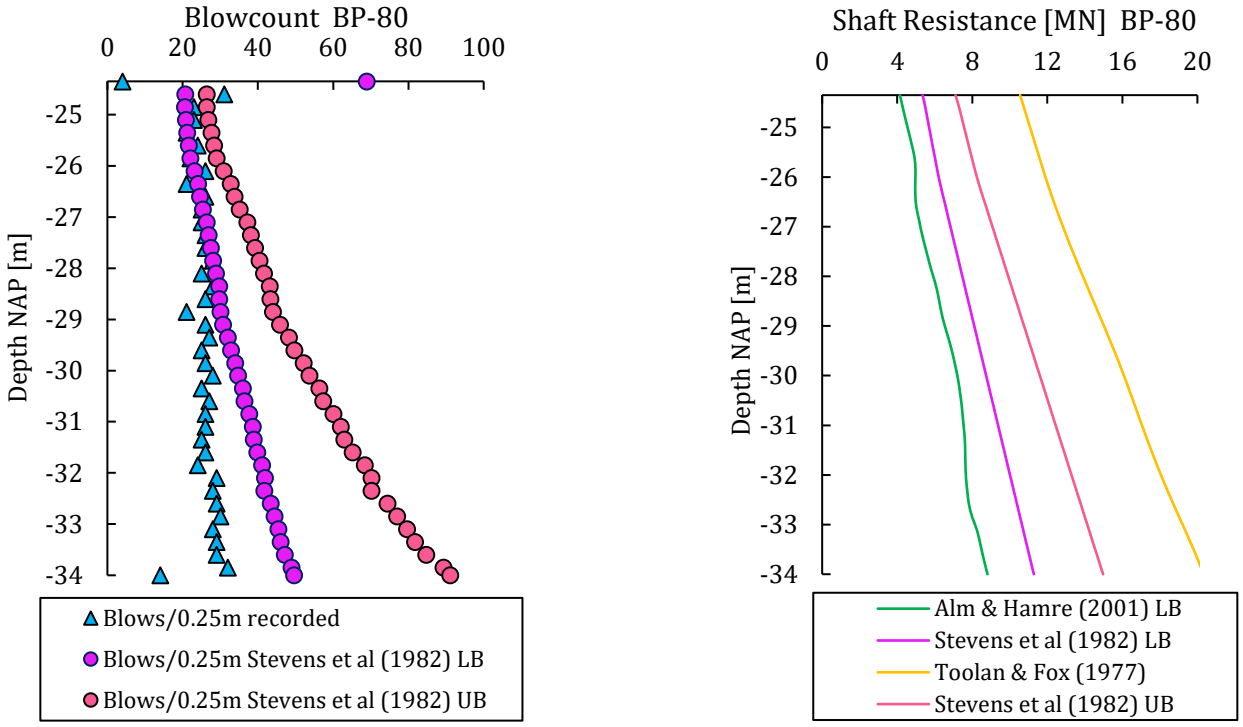

Figure 5.2-10: Comparison of Lower and Upper Bound of Stevens et al (1982) SRD model.

Toe Resistance

The toe resistance of this SRD model can be calculated by using equation [4.3.2]. Although this is a simple equation (bearing capacity factor times effective vertical stresses), some issues that come with it are listed below:

- It can be seen from the post-predictions (e.g., Figure 5.2-4) that the toe resistance can't be greater than $1\,MN$, which may also be derived by multiplying the area of the steel annulus of the pile with the maximum allowable end bearing resistance according to the API table (Figure 4.3-1). This implies that for every pile with a diameter around $1 - 2\,m$ and a wall thickness around $20\,mm$, the maximum toe

resistance that can be mobilized is between $0.7\ to\ 1.5\ MN$, which might be unconservative for driveability analysis.

- Utilizing pre-installation stresses to estimate the toe resistance is not the best approach, as it is known (see Chapter 3.2) that due to soil displacements, grain crushing, re-orientation, etc., the soil stresses are not constant.
- Using a constant bearing capacity factor might not be ideal as well, in case for example of partially plugged piles. Specifically, Gudavalli et al (2013) suggested that Nq should be a function of PLR, which in turns is a function of internal diameter.
- Additionally, the bearing capacity factor as can be seen in Figure 4.3-1 depends on the friction angle and according to Table 4.3-1 it is highly sensitive to even small variations of the friction angle or relative density. For example, at a specific soil horizon where a certain value for the effective vertical stress has been calculated, a relative density of $64\ \%$ (medium-dense sand according to Table 4.3-1) results in a bearing capacity factor equal to 20 (Figure 4.3-1), whereas if the relative density is estimated to be $66\ \%$ (dense sand according to Table 4.3-1), the bearing capacity factor would be 40 (Figure 4.3-1). Hence, a $2\ \%$ difference in relative density might lead to great scatter of estimated toe resistances. In addition, as already mentioned, there are various equations developed over the years for estimating soil relative density (see previous Section), which leads to higher levels of uncertainty.

Overall

- The post-predictions produced with this method are satisfying, since they are in a reasonable range.
- Usually, for a driveability prediction in which the number of blow counts is not known, or in other words, the pile has not been yet driven, it is required to make predictions using both Lower and Upper Bounds. Stevens et al (1982) SRD model, when using its Lower Bound, tends to slightly overestimate the blow counts (especially for the last few meters of installation) required to drive a pile. This implies that an average between the Lower and Upper Bounds (e.g., Best estimate) would still lead to an overestimation that could lead to more expensive choices regarding the hammering equipment (Figure 5.2-10).
- The shaft friction leads to overestimated blow counts, as was the case for Toolan & Fox (1977) method. Shaft friction formulation doesn't consider friction fatigue or the influence of the degree of soil displacements induced during driving.

- This SRD model doesn't consider the fact that during driving soil grains are displaced or even crushed, which means that the pre-installation vertical effective stresses, as well as the lateral earth pressure coefficient do not remain constant through the entire installation process.
- Partially plugged conditions are not taken into account. A modification to this model for that purpose was proposed by Gudavalli et al (2013).
- There is lack of agreement amongst published Nq values. Additionally, Nq is highly sensitive in small variations of relative density or friction angle and the various equations that have been produced over the years do not always agree, leading to higher levels of uncertainty.
- Limits applied on toe resistance might be unconservative for driveability analysis (underestimation of total driving resistance).
- Limits applied on shaft resistance are probably necessary considering that the Lower Bound of this SRD model already overestimates the blows required to drive the steel open-ended piles.

Alm & Hamre (2001) Evaluation

General Observations

Alm & Hamre (2001) SRD model has produced better post-predictions than the other two SRD models. It should be noticed that for the post-predictions presented, the Lower Bound of this method has been used. The advantages of this model are listed below:

- Both shaft and toe resistances are functions of the qc value from CPT. This allows variation of both the shaft and toe model based on local soil variability indicated by the resistance applied on the cone of the CPT.
- Shaft model considers friction fatigue.
- From the post-predictions, a slight underestimation of the initial blow counts (first few meters of installation) can be observed, but overall it is a high reliable SRD model, especially for the piles of the Amaliahaven project.
- Equations are easy to use. The only inputs that are needed are the qc value and the vertical effective stresses.

Unit shaft friction

The unit shaft friction of this model is calculated by equation [4.4.1], which reduces the shaft resistance at a soil horizon with further pile penetration. As already mentioned the shaft friction has larger contribution than the toe resistance in this case. By not taking into account friction fatigue, the other two models lead to overestimation of blow counts, even when applying friction limits (see for example Figure 5.2-7).

Another difference with the other two SRD models is that [4.4.1] is the total shaft resistance which includes internal shaft friction, whereas Toolan & Fox (1977) and Stevens et al (1982) SRD methods model explicitly the internal and external shaft friction. As can be seen in Figure 5.2-9 a slight modification to Toolan & Fox (1977) method, in which their equation has been used to represent the total shaft resistance as the Alm & Hamre (2001) approach, resulted in much better predictions (5.2.1, Figure 5.2-9).

Moreover, since [4.4.1] has been derived through back-calculated SRD profiles for piles with diameters in the range of 0.762 to $2.74\,m$, the potential plug resistance has probably been incorporated to the total shaft friction calculated with [4.4.1], which might lead to slightly higher shaft resistances. This could also explain some overestimated blow counts produced with this method, specifically for the last meters of penetration, as can be seen in Figure 5.2-6. On the other hand though, for piles with smaller diameters, for example $0.35\,m$, which could at least be partially plugged, by not modelling the degree of soil plugging might lead to underestimation of the shaft resistance.

Toe Resistance

Alm & Hamre (2001) SRD model uses a more complicated formula to estimate the toe resistance during driving ([4.4.6]). According to the authors, while the original formulation of the toe resistance was considered as 40% of the qc value (Alm & Hamre (1998)), [4.4.6] will result in a range of 35% to 55% of the qc value when sand density ranges from loose to very dense. Specifically, for the Amaliahaven steel open-ended piles, [4.4.6] led to around 40% the toe resistance predicted by Toolan & Fox (1977) model. As in the case of the shaft model, the toe model doesn't take into account partially plugged conditions, but only fully coring, making it more suitable for large (D>1) offshore piles. This might lead to underestimation of the blow counts for smaller diameter piles.

Overall

- Alm & Hamre (2001) SRD model resulted in the most reliable post-predictions.
- Shaft model takes into account friction fatigue.
- Shaft friction incorporates the plug resistance (inner friction) to the external formulation ([4.4.6]). This might lead to slightly higher shaft resistances.
- Suitable for large offshore (D>1) fully coring piles, as both the toe and shaft resistances have been calibrated for a range of pile diameters between 0.762 to $2.74\,m$, which most probably were fully coring. Moreover, this method doesn't explicitly account for plugging.
- May not be suitable for smaller diameter piles, which may plug.

The performance of the Alm & Hamre (2001) and Stevens et al (1982) models is summarized in Table 5.2-4. For the comparison of these models, first, the Mean Absolute Percentage Deviation or Error (MAPD or MAPE, respectively) is calculated according to [5.2.2] for each and every pile and method examined.

$$MAPE = \frac{100\%}{n}\sum_{1}^{n}\frac{\left|Actual_{\frac{blows}{0.25m}} - Predicted_{\frac{blows}{0.25m}}\right|}{Actual_{\frac{blows}{0.25m}}} \qquad 5.2.2$$

where, n is the number of fitted points. MAPD shows the average deviation of the predicted blow count curve from the actual - recorded blow count curve, and is commonly used in practice to evaluate how good a prediction or a forecast is compared with recorded data. By calculating the MAPD or MAPE, one can also define the average (absolute) match percentage (100% - MAPD or MAPE). The latter is presented in Table 5.2-4 as '% Match', and shows the percentage of matching of the predicted and actual blow count curves. The higher the % Match the closest the prediction is to the actual measurements.

Moreover, besides the percentage of match between the actual and predicted curves, it is is important to know if there is a tendency for the prediction method to under or over - estimate the blows/0.25 m. This tendency is also presented in Table 5.2-4, as '% Under', which shows the percentage of the predicted blow count curve that lies below the actual blow count curve (shows the underestimation of the blow counts). Thus, a percentage of 80% Under, means that 80% of the predicted blows are underestimated (irrespectively of the % Match).

It can be seen that the predictions of the Alm & Hamre (2001) model have a higher (better) match in 7 out 10 piles examined than the Stevens et al (1982) model for the steel open-ended piles of the Amaliahaven project.

It is important to clarify that Table 5.2-4 gives just an indication of how the models perform, while the reader should always inspect the graphs of the blow counts and SRD as presented earlier.

Table 5.2-4: Percentage of match (% Match) between recorded and predicted blow count curves using Alm & Hamre (2001) and Stevens et al (1982) models for the Amaliahaven steel open-ended tubular piles. The % Under shows the percentage of the predicted blow count curve that lies below the recorded one (underestimation of blow counts).

	Alm & Hamre (2001)		Stevens et al (1982)	
	% Match	% Under	% Match	% Under
BP-920	77 %	88 %	78 %	33 %
BP-899	79 %	82 %	76 %	39 %
BP-853	78 %	70 %	89 %	58 %
BP-838	76 %	77 %	88 %	48 %
BP-800	86 %	59 %	78 %	44 %
BP-02	77 %	21 %	61 %	6 %
BP-33	83 %	38 %	68 %	11 %
BP-48	87 %	56 %	81 %	17 %
BP-64	83 %	43 %	75 %	29 %
BP-80	87 %	45 %	71 %	15 %

5.3 SRD estimations of Unified Method (2020)

Implementing Unified Method (2020) in AllWave PDP

Initially, this brief section will explain how the Unified Method can be implemented in AllWave PDP software.

One of the advantages of this software is that it allows users to manage the yield stresses or quake values of the springs used to model the soil around and at the tip of the pile. As mentioned before, the shaft and toe resistances are modeled through elasto-plastic springs (Figure 5.2-2), in which the yield stress (either the shaft's or the toe's) can be modified.

The yield stress is *the maximum soil resistance* that can be mobilized during a hammer blow and is reached when the pile's displacement becomes greater than the quake value. It is clarified that the traditional SRD models and the Unified Method are used to define the *maximum* shaft/toe resistance or yield stress of the springs and therefore, the *mobilized SRD* is not an input but an output (product of the driveability analysis).

The quake is the term used to describe the maximum soil displacement until which, the behaviour of the soil can be assumed elastic. If the pile's displacement from a hammer blow is greater than the quake values of the springs, the soil behaves plastically. The reader is referred to Figure 5.2-2, Table 5.2-1, Table 5.2-2, Table 5.2-3, which show the springs used to model the shaft and toe, as well as quake values used by the traditional driveability models. Moreover, these tables show how the aforementioned SRD approaches, model the yield stresses of the shaft and the toe.

Therefore, a similar approach needs to be followed in order to implement the Unified Method SRD model into AllWave PDP. It should be mentioned that this section implements the Unified Method in its 'raw' form (as intended to be used in pile design and not in driveability studies). For that reason, equations [4.5.1] and [4.5.6] have been used to model the shaft and toe yield stresses.

A typical quake is about 2.5 mm, but it should be stated that this is not a fixed value and signal matching can reveal appropriate soil resistances and quakes. Since, signal matching has not been done for the purposes of this Thesis, quake values similar to those used by

the traditional driveability models are utilized. Table 5.3-1 below summarizes the characteristics of the soil springs.

Table 5.3-1: Unified Method (2020) soil spring parameters.

	F_{y1} [MPa]	F_{y2} [MPa]	u_1 [mm]	u_2 [mm]	Smith Damping factor [s/m]
Toe model *	$q_{b0.1} = [0.12 + 0.38 * A_{re}] * q_p$	0.1*F_{y1}	2.5	2	0.5
Shaft model	$(q_c/80) * A_{re}^{0.3}$	F_{y1}	2.5	2	0.25
Fatigue factor	$\left[\max\left(1, \frac{h}{D}\right)\right]^{-0.4}$	-	-	-	-

- q_p is taken as the qc averaged $+/-1.5D$ from the pile tip.

1. Toe resistance is applied on the entire base area.
2. Shaft resistance is applied only at the outer shaft area.

For the shaft model, equation [4.5.1] has been slightly modified. A list of changes is presented below:

- f_t/f_c is taken as 1, since during pile driving a compression load is mainly applied.
- $\Delta\sigma'_{rd}$ can be ignored for large diameter piles ($D > 1$). By including it to [4.5.1], one would notice an insignificant change to the radial effective stresses (for large diameter piles) and this can also be understood by inspecting [4.5.4], which shows that $\Delta\sigma'_{rd}$ is inversely proportional to pile diameter.
- δ_f is assumed by this method to be around 29^0 ($+/-\ 5^0$), due to grain crushing etc., as explained in Chapter 4.5. Hence, $tan\delta_f = tan29 \approx 0.55$ and $tan29 * \left(\frac{q_c}{44}\right) * A_{re}^{0.3} * \left[\max\left(1, \frac{h}{D}\right)\right]^{-0.4}$ can be written as $\left(\frac{q_c}{80}\right) * A_{re}^{0.3} \cdot \left[\max\left(1, \frac{h}{D}\right)\right]^{-0.4}$.
- PLR measurements have been made at the end of installation for ten piles in total from both APM and RWG sites, and the piles were fully coring (so $PLR \approx 98 - 99\%$).

Therefore, the shaft and toe yield stresses are modeled as indicated in Table 5.3-1 with their quake values and Smith's (1960) damping factors being the same as those suggested by Alm & Hamre (2001).

AllWave PDP allows the user to manually insert both the yield stresses and the quake values and damping factors for the shaft and toe model. It should be clarified that the yield stress of the shaft is the one indicated in Table 5.3-1, while the software also allows to model the fatigue curve by changing the fatigue factors that are shown in Figure 5.3-1, below.

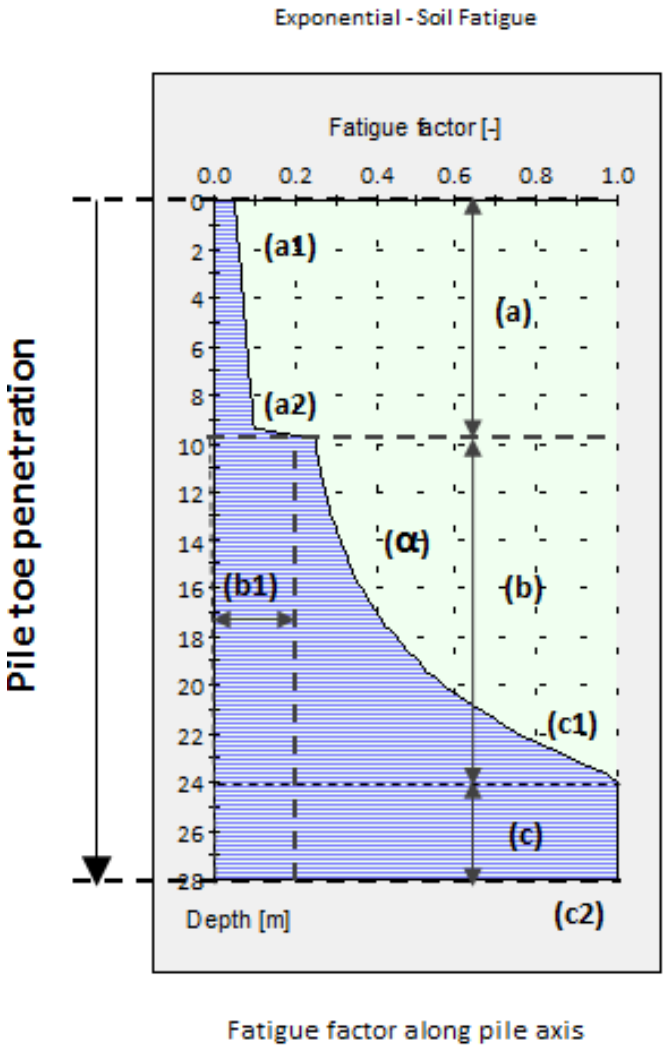

Figure 5.3-1: Fatigue curve and factors (Allnamics: AllWave PDP).

In order to implement the Unified Method into the software, one can simply modify the Exponential decay model (a model similar to Alm & Hamre (2001) suggested by Allnamics), using the following equations:

Shaft friction Exponential decay model:

$$f_s = f_{sres} + (f_{si} - f_{sres}) * e^{k(d-p)} \qquad 5.3.1$$

With $f_{si} = f_{s,CPT}$, in which $f_{s,CPT}$ is the sleeve friction as measured in a CPT, while the rest of the parameters are the same as the Alm & Hamre (2001) model (Chapter 4.4).

Since the exponential fatigue factor of equation [5.3.1] tends to zero, when $d \ll p$, it is important to include the term f_{sres} in order to eventually have a residual shear stress applied on the pile (or a lower Bound for the shaft friction). On the contrary, the fatigue factor of the Unified Method (Table 5.3-1) doesn't need to explicitly model the residual stress, but it is already incorporated. That means that [5.3.1] can be written for the Unified Method as can be seen in [5.3.2] below:

$$f_s = f_{si} * e^{k(d-p)} \qquad 5.3.2$$

By equating f_{si} with $(q_c/80) * A_{re}^{0.3}$ the only factor that remains to be modeled is the fatigue factor for which $e^{k(d-p)}$ is replaced by $(h/D)^{-0.4}$ by substituting k with [5.3.3]:

$$k = \frac{-\ln\left(\frac{p-d}{D}\right)^{-0.4}}{p-d} = \frac{-\ln\left(\frac{h}{D}\right)^{-0.4}}{h} \qquad 5.3.3$$

where p is the penetration depth, and d is the level in which the shaft friction is calculated.

The user can calculate the term $\left[\max\left(1, \frac{h}{D}\right)\right]^{-0.4}$ and clarify if k needs to be 0 in case $\frac{h}{D} < 1$ or equal to [5.3.3].

The rest of the fatigue factors are listed below:

- $(a1) = (a2) = (\alpha) = (b1) = (c) = 0$
- $(c2) = (c1) = (d) = 1$, with (d) being a fatigue factor for the toe.

By following the aforementioned procedure, the resulting fatigue curve will be similar in form as can be seen in the example of Figure 5.3-2. It can be observed that friction fatigue occurs at some distance from the pile tip, as the area close to the pile tip has not been sheared as much as the soil interface at shallower parts.

By this analytical modeling of the Unified Method, the model is implemented into the software and used based on the authors' suggestions. Additionally, in this way, shaft friction changes constantly with increasing penetration at each level, and therefore there is no need for calculating a constant pseudo-average shaft friction as was done by many researchers like Prendergast et al (2020), Schneider et al (2010), Byrne et al (2012), Byrne et al (2018), etc.

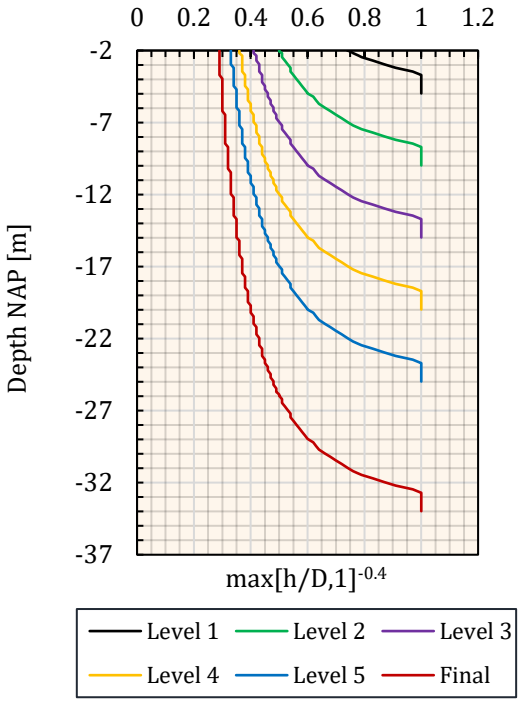

Figure 5.3-2: Example of fatigue curves of Unified Method for different pile penetration levels.

Two piles (BP-920 and BP-853) of the Amaliahaven project have been examined using the aforementioned procedure, and the results are presented in Figure 5.3-3.

It is mentioned that only two piles have been examined because this method highly overpredicts the blows required to drive a steel open-ended pile, and more post-predictions wouldn't be needed for additional insight. Moreover, due to the high overestimation, the actual blow counts recorded are not included in Figure 5.3-3, due to scale issues. Toolan & Fox (1977) SRD model is also used for comparison. The reader can also examine the results of the post-predictions of the other two SRD models (Alm & Hamre (2001) and Stevens et al (1982)) in Figure 5.2-4, and Figure B 1.

The results are commented in the following sections.

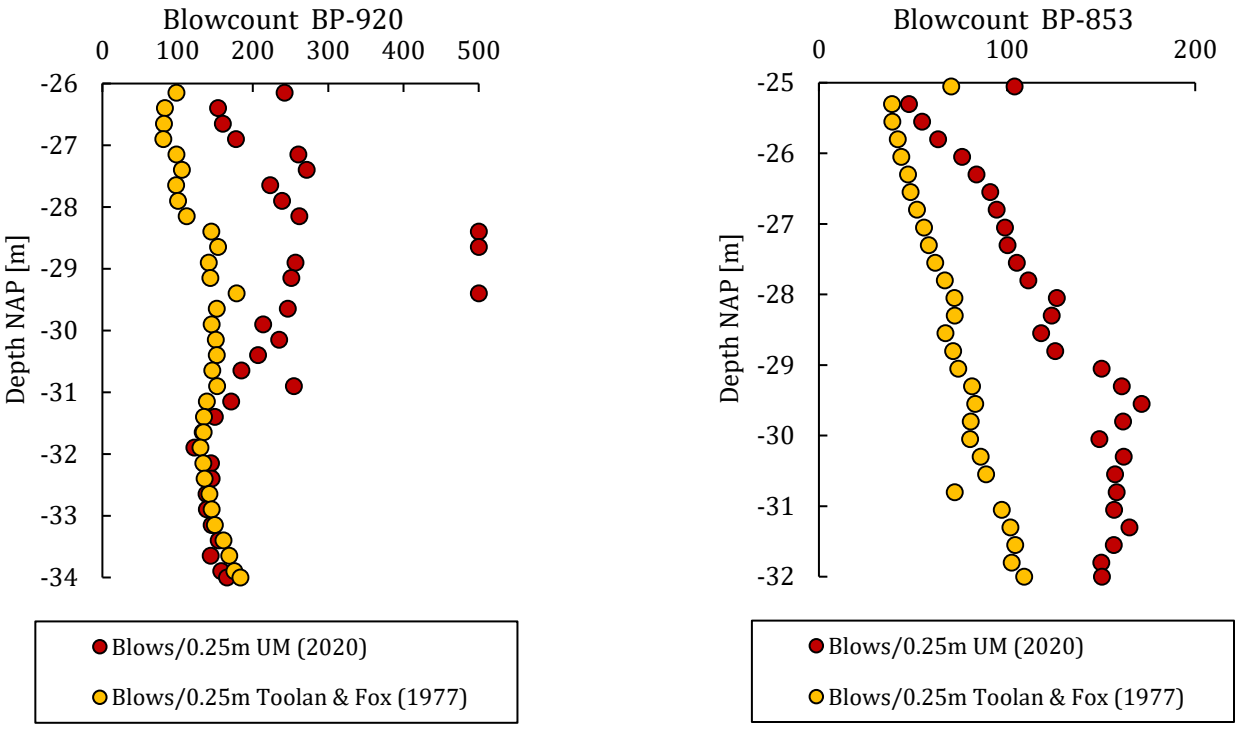

Figure 5.3-3: Driveability post-predictions for combi-wall piles BP-920 and BP-853, using the Unified Method (2020) SRD model. APM terminal.

Unified Method (2020) Evaluation

General Observations

It can be observed from Figure 5.3-3 that the Unified Method SRD model leads to high overestimation of the blow counts required to drive the pile. In some cases, (pile BP-920) it results in blows/0.25 m greater than 500, while refusal can also be set by the contractor to 100, 120, 250 blows/0.25 m. To understand why a high overestimation is produced, a 'closer look' to the shaft and toe resistances is required. Therefore, this model, in its 'raw' format cannot be used for driveability studies.

Unit shaft friction

The shaft model of the Unified Method ([4.5.1]) incorporates some important parameters, which were also mentioned in Chapter 3 and 4.5. These are listed below:

- [4.5.1] is a function of the qc value of the CPT. The advantage is that the cone can also be seen as a small-scale pile inserted into the soil, for which toe resistance and sleeve friction are measured. Moreover, since the last few years, there have been various attempts to correlate empirically the cone resistance with a great number of soil parameters, such as relative density, friction angle, stiffness, etc., having formulas that depend on the CPT retains consistency on interpreted soil behaviour.
- [4.5.1] varies with the effective area ratio, A_{re}, and thus, it takes into account the fact that τf varies with the degree of soil displacement during installation and that it is lowest for fully coring piles and largest for closed-ended piles, as has been confirmed by Gavin and Lehane (2003).
- Since the effective area ratio, A_{re} is a function of the degree of soil plugging, [4.5.1] can be used as a general formulation of the shaft resistance to any kind of pile, meaning open-ended fully coring, partially plugged, or even closed-ended pile.
- Additionally, [4.5.1] takes into account friction fatigue, but in contrast to Alm & Hamre (2001) model, it also varies with the diameter of the pile. In general, this normalization is made so that the radial effective stresses applied at the outer shaft area, are consistent with observations made by White et al (2004), while it also resulted in improved measured to calculated capacities ratios than without including the pile diameter (Chapter 4.5).

- Moreover, during loading, the thin interface zone between pile and shaft that contracts with increasing number of cyclic loading, will tend to dilate upon further shearing (e.g., re-orientation or crushing of soil grains). The restrain to dilation by the surrounding soil mass leads to an increase in the radial effective stresses on the pile shaft (Lehane et al (2020)). This increase is also taken into account in [4.5.1] by incorporating the factor $\Delta\sigma'_{rd}$ to the formulation. As mentioned, earlier, for large offshore piles (e.g., $D > 1$) the contribution of this term to the total shaft friction becomes insignificant. However, for smaller diameter piles its contribution is important and it should be considered.

Therefore, a question one may ask, is:

1. W*hy this model, which takes into account various important phenomena that the other models don't, results in high overestimated blow counts?*

To answer this question, it is important to compare the shaft resistances produced by this method with the shaft resistances produced by the Alm & Hamre (2001) method, the most suitable (at least in this case) SRD model. For that reason, Figure 5.3-4 below, depicts the static component of the shaft resistances mobilized during driving of pile BP-920 at the APM terminal.

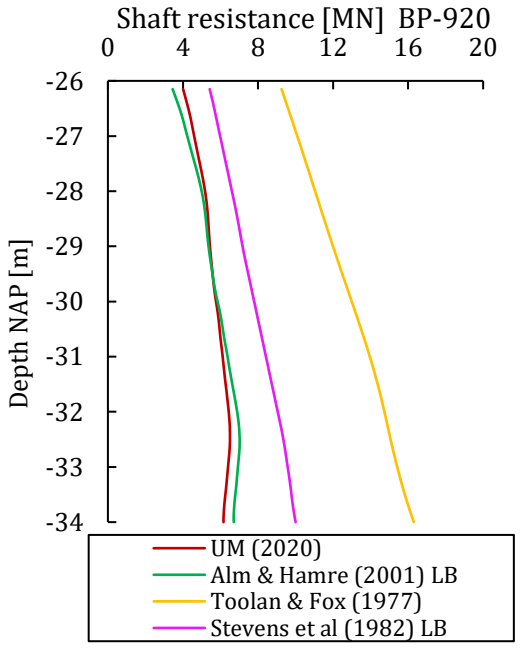

Figure 5.3-4: Static shaft resistances mobilized during driving of pile BP-920, at the APM site, produced by Alm & Hamre (2001), Toolan & Fox (1977), Stevens et al (1982), and Unified Method (2020) SRD models.

Surprisingly, it can be observed from Figure 5.3-4 that the shaft friction produced by the Unified Method is almost the same as the one produced by Alm & Hamre (2001) model, which has been proven to be very reliable. This implies that the overestimation of the hammer blows required to drive the pile, comes from the toe resistance model and not from the formulation of the shaft resistance. This will be examined and explained in the next section. The similarity in shaft resistance of these two models was observed in every of the 10 piles of the APM and RWG sites.

The second question that arises is:

2. W*hy this model, which has been calibrated to estimate the shaft capacity around 14 days after the installation, produces (mobilized) shaft resistances that are very similar to* Alm & Hamre (2001) *model that has been calibrated using driving records?*

Since the Unified Method is calibrated to estimate shaft capacities around 14 days after the installation, one would expect that this model would overestimate the shaft resistance mobilized during driving. That is because, as explained in Chapter 3.4, certain time after the installation process, the soil regains its shaft capacity and tends to even increase. Some reasons that eventually lead to similar *mobilized* shaft resistance are listed below:

- Alm and Hamre (2001) mentioned in their paper that the Lower Bound of this method was very close or slightly above the average back-calculated SRD profiles from various sites that they examined, meaning that the Lower Bound could produce in some cases a greater overall SRD than the actual one.
- The Alm & Hamre (2001) model includes the inner shaft friction (plug resistance) to its external shaft formulation ([4.4.1]). On the other hand, the Unified Method takes into account the inner plug resistance to the toe formulation and models only the external shaft friction.
- In addition, Lehane et al (2020), examined measured to calculated shaft resistance ratios for open-ended piles and concluded that the Unified Method has an average Qm/Qc ratio of about 1.02 with the standard deviation being around 0.22. This means that this method might overestimate or underestimate the shaft capacity by about 20%.
- Furthermore, the Unified Method has been calibrated through static load tests using piles with diameter ranging from 300 to 800 mm, with 90% of the piles examined having a diameter less than 800 mm, while the Alm & Hamre (2001) model used driving data of piles with diameter ranging from 0.762 to 2.74 m. This scale

difference might also be the cause for the Unified to produce less shaft resistance for large offshore piles even though it is calibrated with a median set up factor of 14 days after the installation.

In order to further investigate the shaft friction estimated by these two methods a simple example case is presented below. Assuming the qc value as can be seen in Figure 5.3-5, the unit skin friction without including the fatigue factor, for an open-ended pile with a diameter of $2\,m$, a wall thickness of $40\,mm$ and length of $15\,m$ (fully coring), for the two models is presented in Figure 5.3-5.

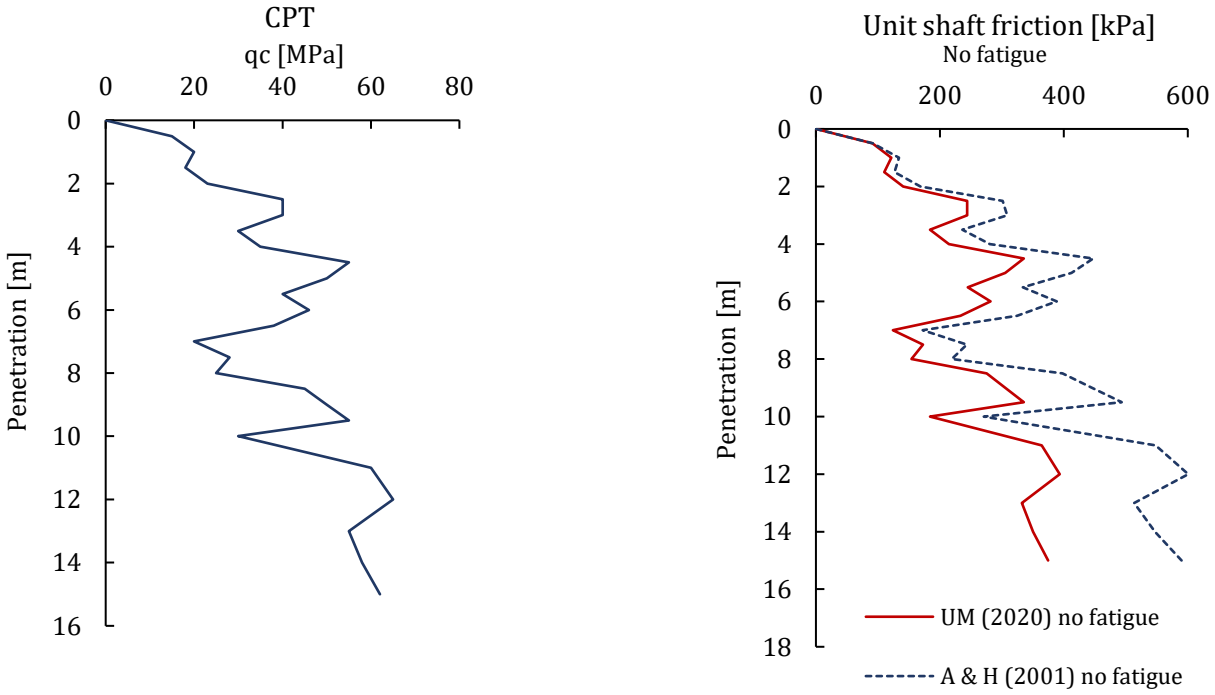

Figure 5.3-5: Example case, in which the unit shaft friction without including friction fatigue is estimated with the Unified Method (2020) and Alm & Hamre (2001) SRD models.

Again, the Alm & Hamre (2001) formulation led to a greater initial pile side friction than the Unified Method for a large diameter (assumed fully coring) offshore pile (Figure 5.3-3). Now, in Figure 5.3-6 the fatigue factors are plotted alongside with the shaft friction developed in various penetration depths for the same example case.

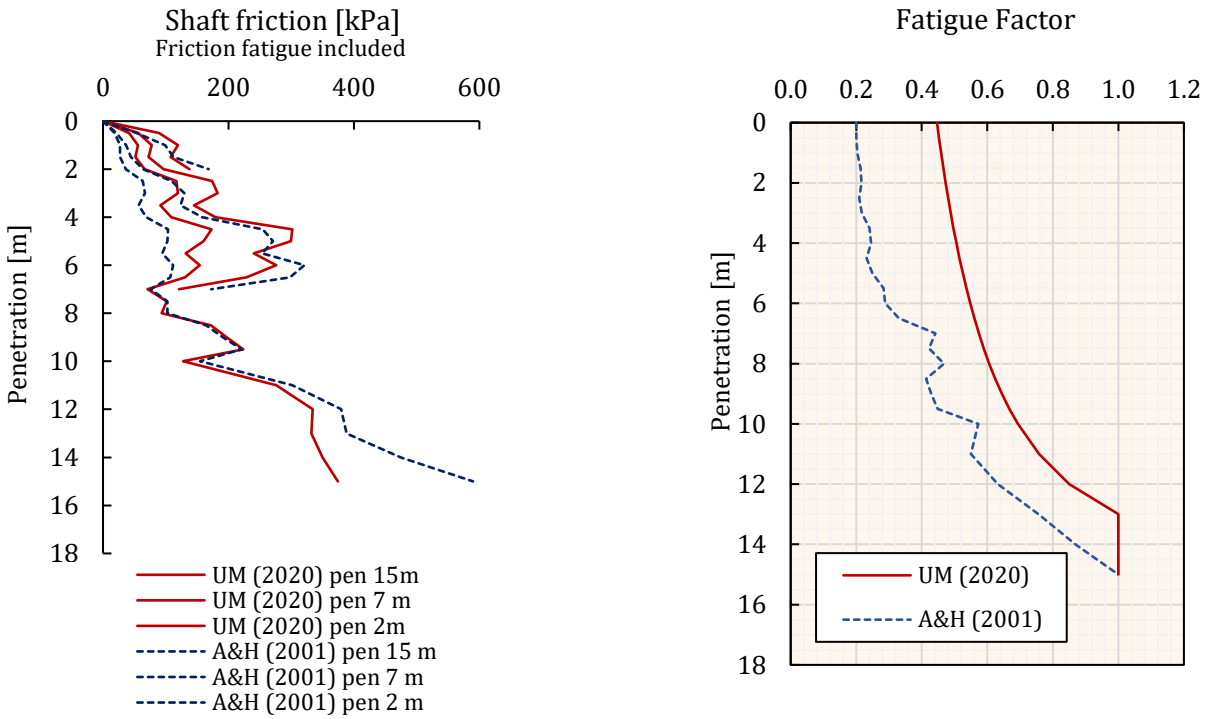

Figure 5.3-6: Example case, in which the shaft friction including friction fatigue and the fatigue factors is estimated with the Unified Method (2020) and Alm & Hamre (2001) SRD models.

It can be observed in Figure 5.3-5 that on hand, the Alm & Hamre (2001) model assumes a high initial pile side friction, which is reduced rapidly by the exponential fatigue factor. This is probably done due to incorporation of the inner plug resistance to the external shaft formulation. On the other hand, the Unified Method estimates a lower initial pile side friction (only external is modeled), but it is reduced in a much slower rate, due to its steep fatigue curve. In addition, one can notice that the Unified Method estimates higher resistances for soil horizons further away from the pile tip, while the Alm & Hamre (2001) method leads to higher shaft friction in an area around and close to the pile tip.

Therefore, the aforementioned observations made by the post-predictions and the example case imply that the Unified Method, although it is a static capacity approach, predicts *external* shaft resistance very similar to the *total* (inner and outer) shaft resistance produced by the Alm & Hamre (2001) model for large offshore piles.

Another question that arises is:

3. *For large offshore piles ($D \approx 2m$), both the Alm & Hamre (2001) and the Unified Method estimate mobilized shaft frictions that are eventually very similar in shape and magnitude. What happens though for piles with smaller diameters?*

To answer to this question, a second example case is presented below, in which the soil conditions (CPT) are the same as in the previous example, but now a steel open-ended pile with diameter $0.34\,m$, wall thickness $14\,mm$ and length of $15\,m$ is examined in Figure 5.3-7. It should be mentioned that the Final Filling Ratio in this case is taken as 0.4, while this example case has been inspired by Prendergast et al (2020), who examined the installation of piles with the same characteristics and plug observations in Blessington's dense sand.

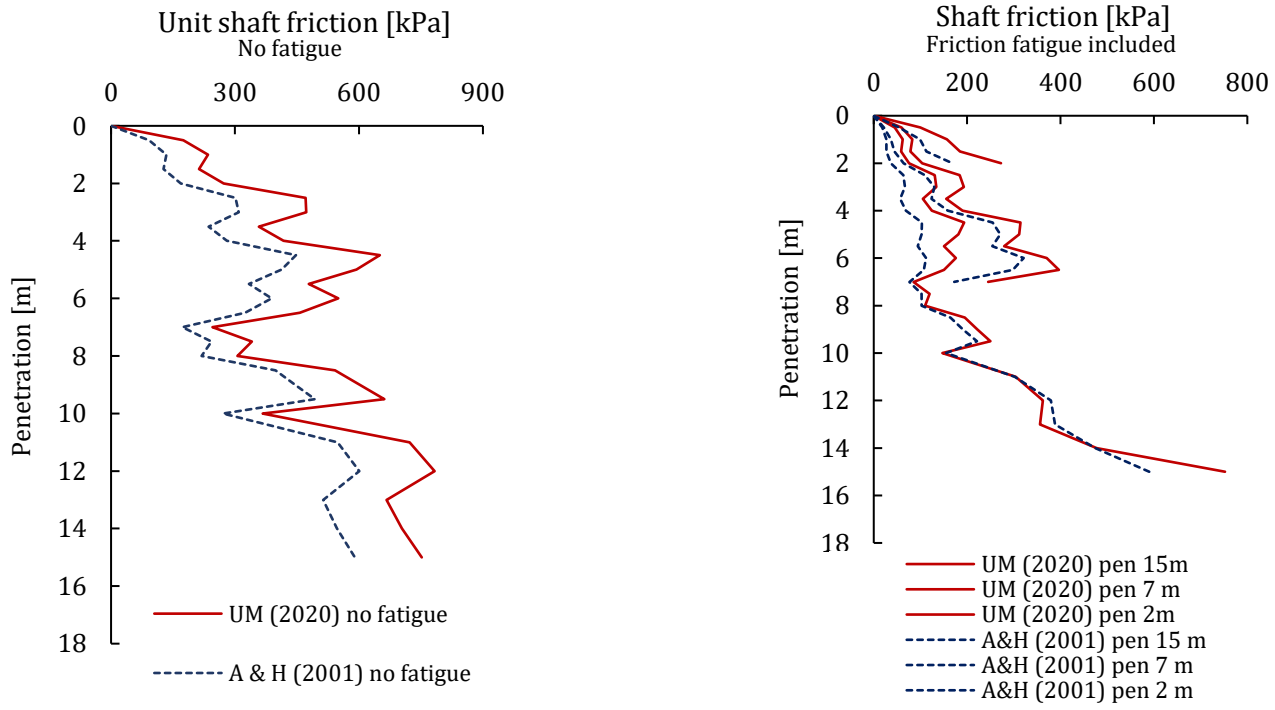

Figure 5.3-7: Example case 2, in which shaft friction estimations of a small diameter plugged pile in dense sand are made by Unified Method (2020) and Alm & Hamre (2001) SRD models.

Figure 5.3-8 below presents the fatigue curves produced by the two models for the second example case.

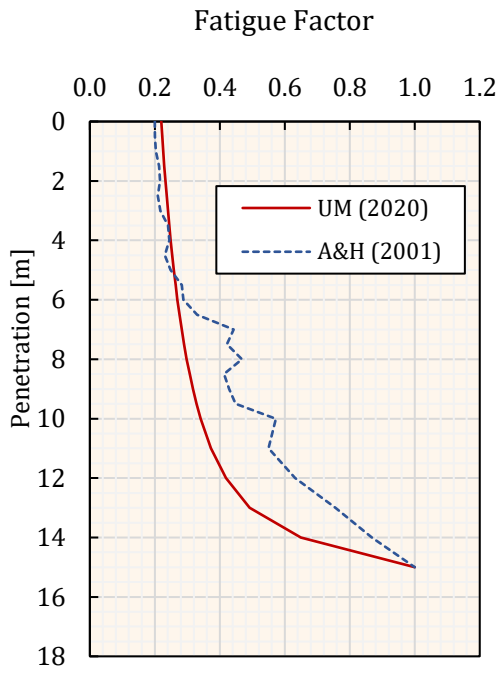

Figure 5.3-8: Fatigue curves produced by Unified Method (2020) and Alm & Hamre (2001) SRD models for the second example case.

In the second example case (Figure 5.3-7, Figure 5.3-8), for the smaller diameter plugged pile, the Unified Method estimates in general greater (external only) shaft resistance than the Alm & Hamre (2001) model. This can be attributed to the fact the Alm & Hamre (2001) model has been calibrated for large offshore piles that fully core, so it doesn't take into account the increase of the plug inner resistance (*of a plugged pile*) to the total shaft resistance. In addition, it can be observed that the curves produced by Alm & Hamre (2001) remained the same as in the previous example, because the soil conditions are the same and this model doesn't take into account the pile diameter.

In addition, the Unified Method produces a fatigue factor that is less steep than in the first example (Figure 5.3-6), with lower residual values. That happens, because as mentioned in the previous sections, the fatigue factor of this method is also a function of the pile outer diameter. Therefore, the initial radial effective stresses applied on the outer shaft area are reduced rapidly, and the resulting (*external*) shaft resistance is again similar in shape than the the *total* (inner and outer) shaft resistance produced by Alm & Hamre (2001), but generally higher, especially for the first few meters of installation.

Toe Resistance

The toe resistance of this model is calculated by using equation [4.5.6] and applied at the entire base area of the pile since it accounts for the inner plug resistance. On the contrary, the Alm & Hamre (2001) model assumes toe resistances during driving around 0.35 to 0.55 times the qc value applied only at the steel annulus of the pile.

For steel open-ended piles, with a diameter around $1.5\,m$ and a wall thickness around $20\,mm$ as in case of the piles of the APM and RWG sites, the Alm & Hamre (2001) model will estimate a toe resistance $[MN]$, acting on the entire base area of an equivalent closed-ended pile (with diameter around $0.34\,m$) to be in the range of 0.03 - $0.05\,[m^2]$ times the qc value.

On the other hand, using [4.5.6] for the piles mentioned earlier, would result in a toe resistance $[MN]$ around $0.25\,[m^2]$ times the qc value. This means that the Unified Method estimates a toe resistance for these piles, approximately $4\ to\ 8$ times the one calculated by Alm & Hamre (2001) model.

The toe resistance for a pile with $D_{out} = 1.5\,m$ and $t = 20\,mm$, installed in soil conditions as shown in Figure 5.3-5 (same CPT), predicted by the two models, as well as the toe resistance predicted for pile BP-920 are presented in Figure 5.3-9.

As can be seen (Figure 5.3-9), the toe resistance produced by the Unified Method for the soil conditions of the first example case, is on average around 4 times that of the Alm & Hamre (2001), and on average around 2 times the toe resistance calculated as the qc value applied directly to the steel annulus of the pile. The same observations can be made from the (static) toe resistance mobilized during driving of the steel open-ended BP-920 pile of the APM site. The toe resistance of the Toolan & Fox (1977) model is also plotted for pile BP-920, as it is an average of qc (above and below tip) that is applied on the steel annulus.

Therefore, the aforementioned observations verify the answer given to the first question that the overestimation of the blow counts required to drive the steel open-ended piles of both APM and RWG sites, comes from overestimation of the toe resistance produced by the Unified Method.

It is mentioned again that the piles are fully coring and the same trend can be noticed in every of the ten piles examined.

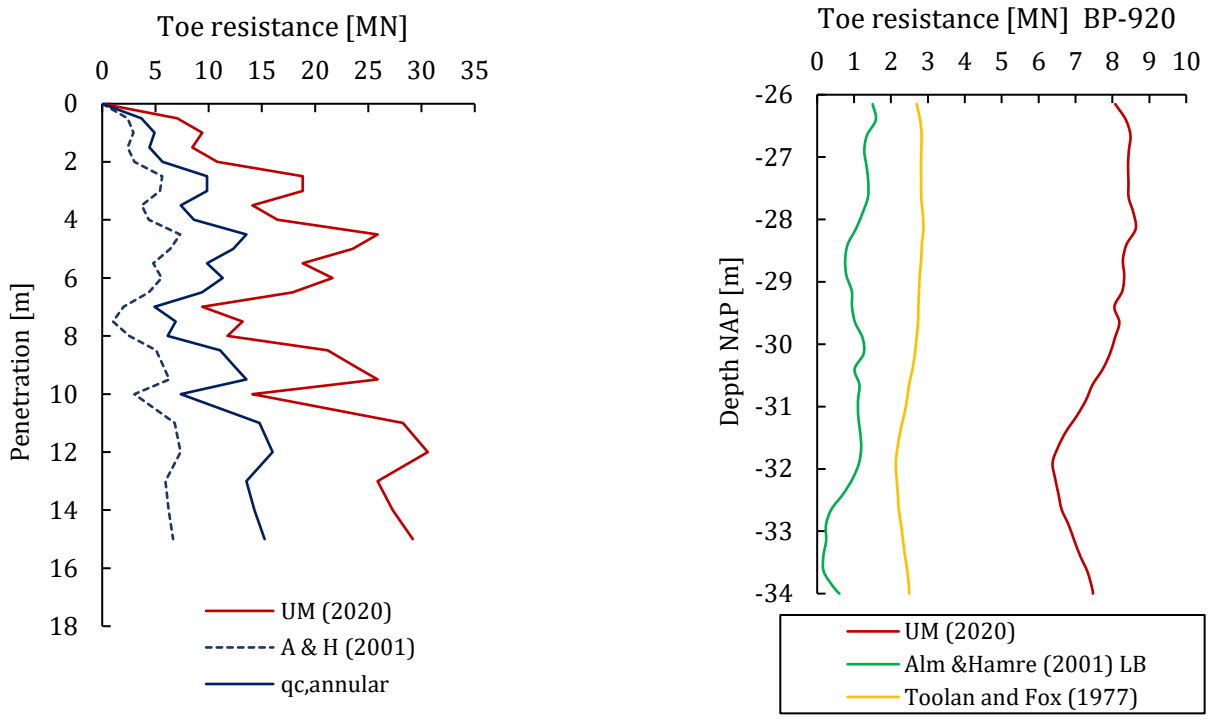

Figure 5.3-9: An example of toe resistances produced for a pile with $D = 1.5m$ and $t = 20mm$ with the Unified Method (2020) and Alm & Hamre (2001) SRD models. On the right side, the toe resistances produced for pile BP-920 of the APM site.

Hence, the question now is:

4. *Why does the Unified Method estimate a toe resistance that large (*$5 - 8$ *times that of the Alm & Hamre (2001)) for the piles examined?*

The Unified Method has been calibrated to estimate pile tip resistance at failure, which is defined as the toe resistance mobilized at displacements $0.1 * D$. Thus, for the Amaliahaven piles, this resistance is mobilized when the toe is displaced $0.1 * 1.42 = 0.142 \approx 14cm$. However, during a typical hammer blow, the pile will displace a few millimeters, meaning that the toe resistance that should be mobilized is less than that at failure. More details are also explained in the next Chapter.

Overall

- By observing the results of the post-predictions made for the Amaliahaven project, but also those of the example cases, it can be concluded that the Unified Method

highly overpredicts the blow counts required to drive a pile, and even suggests (falsely) refusal.

- Contrary to the rest of the SRD models examined, the overestimation by the Unified Method comes from the toe resistance formulation.
- Interestingly, the *mobilized* shaft resistance produced by the Unified Method is very similar to the one produced by Alm & Hamre (2001) model, although the first is calibrated to predict shaft capacities around 14 days after the installation. The main reason behind that, is that the Unified Method models only the shaft friction that is developed at the outer shaft area of the pile, while the Alm & Hamre (2001) approach models both the inner and outer shaft resistance. Therefore, although the shaft resistance of the Unified Method includes a set up of 14 days, since only external shaft resistance is modeled, the mobilized shaft resistance is similar in magnitude with that of the Alm & Hamre (2001) model.
- For large diameter piles, the shaft resistance estimated by the Unified Method is very similar to that of Alm & Hamre (2001) model and lower near the pile tip, whereas for smaller diameter piles, which can also plug during driving, the Unified Method predicts greater shaft resistance.

1. The shaft resistance model considers:
   - Variation of τf with the degree of soil displacement during installation. This allows utilization of [4.5.1] for all cases: fully coring, partially plugged, closed-ended piles.
   - Friction fatigue, which is a function of h and D.
   - Increase of radial effective stresses during loading, due to constrain of dilation of the thin interface zone by the surrounding soil mass.

2. Equation [4.5.6] that estimates the toe resistance:
   - Can be used in all cases, meaning fully coring, partially plugged and closed-ended piles, as it assumes an equivalent closed-ended pile, which in turns implies that the inner plug resistance is incorporated to the base resistance model.
   - Considers the plug resistance of a partially plugged pile by utilizing the effective area ratio, which is a function of IFR or PLR.
   - Results in mobilized toe resistance at displacements of $0.1 * D$, making the method unsuitable for pile driveability analysis in its 'raw' format.

6. Unified SRD Method

The observations made for the Unified Method in the previous Chapter leads to the conclusion that both the shaft and the toe model need to be modified, so that this method can be used for driveability analysis. In this Chapter, an effort is made to suggest general formulations for the shaft and toe resistances, in order to be able to utilize this model in driveability predictions for various case studies (Chapter 7). To distinguish between the Unified Method from the modified format used in SRD estimations, the latter is referred to as Unified SRD Method.

6.1 Shaft Resistance During Driving

Three very important factors already included in the unmodified form of [4.5.1] and will also be incorporated in the modified formulation are:

3. Variation of τf with the degree of soil displacement during installation (green color in [6.1.1]).
4. Friction fatigue as function of h and D (blue color in [6.1.1]).
5. Increase of radial effective stresses during loading, due to constrain of dilation of the thin interface zone by the surrounding soil mass (orange color in in [6.1.1]).

Since this method has been calibrated to estimate shaft capacities around 14 days after the installation, a set up factor needs to be applied in order to reduce the static shaft capacity to external shaft resistance during driving. Although it has been observed that this model estimates shaft capacities similar to the Alm & Hamre (2001) shaft resistances during driving, Lehane et al (2020) mentioned that the ratio of measured to calculated shaft capacities for open-ended piles is on average 1.02, with a standard deviation of 0.22. This means that this model might overestimate or underestimate the radial effective stresses developed during driving, by about 20%. Additionally, it was explained that the Alm & Hamre (2001) model includes the inner shaft friction (plug resistance) for large offshore piles to the external shaft formulation, making it slightly higher than the Unified Method, which incorporates the plug resistance to the base resistance formulation.

In Chapter 1.5, it was mentioned that one of the limitations of this research is that a set up factor has not been established for the steel open-ended piles of the Amaliahaven project. This could have been done by utilizing a PDA system to measure transferred

energy and estimate soil resistances and quake values during pile installation, and by taking the same measurements about 2 weeks later by re-striking the same piles. This information could be used to:

1. Assess how much shaft capacity would have been regained over a period of two weeks.
2. Asses the driving resistance estimated by the examined models, and additionally,
3. Evaluate the shaft capacity estimated by the Unified Method.

Instead, in this research, a set up factor has been estimated using [3.4.1], and included in equation [4.5.1]. This set up formulation was established by Lehane et al (2017), who utilized the same database that was used for the calibration of the Unified Method.

Thus, [3.4.1], by setting $d_{offset} = 0$, will result in a set up factor of ≈70%. Jardine et al (2006), Karlsrud et al (2014), and Gavin et al (2013) have also confirmed a set up factor of around 0.7 in their studies in dense sand deposits. Further information can be read in Chapter 3.4.

Therefore, the modified form of the (external) shaft resistance of the Unified Method is presented below, in [6.1.1], in which all factors have been previously clarified:

$$\tau f_{SRD} = set\_up * \left((q_c/44) * A_{re}^{0.3} * \left[\max\left(1, \frac{h}{D}\right) \right]^{-0.4} + \Delta\sigma'_{rd} \right) * tan\delta_f \qquad 6.1.1$$

With $set\_up = 0.7$.

[6.1.1] is the external shaft friction formulation and is applied on the outer shaft area only. The plug resistance is incorporated to the base resistance formulation.

6.2 Toe Resistance During Driving

It was mentioned in previous sections that the Unified Method estimates the base resistance at displacements of $0.1 * D$. Hence, for large offshore piles, like the ones examined from the Amaliahaven project, this resistance is mobilized, when the toe is displaced $0.1 * 1.42 = 0.142 \approx 14cm$. However, for typical hammer blows ($25 - 40$ blows/0.25 m), the pile displaces a few millimeters per blow, meaning that the toe resistance that should be mobilized is less than that at failure.

The difficulty in modelling the mobilized toe resistance, is that the pile displacement induced per hammer blow is not known before the pile installation. Additionally, as stated in previous sections, all of the models examined so far, assume a typical quake (maximum elastic soil displacement) of about $2.5\,mm$ and use elasto-plastic springs to model the yield stress of the toe spring model. Therefore, for a hammer blow that induces a pile tip displacement $\geq 2.5\,mm$, the full toe resistance is assumed to be mobilized. Hence, it is reasonable to expect overestimation of the blow counts required to drive the pile, when using the 'raw' format of this method, since for $2.5\,mm$ of vertical pile tip movement, the toe resistance mobilized is assumed to be equal to the one mobilized at $0.1 * 1.42 = 0.142 \approx 14cm$ (Figure 5.3-9). Thus, it is clear that the toe resistance of this method needs to be reduced, so that it corresponds to the toe resistance during driving.

It should be mentioned here, as part of the limitations of this Thesis that only elasto-plastic springs have been examined (Figure 5.2-2), as a simplification to actual non-linear soil behaviour. Moreover, typical quake values are also used for the toe model, since actual quakes have not been estimated, through for example, signal matching. Additionally, suggestions of quake values vary, and there hasn't been established yet a generally accepted formula that can estimate quake values for various soil conditions, based for example, on soil properties, pile dimensions etc., so this is a field that requires a lot of attention and more research in the future. However, quake values can be estimated, if the yield stress of the spring is known and by using equation [6.2.1], suggested by Lysmer & Richart (1966), for the soil stiffness in small strains. But as stated above, the yield stress of the spring is generally not known.

$$k = \frac{4}{\pi}\left[\frac{E_0}{1 - v^2}\right] \qquad 6.2.1$$

where, E_0 is the small strain Young's modulus and v the Poisson's ratio.

Therefore, without project specific actual measurements, the options are to either assume a typical quake value, (e.g., $2.5\,mm$), or to assume a maximum toe resistance for the spring, (e.g., the qc value from the CPT times A_{re}, applied on the entire base area), and define the quake from [6.2.1]. Both methods include uncertainty, but usually to the toe resistance is the one modelled and the quake is assumed.

Base displacement models

Byrne et al (2012), Byrne et al (2018) and Prendergast et al (2020) suggested to use the Gavin and Lehane (2007) base-displacement model, in order to approximate the base resistances encountered during driving, by estimating the actual settlements from each hammer blow from the driving records. By doing so, they showed improved predictions of blow counts, when using axial static capacity design methods, like ICP and UWA. This model is presented in Figure 6.2-1, below.

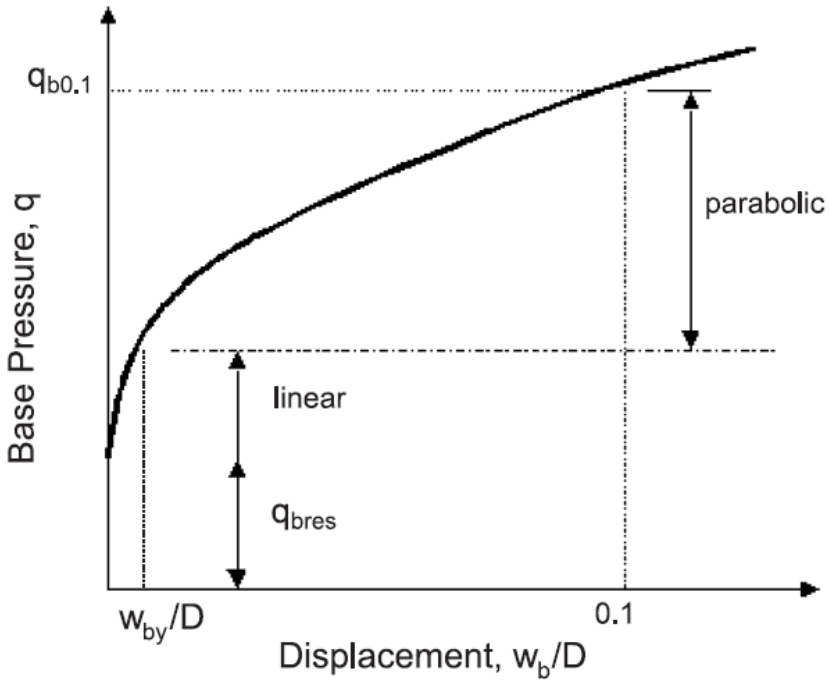

Figure 6.2-1: Idealized base load transfer curve by Gavin and Lehane (2007).

For clarification:

- $q_{b0.1}$ is the resistance at the base of a pile at displacement $w_b = 0.1 * D$.
- q_{bress} is the residual base pressure.
- w_b is the displacement of the pile base.
- D is the external pile diameter.

The load-displacement relationship can be subdivided in three stages:

1. A stage in which no base movement occurs until the residual base pressure (q_{bress}) is exceeded.
2. A linear stage with an average operational Young's modulus of Eo, where q_b exceeds q_{bress} up to $w_b/D = w_{by}/D$.
3. A non-linear stage up to $\frac{w_b}{D} = 0.1$ when the base pressure becomes equal to $q_{b0.1}$.

The graph of Figure 6.2-1 can be plotted using [6.2.2],[6.2.3] below:

$$q_b = k * \frac{w_b}{D} + q_{bress} \quad for \ \frac{w_b}{D} < \frac{w_{by}}{D} \tag{6.2.2}$$

$$q_b = \left[k * \left(\frac{w_{by}}{D}\right)^{1-n} * \left(\frac{w_b}{D}\right)^{n}\right] + q_{bress} \quad for \ \frac{w_{by}}{D} < \frac{w_b}{D} < 0.1 \ with \frac{w_{by}}{D} \geq 0.003 \tag{6.2.3}$$

Moreover, the term $\frac{w_{by}}{D}$ can be calculated by [6.2.4]:

$$\frac{w_{by}}{D} = \frac{\pi}{4} * q_p * \frac{1 - v^2}{E_o} \leq 1.5\% \tag{6.2.4}$$

in which, q_p for open-ended piles is taken from [6.2.5], which can be used to estimate base resistances up to $1 * D$:

$$q_p = q_{plug} * A_{plug} + q_{ann} * A_{ann} \quad 6.2.5$$

where, $q_{plug} = qc * (0.8 - 0.7 * FFR)$ and $q_{ann} = qc$, with FFR the final filling ratio, and A_{ann} and A_{plug} the pile annulus and plug areas, respectively. In case of closed-ended piles $q_p = qc$.

Additionally, according to the authors, the value of n in [6.2.3] is calculated by equating its prediction of $q_{b0.1}$ for $\frac{w_b}{D} = 0.1$ with [6.2.6], which is how UWA-05 calculates $q_{b0.1}$.

$$q_{b0.1} = q_{c,avg} * (0.15 + 0.45 * A_{rb,eff}) \quad 6.2.6$$

Lehane et al (2020b) suggested the following formulation, [6.2.7] to produce an idealized base load transfer curve, when using the Unified Method. The Gavin and Lehane (2007) model presented earlier, is actually a general format of equation [6.2.7], as the authors suggest, and moreover, this formula approximates the recommended API (2011) base-displacement model. The base load displacement curve produced by this equation, was in good agreement with base responses measured in tests. Measurements only for closed-ended piles were available though.

$$\frac{w_b}{D} = 0.01 * \left(\frac{\frac{q_b}{q_{b0.1}}}{1 - 0.9 * \frac{q_b}{q_{b0.1}}} \right) \quad 6.2.7$$

It should be mentioned, that [6.2.7] is easier to use than the equations presented for the Gavin and Lehane (2007) model, as the latter model needs calibration of the n value, as well as a very careful estimation of the initial soil stiffness.

Finally, Table 6.2-1 presents recommended values for estimating the pile base response, available in the API (2000) edition.

Table 6.2-1: API (2000) recommendations for idealized base load transfer curves.

$\frac{w_b}{D}$	$\frac{q_b}{q_{b0.1}}$
0.002	0.25
0.013	0.5
0.042	0.75
0.073	0.9
0.1	1

These three models are presented in this Chapter, because an attempt will be made to define a base resistance for the toe model of the Unified Method, during driving. Assuming a typical quake value of $2.5\,mm$, a corresponding toe resistance will be calculated using one of these models. For that reason, a recent case study (Han et al (2020)) will be investigated, in order to examine the performance of these models, when the equations of the Unified Method are utilized.

Evaluation of Q - z curves based on a case study

Han et al (2020) used a twin-walled instrumented $660\,mm$ diameter pile with a wall thickness of $38\,mm$ and measured plug and steel annular resistances, as well as residual loads after the installation. The pile also partially plugged during driving, with a PLR of 77.7%. Using the equations of the Unified Method and the base displacement models presented earlier, an attempt will be made to approach the actual base response of the pile, in order to examine the applicability of the three aforementioned Q - z models in combination with the Unified Method. This case study will also show how the base formulation [4.5.6] performs in predicting the annular and plug resistance at displacements of $0.1 * D$.

Han et al (2020) measured explicitly the inner plug and tip annular resistances, alongside with the corresponding residual loads. Because [4.5.6] of the Unified Method is applied on the entire base area of the pile and accounts for both the tip and plug resistance, the resistances measured [kN], including the residual loads, were added together and divided by the total pile base area, in order for comparisons to be possible.

Table 6.2-2 below, shows the measured resistances, after being modified to correspond to the entire base area.

Table 6.2-2: Cumulative measured resistance at the entire pile base area, Han et al (2020).

$\frac{w_b}{D}$	q_b (cumulative pressure in the entire base area - including residual loads), [MPa]
0.05	5.2
0.1	7.4
0.225	10

Thus, in order to produce predictions of idealized base load transfer curves, the aforementioned equations have been utilized, in which $q_{b0.1}$ in all the equations presented is estimated by the Unified Method, using [4.5.6]. It should be clarified that for [6.2.1], the Young modulus in small strains (v assumed 0.1 Gavin and Lehane (2007)) is calculated by [6.2.8] below, proposed by Baldi et al (1989).

$$E_0 = 2 * (1 + v) * G_0 \quad with \quad G_0 \approx qc \cdot * 185 * q_{c1N}^{-0.75} \qquad 6.2.8$$

in which, $q_{c1N} = (qc/Pa) * \left(\frac{\sigma'_{vo}}{Pa}\right)^{0.5}$.

Additionally, the value of n in [6.2.3] is calculated by equating its prediction of $q_{b0.1}$ for $\frac{w_b}{D} = 0.1$ with [4.5.6]. A best fit was found when $n \approx 0.12$.

Moreover, [6.2.9] was developed, in order to approximate the curve suggested by API (2000) in Table 6.2-1. Again for $q_{b0.1}$, equation [4.5.6] has been used, and it is also denoted as $qb_{0.1,UM}$ in [6.2.9] for clarity.

$$\frac{qb}{qb_{0.1,UM}} = 2.23 * (\frac{w_b}{D})^{0.347} + \frac{q_{res}}{qb_{0.1,UM}} \quad with\ w_b/D \leq 0.1 \qquad 6.2.9$$

Finally, it is mentioned that the residual loads are about 4% of the qc value (or about 14% the $qb_{0.1,UM}$), assuming that they are applied on the entire base area. Figure 6.2-2 below depicts the idealized base load transfer curves produced with the aforementioned models and by incorporating the formulations of the Unified Method.

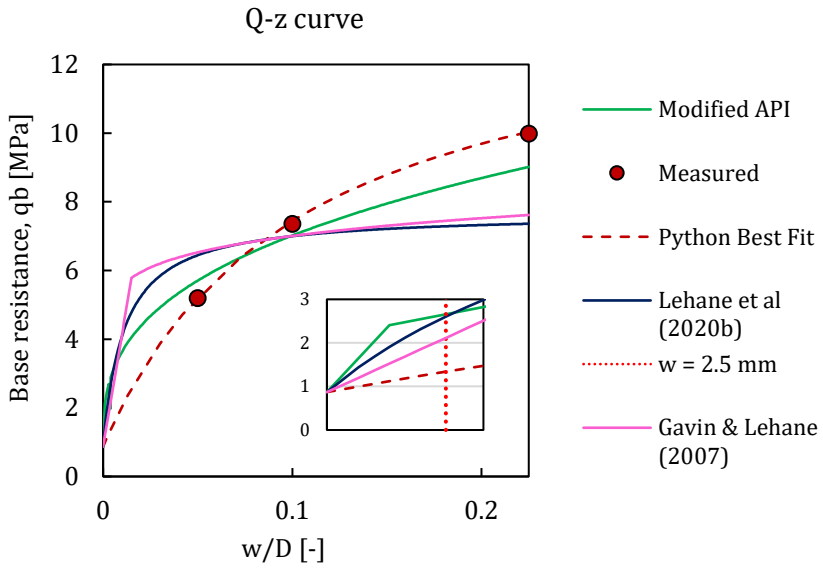

Figure 6.2-2: Idealized base load transfer curves produced for the case examined by Han et al (2020).

What should be highlighted first from Figure 6.2-2, is that the Unified Method leads to an excellent estimation of the resistance mobilized at $0.1 * D$ displacements, for a partially plugged pile. Moreover, it is mentioned that the aforementioned models are suitable for pile tip displacements up to $0.1 * D$. Additionally, by observing Figure 6.2-2, it can be said that the models produce a similar base displacement response, but better results have been produced with [6.2.9], the modified API curve. For that reason, it is also used to modify the toe resistance of the Unified Method.

Specifically, by utilizing [6.2.9], using various pile diameters and pile tip displacements induced per hammer blow, one can define the percentage of total base resistance mobilized during driving.

For the Amaliahaven steel open-ended piles, with diameter $1.42\,m$, Table 6.2-3 below presents the various ratios of $\frac{qb}{qb_{0.1,UM}}$.

While Paik et al (2003) measured that residual stresses were in the range of $11-14\%$ of the CPT qc for $356\,mm$ (diameter) open and closed-ended piles in dense sand, Byrne et al (2018) suggested values $1-10\%$ of the qc in medium dense sands for large offshore steel open-ended monopiles. Clearly, there is an uncertainty on the residual loads, and thus a 10% of the $qb_{0.1,UM}$ (a bit lower than 14% of $qb_{0.1,UM}$ measured by Han et al (2020) for a pile with diameter of $660\,mm$) is incorporated in [6.2.9], for all the post-predictions to be presented.

Table 6.2-3: Various ratios of $\frac{qb}{qb_{0.1,UM}}$, based on displacements induced per hammer blow. Residual loads of $10\%\ qb_{0.1,UM}$ are included in the values presented below.

Diamter [mm]		1420	
Blows/0.25m	mm/Blow	w_b/D	qb/qb_{01}
10	25.0	0.0176	0.65
15	16.7	0.0117	0.58
20	12.5	0.0088	0.53
25	10.0	0.0070	0.50
30	8.3	0.0059	0.47
35	7.1	0.0050	0.46
40	6.3	0.0044	0.44
45	5.6	0.0039	0.43
50	5.0	0.0035	0.41
55	4.5	0.0032	0.40
60	4.2	0.0029	0.39
65	3.8	0.0027	0.39
70	3.6	0.0025	0.38
75	3.3	0.0023	0.37
80	3.1	0.0022	0.37
85	2.9	0.0021	0.36
90	2.8	0.0020	0.36
95	2.6	0.0019	0.35
100	2.5	0.0018	0.35
115	2.2	0.0015	0.34
120	2.1	0.0015	0.33
125	2.0	0.0014	0.33

Therefore, it can be seen from Table 6.2-3 that a toe resistance of about 0.35 is mobilized for a typical quake value of $2.5\ mm$ (including 10% increase for residual loads as mentioned earlier). Thus, the toe resistance during driving is formulated as can be seen in [6.2.10]:

$$qb_{SRD} = 2.23 * (\frac{w_b}{D})^{0.347} * (0.12 + 0.38 * A_{re}) * qc + q_{res} \qquad 6.2.10$$

in which, $q_{res} = 0.1 * (0.12 + 0.38 * A_{re}) * qc$. It is mentioned here that, as the initial toe model, the modified version is also applied in the entire base area. Using then equation

[6.2.10], one can plot the range of $\frac{qb}{qb_{0.1,UM}}$ (with or without residual loads) for various normalized to diameter toe displacements, as can be seen in Figure 6.2-3, which includes the aforementioned $10\%\ qb_{0.1,UM}$ of residual loads.

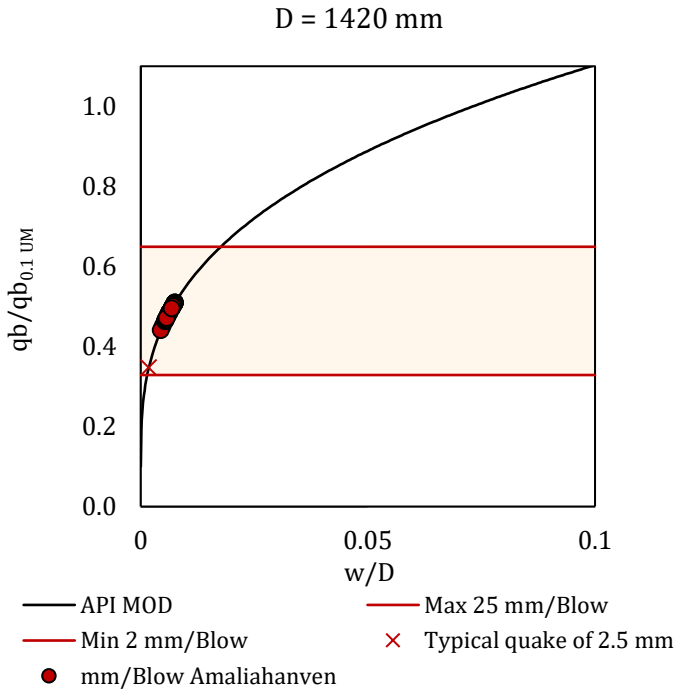

Figure 6.2-3: Idealized base load transfer load and base resistance mobilization from the blow counts of the Amaliahaven project (both APM and RWG sites). Residual loads are included.

One should also notice though, that some pile tip displacements per one hammer blow might not be representative as to define a $\frac{qb}{qb_{0.1,UM}}$ ratio, as for example, the case of 10 blows/0.25 m for a large offshore pile, which is not common (Table 6.2-3). Typically, blows/0.25 m are in the range of $20-40$ blows/0.25 m for normal driving conditions.

Figure 6.2-3, includes also average $\frac{qb}{qb_{0.1,UM}}$ ratios, or the average toe resistance mobilized during driving of the Amaliahaven piles (including $10\%\ qb_{0.1,UM}$ of residual loads). Although for driveability post-predictions, 10 piles have been used, 5 for the APM and 5 for the RWG terminal, Figure 6.2-3 includes the aforementioned ratios of 33 piles across the entire port extension (from both terminals). For clarity, the aforementioned ratios are also plotted separately in Figure 6.2-4.

Since the blows/0.25 m of the Amaliahaven project are more or less constant with depth (for example see Figure 5.2-6), this allowed to define average blows/0.25 m for the entire

installation of each of the examined piles, from which, an average penetration in mm per one blow was estimated (for each and every of the 33 piles). Doing this procedure, one can define the mobilized toe resistance using [6.2.10] for all the piles (red dots in Figure 6.2-3). It is mentioned again that for this procedure (Table 6.2-3, Figure 6.2-3), residual loads were taken into account. APPENDIX C includes ratios of $\frac{qb}{qb_{0.1,UM}}$ and $\frac{w_b}{D}$ for various pile diameters (Table C 1), but in this case *no residual loads* have been applied, so that the user can select the most suitable residual load based on their case.

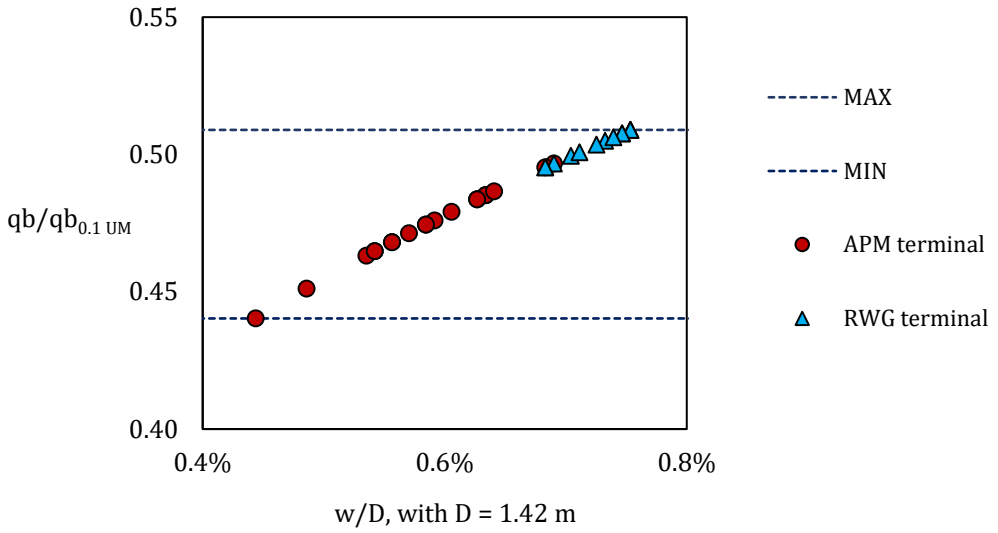

Figure 6.2-4: $\frac{qb}{qb_{0.1,UM}}$ ratios calculated from mm/blow of the Amaliahaven project from 33 piles across the entire site. Residual loads of 10% $qb_{0.1,UM}$ are included.

6.3 Evaluation of the Unified SRD Method

The formulas suggested for the Unified SRD Method (modified format of the Unified Method) are listed in Table 6.3-1, below.

Table 6.3-1: Unified SRD Method suggested driveability formulas.

Unified SRD Method	
Shaft Resistance	$Q_{shaft} = \pi * D * \int_0^L tf_{SRD} dz$
	$\tau f_{SRD} = set\_up * \left((q_c/44) * A_{re}^{0.3} * \left[\max\left(1, \frac{h}{D}\right) \right]^{-0.4} + \Delta\sigma'_{rd} \right) * tan\delta_f$ with $set\_up = 0.7$ and $\delta_f = 29^0$
	$A_{re} = 1 - PLR * \left(\frac{D_i}{D}\right)^2$ and $PLR = \tanh\left[0.3 * \left(\frac{D_i}{D_{CPT}}\right)^{0.5}\right]$
	$\Delta\sigma'_{rd} = \left(\frac{q_c}{10}\right) * \left(\frac{q_c}{\sigma'_v}\right)^{-0.33} * \left(\frac{D_{CPT}}{D}\right)$
Toe Resistance	$Q_b = q_{b_{SRD}} * \pi * \frac{D^2}{4}$
	$qb_{SRD} = 2.23 * \left(\frac{w_b}{D}\right)^{0.347} * (0.12 + 0.38 * A_{re}) * qc + q_{res}$ with a typical $w_b = 2.5\,mm$ and $q_{res} = 0.1 * (0.12 + 0.38 * A_{re}) * qc$

Driveability post-predictions, as those presented in Chapter 5, have also been made for the Unified SRD Method for 10 piles of the Amaliahaven project, 5 for each of the APM and RWG sites. Here the predictions of 4 piles are presented (Figure 6.3-1, Figure 6.3-2, Figure 6.3-3, Figure 6.3-4), while the rest can be found in APPENDIX D (Figure D 1, Figure D 2, Figure D 3, Figure D 4, Figure D 5, Figure D 6). Quake and damping factors for the toe and shaft models are the same as those presented in Table 5.3-1. The only difference is that an average $qc +/-4Deq$ has been used in order to avoid a greater average of the qc values, which could be more appropriate for pile design.

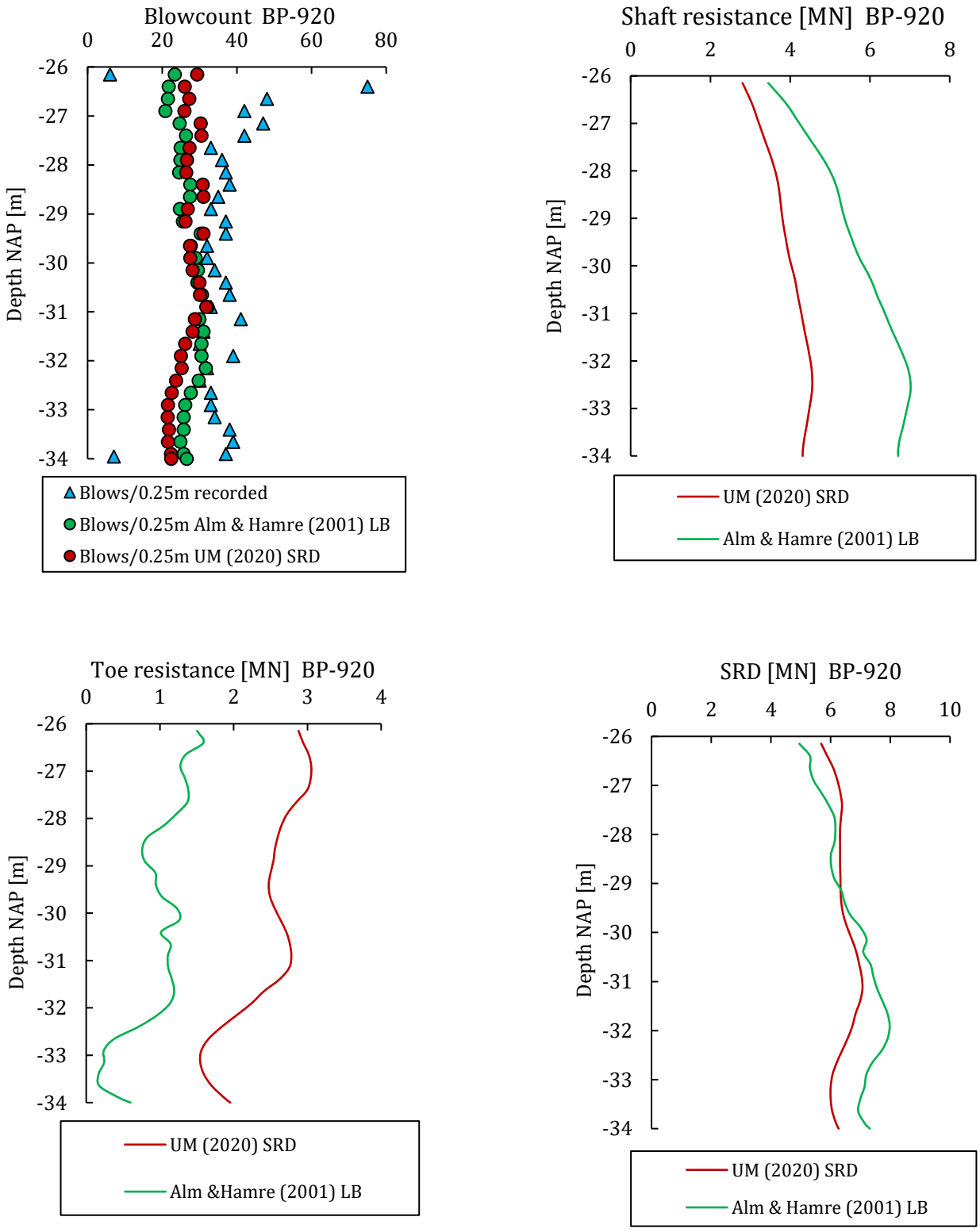

Figure 6.3-1: Driveability post-prediction for combi-wall pile BP-920, using Alm & Hamre (2001) and the Unified SRD Method models. APM terminal.

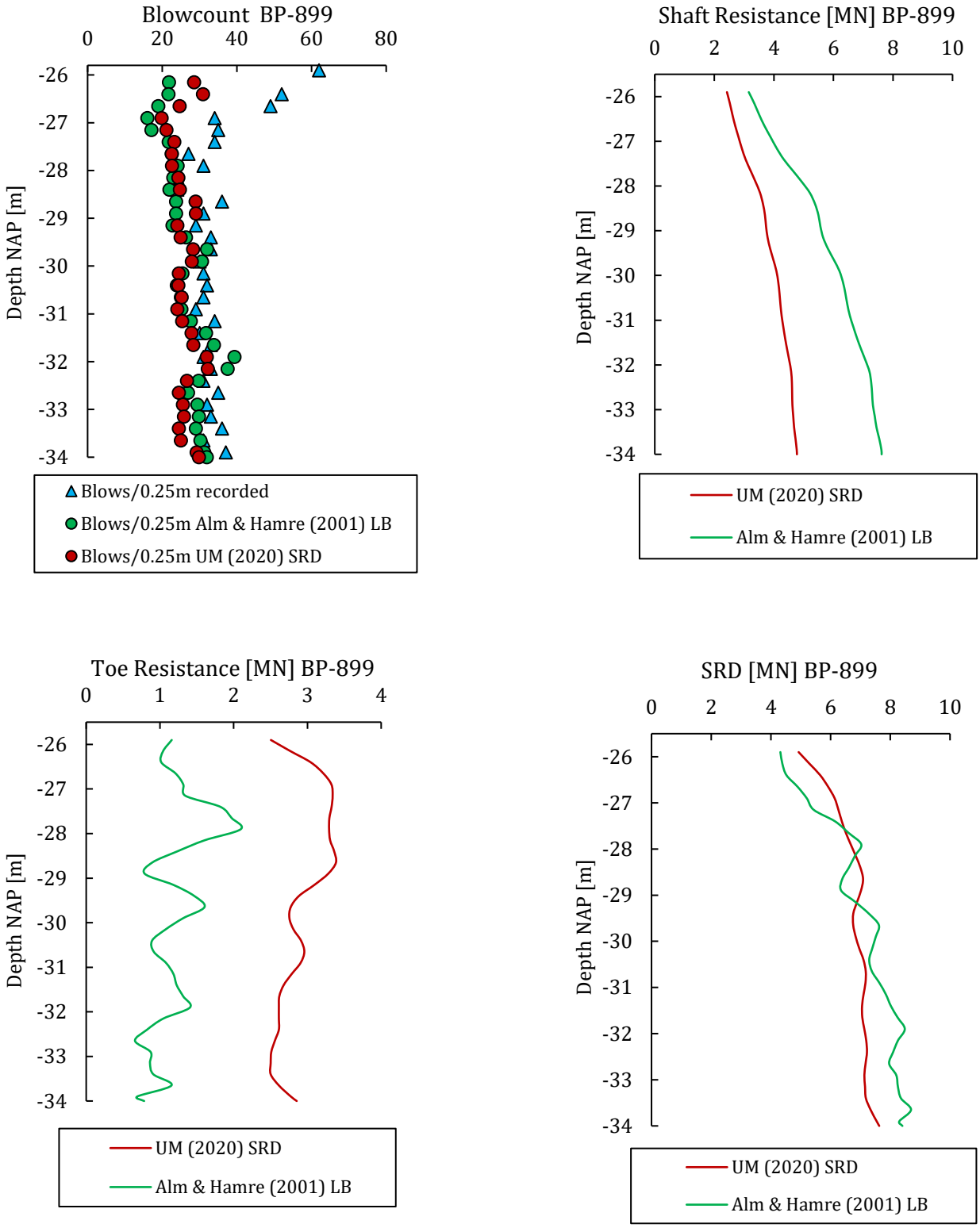

Figure 6.3-2: Driveability post-prediction for combi-wall pile BP-920, using Alm & Hamre (2001) and the Unified SRD Method models. APM terminal.

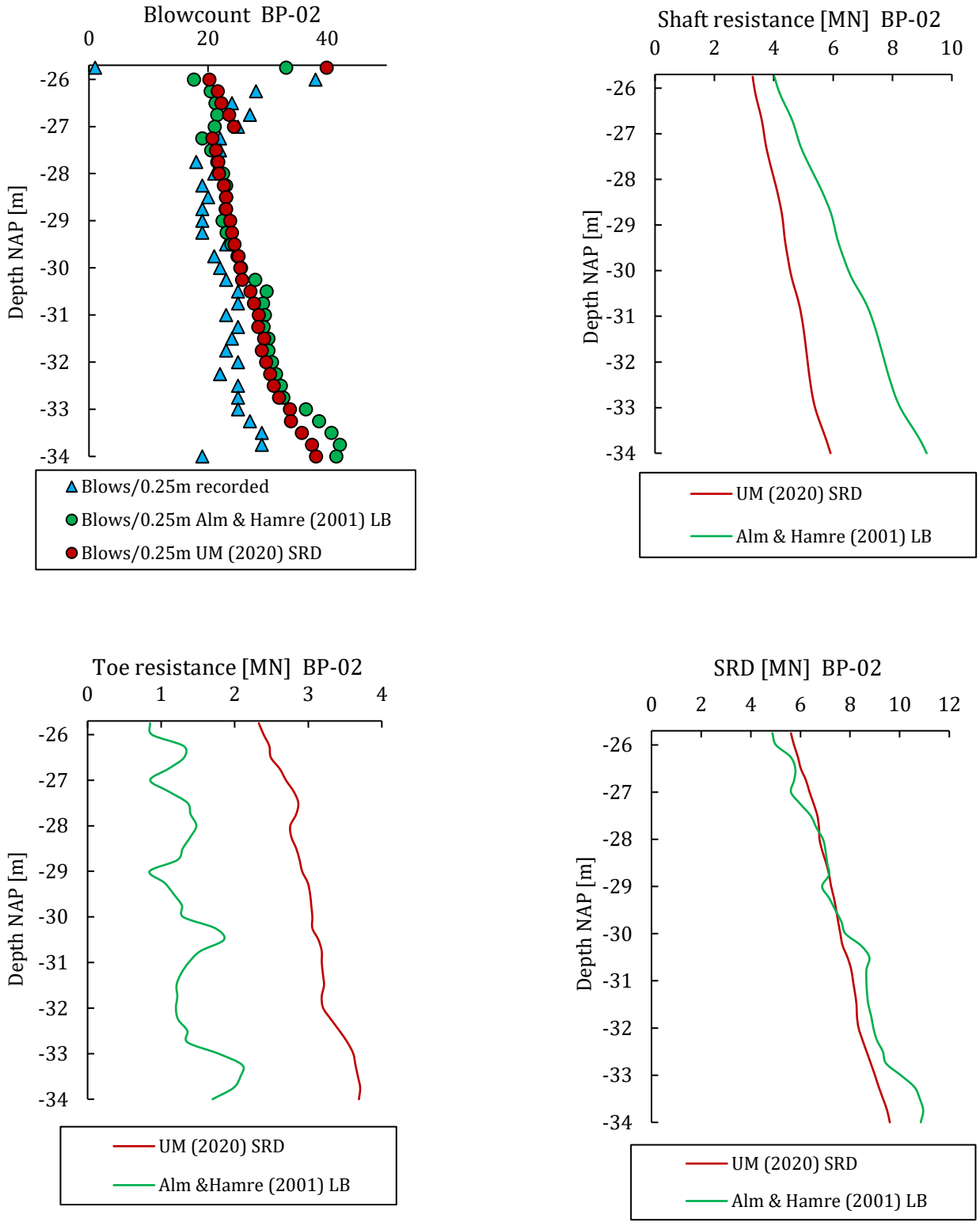

Figure 6.3-3: Driveability post-prediction for combi-wall pile BP-899, using Alm & Hamre (2001) and the Unified SRD Method models. RWG terminal.

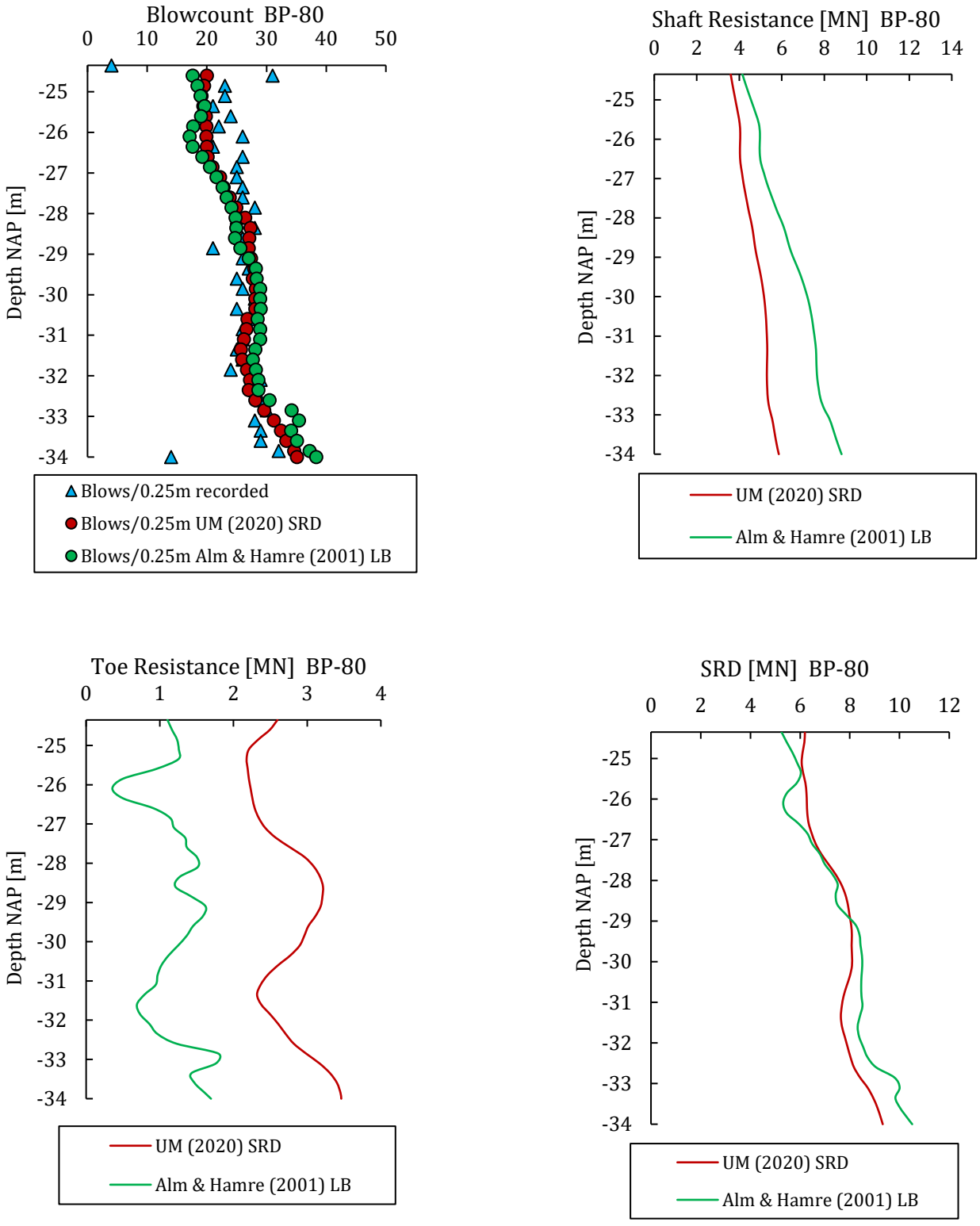

Figure 6.3-4: Driveability post-prediction for combi-wall pile BP-80, using Alm & Hamre (2001) and the Unified SRD Method models. RWG terminal.

Overall performance

The % Match and % Under, as were described at the end of Chapter 5.2, are presented in Table 6.3-2 to examine the overall performance of the Unified SRD Method, Alm & Hamre (2001) and Stevens et al (1982) models. The performance of the Unified SRD Method against the other 2 models is also depicted in Figure 6.3-5.

Table 6.3-2: Percentage of match (% Match) between recorded and predicted blow count curves using the Unified SRD Method, Alm & Hamre (2001) and Stevens et al (1982) models for the Amaliahaven steel open-ended tubular piles. The % Under shows the percentage of the predicted blow count curve that lies below the recorded one (underestimation of blow counts).

	Alm & Hamre (2001)		Unified SRD Method		Stevens et al (1982)	
	% Match	% Under	% Match	% Under	% Match	% Under
BP-920	77 %	88 %	75 %	94 %	78 %	33 %
BP-899	79 %	82 %	80 %	88 %	76 %	39 %
BP-853	78 %	70 %	84 %	76 %	89 %	58 %
BP-838	76 %	77 %	79 %	84 %	88 %	48 %
BP-800	86 %	59 %	88 %	88 %	78 %	44 %
BP-02	77 %	21 %	82 %	21 %	61 %	6 %
BP-33	83 %	38 %	87 %	30 %	68 %	11 %
BP-48	87 %	56 %	87 %	56 %	81 %	17 %
BP-64	83 %	43 %	86 %	36 %	75 %	29 %
BP-80	87 %	45 %	91 %	45 %	71 %	15 %

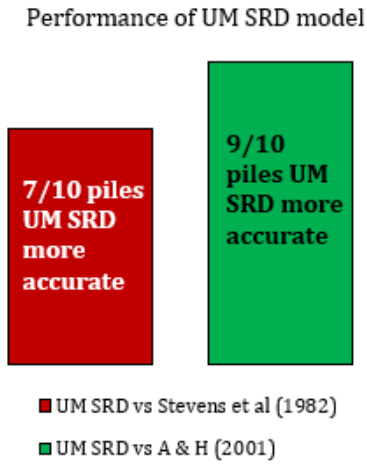

Figure 6.3-5: Performance of Unified SRD Method against Alm & Hamre (2001) and Stevens et al (1982) models for the Amaliahaven piles.

From the post-predictions made for the Amaliahaven piles of both sites, APM and RWG terminals, it can be observed that the modified format of the Unified Method, referred to as Unified SRD Method (UM (2020) SRD), leads to better SRD estimations than the other models examined (Table 6.3-2, Figure 6.3-5).

It can be said that for large offshore open-ended tubular piles, as those utilized in the Amaliahaven project, both the Unified SRD Method and Alm & Hamre (2001) model resulted in very good post-predictions, although the Unified Method has been calibrated for smaller diameter piles (< 800), in contrast to the Alm & Hamre (2001) method that was calibrated based on pile diameters in the range of about $0.76 - 2.7\,m$.

It was noticed in Chapter 5.3 that the shaft resistances produced with the unmodified Unified Method and the Alm & Hamre (2001) model were very similar in shape and magnitude. However, the Unified Method is basically an axial capacity pile design method, and the shaft resistance produced, is referred to external shaft capacity developed around 2 weeks after installation. Therefore, it is very important to re-calibrate it so that it represents shaft resistances during driving, and thus a set up factor was utilized. Moreover, it was mentioned at the beginning of this Chapter that the shaft model of this method already incorporates factors that are important (for the shaft resistance) and affect both predicted driveability and capacity, such as friction fatigue and the degree of soil displacements during installation (A_{re}). Additionally, it was also observed that the Alm & Hamre (2001) model might lead to higher shaft resistances, because it incorporates the inner plug resistance (inner shaft friction) to the external shaft formulation [4.4.1]. Therefore, it is reasonable to expect that the Unified SRD Method will estimate lower shaft resistances than the Alm & Hamre (2001) model, for fully coring piles.

On the other hand, the toe model of the Unified SRD Method incorporates the plug resistance by utilizing the A_{re} factor, which is a function of PLR. The initial resistance was calibrated to toe resistance during driving by utilizing equation [6.2.10], assuming a typical quake value of $2.5\,mm$. Since the end bearing pressure is applied on the entire base area (steel annulus and plug area) it is reasonable to lead to higher toe resistances than the Alm & Hamre (2001) model, which applies the toe resistance only at the pile annulus.

With the aforementioned observations, it is reasonable to expect similar SRDs from these two models, for fully coring piles. However, the main factor that leads to better overall predictions by the Unified SRD Method, is the incorporation to the equations of both the shaft and the toe of the A_{re}, which allows to take into account the effect of the degree of soil displacements on the radial effective stresses, and account for inner plug resistance.

7. Application to other Case Studies

In this Chapter, three case studies are also examined, in which the predicted blows/0.25 m of the Unified SRD Method are compared to those of the Alm & Hamre (2001) model and the actual - recorded ones. The projects that are used for further comparison are the SIF, HHTT and Euripides. The results of the post-predictions are presented in Chapter 7.1, while 7.2 includes a discussion with respect to the SRD estimations made for all of the three case studies examined.

7.1 SIF, HHTT & EURIPIDES Projects

The piles' length, diameter and wall thickness, as well as the hammers used, are presented below, in Table 7.1-1, while, Figure 7.1-1 and Figure 7.1-2 show the locations of the projects. A short description of the projects follows. All soil profiles consist of dense sand.

Table 7.1-1: Pile properties and hammers used for SIF, HHT and Euripides project.

		Pile	Hammer
SIF	Length [m]	32.28	
	Diameter [m]	1.42	Delmag D100-13
	Wall thickness [mm]	21	
	Number of piles examined	2	
HHT	Length [m]	35.3	
	Diameter [m]	1.42	IHC S-280
	Wall thickness [mm]	18 - 24	
	Number of piles examined	4	
EURIPIDES	Length [m]	47	
	Diameter [m]	0.762	IHC S-90
	Wall thickness [mm]	36	
	Number of piles examined	1 (re-driven in second location)	

Figure 7.1-1: Location of APM, RWG, SIF and HHT terminals in the Maasvlakte area (photo taken from Google Earth, 2022).

Figure 7.1-2: Eemshaven. Location of the Euripides project area (photo taken from Google Earth, 2022).

Similar to the Amaliahaven project, with the expansion of the APM and RWG terminals, the SIF project is about the construction of a deep sea quay wall with a retaining height of about $30\,m$ in the Arianehaven of Rotterdam, Maasvlakte. The project was completed around December, 2021. The expansion of the SIF terminal fits in with the Port Authority's aim to play an important role in the development of offshore wind projects in the North Sea. This expansion of the quay wall gives SIF the opportunity to expand its services to the offshore wind industry by taking care of the storage, construction and supply of the turbines, blades and towers for offshore wind farms. In addition, the HHTT project is also about the construction of a deep sea quay wall which was completed around December 2019, in the Rotterdam, Maasvlakte area. The project involved the construction of a 1200 m long deep sea quay wall for large sea vessels, and the connection of the new quay to the existing quay, a quay wall over a length of 1000 m for five inland vessels. Both projects used combined walls with steel open-ended tubular piles, as in the case of the Amaliahaven project. More information about these projects can be found on the official website of the Port of Rotterdam.

Moreover, an extensive axial pile load testing program was conducted under a joint industry project by Fugro Engineers of The Netherlands and Geodia S.A. of France on a highly-instrumented 0.76 m outer diameter pipe pile driven open-ended in very dense sands at Eemshaven, The Netherlands (Figure 7.1-2). The project is known as EURIPIDES (European initiative on piles in dense sands), and the pile load tests were performed to obtain reliable data in order to improve offshore pile design criteria. The program consisted of a series of static compression, tension and cyclic load tests. Details can be found in the papers of Niazi et al (2010), Schneider et al (2010), and Xu et al (2008).

For the SIF project only 2 piles are examined, as measured energy wasn't obtained for the purposes of this Thesis. It is mentioned that hammer energy is a very important factor for a reliable driveability prediction. When doing post-predictions though, in order to evaluate how the soil model estimates driving resistances, it is required to constrain the variables only to the soil models used. Thus, in a pile-hammer-soil system, in which the variables are both the hammer energy and the soil model, uncertainty increases. Therefore, an assumption is made for the ratios of potential to rated energy, and impact to potential energy, as done in practice for actual driveability predictions. Specifically, the aforementioned energy ratios are assumed to be 60% and 80%, respectively, which means a constant stroke height of about $2\,m$ and impact energy 80% of potential energy, which is the suggested value for diesel hammers in commonly used driveability software. A square hammer cushion has been used (steel cables), with side of $1\,m$ and $60\,mm$ thickness, according to the records collected. Figure 7.1-3 below shows the CPTs for the 2 piles as well as the qc values from the CPTs with the recorded blows/0.25 m.

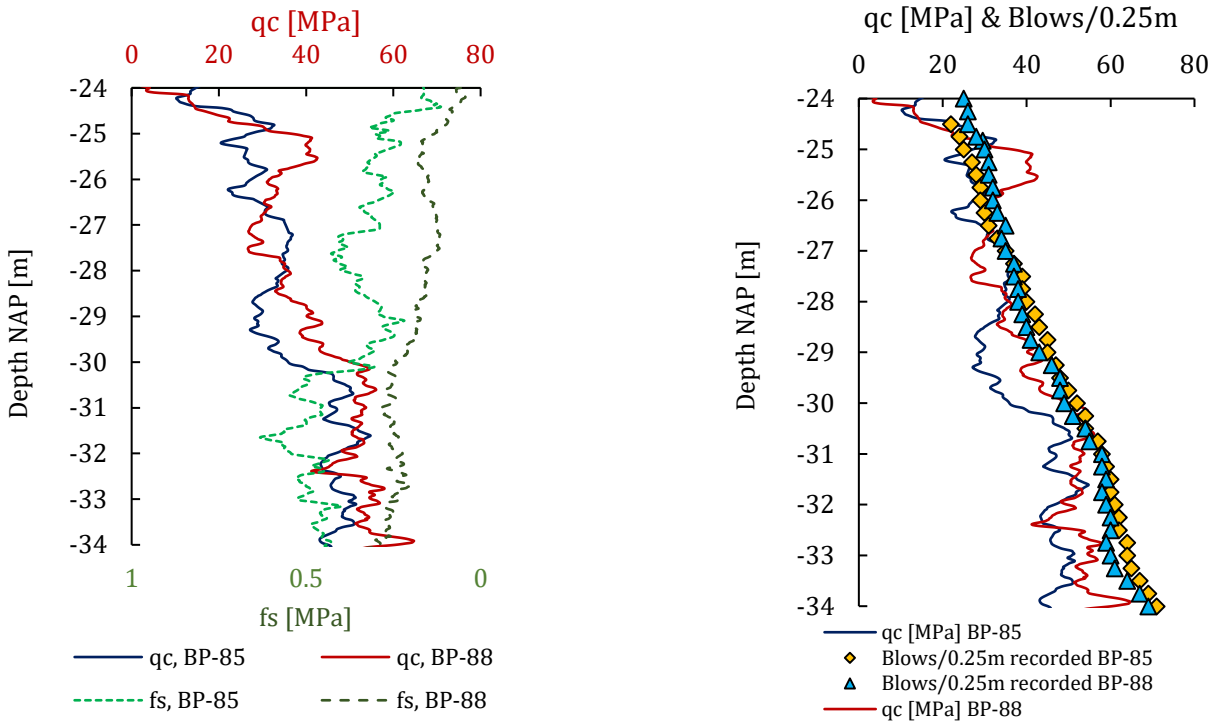

Figure 7.1-3: CPTs and blows/0.25 m from SIF project for the two piles examined.

It can be seen in Figure 7.1-3 that the blow counts recorded follow the trend of the CPTs, which are the closest CPTs to the piles examined, performed prior to installation of the combi wall piles, prior to excavation that took place, similarly to the Amaliahaven project. It is referred here that the ground surface was initially at around $5-6\,m$ from NAP, while the working level was around $-2\,m$ from NAP. Moreover, the water table was lowered at $-3\,m$ NAP during construction works.

In Figure 7.1-4, the blows/0.25 m are presented, as estimated by the Unified SRD Method and the Alm & Hamre (2001) model. As mentioned, the impact energy is assumed constant, as well as the stroke height of the ram.

For comparison, a much more unconservative analysis is also presented in Figure 7.1-5 for pile 88, for which the ratio of potential to rated energy is assumed 1, which means that the ram, during the driving process, will constantly have the maximum stroke height, which for this hammer is about $3.4\,m$. This comparison is performed by using only the Unified SRD Method.

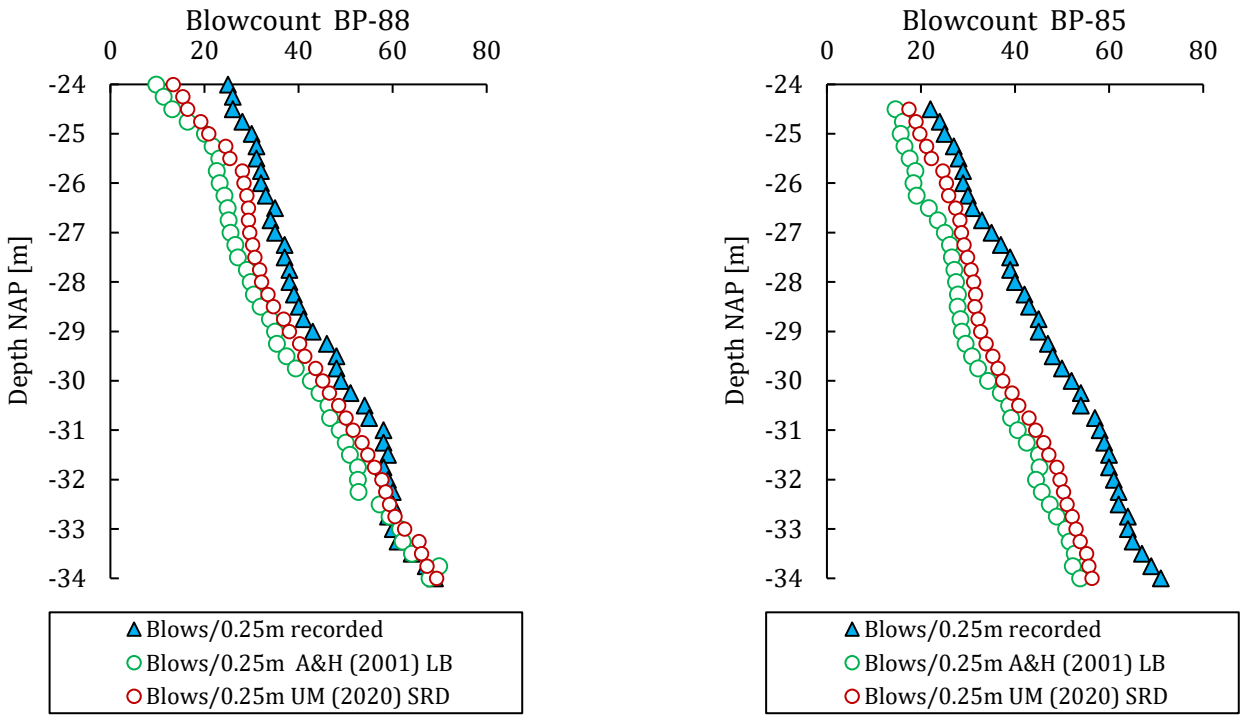

Figure 7.1-4: Blows/0.25 m predicted by Alm & Hamre (2001) model and the Unified SRD Method for BP-88 and BP-85 of the SIF project.

It can be observed from Figure 7.1-5 that the blows/0.25 m predicted using a greater stroke height have reduced and that is because with a lower drop height less energy is produced and installation process becomes more difficult.

Again, it is stated that energy records weren't obtained for the SIF project, and the results produced and presented could be seen as an indication only on how these methods perform in actual predictions. During the driving process, due to losses of energy, or due to not constant hammer strikes, the energy transferred into the piles varies. This variation, which is absent in the current analysis, might be the cause for lower blow counts predictions (BP-85), although the CPTs are very similar. However, both predictions (Figure 7.1-5) are very satisfying, and wouldn't lead to an unconservative or conservative (e.g., higher costs) hammering equipment.

In an actual driveability prediction, in which neither the blow counts nor the driving energy is known, the engineer has to define at least an Upper Bound of the predicted driving resistance, based on the lowest acceptable driving energy for a specific hammer.

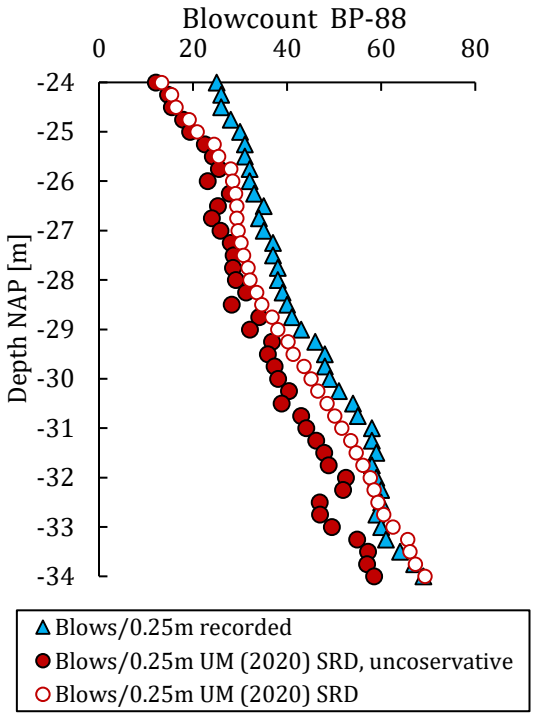

Figure 7.1-5: Comparison of predicted blows/0.25 m using Unified SRD Method, for pile BP-88 of the SIF project, assuming (filled red dots) a constant maximum drop height of 3.4 m, and (not filled red dots) a constant drop height of 2 m.

From the HHTT project 4 piles are examined. The CPTs from these piles are presented in Figure 7.1-6. Similarly to the other projects, blow counts have been estimated and compared to recorded ones (Figure 7.1-7, Figure 7.1-8). However, it is mentioned that for these piles impact energy was recorded. Again, no hammer or pile cushion has been used to model the hydraulic hammer. Pile properties can be found in Table 7.1-1. As in the Amaliahaven and SIF projects, an excavation takes place and the ground level during construction is around $-2\,m$ from NAP and the water table at that time around $-3\,m$ from NAP.

It can be observed from Figure 7.1-6 that the qc value, as in the case of the Amaliahaven project, doesn't show a clear depth trend, meaning that the qc mainly fluctuates around a median value rather than increase or decrease with depth. Hence, the blows/0.25 m recorded at both the Amaliahaven and HHTT (at least for the piles examined) are more or less constant for the entire depth. On the other hand, the qc value in the SIF project clearly increases with depth and this is also depicted in the blows/0.25 m. It is mentioned again that all three projects utilize piles with very similar properties.

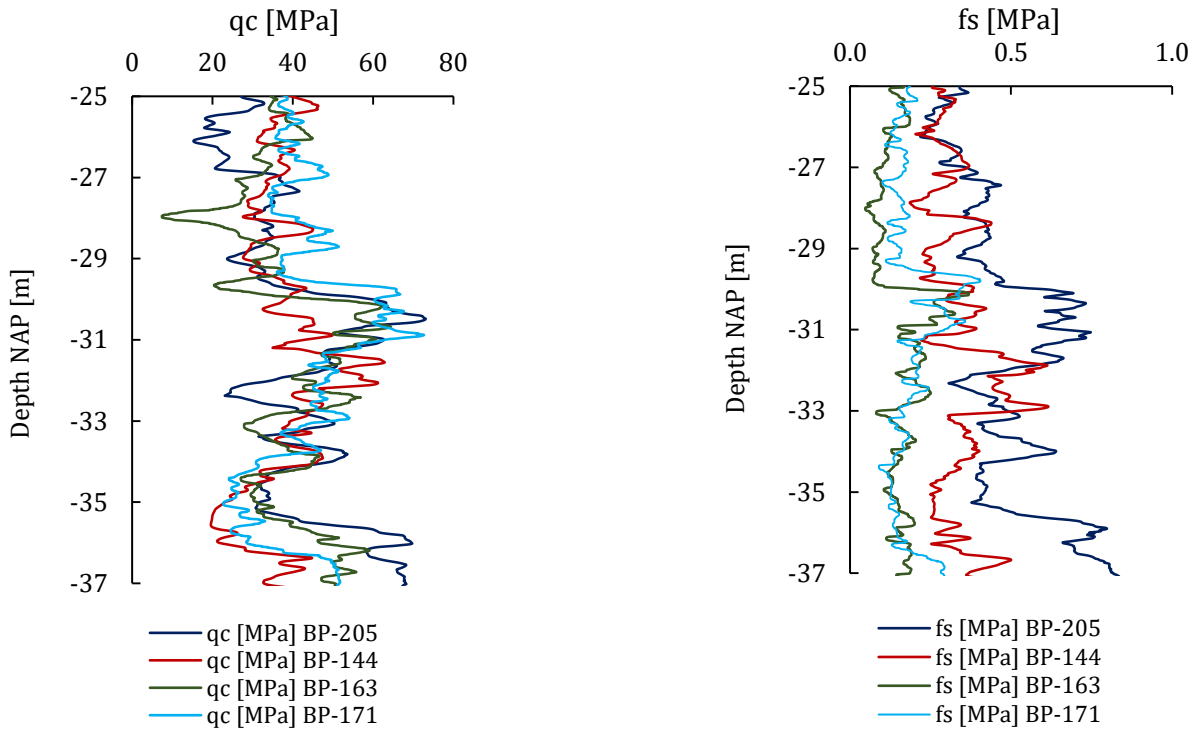

Figure 7.1-6: CPTs from the HHTT project.

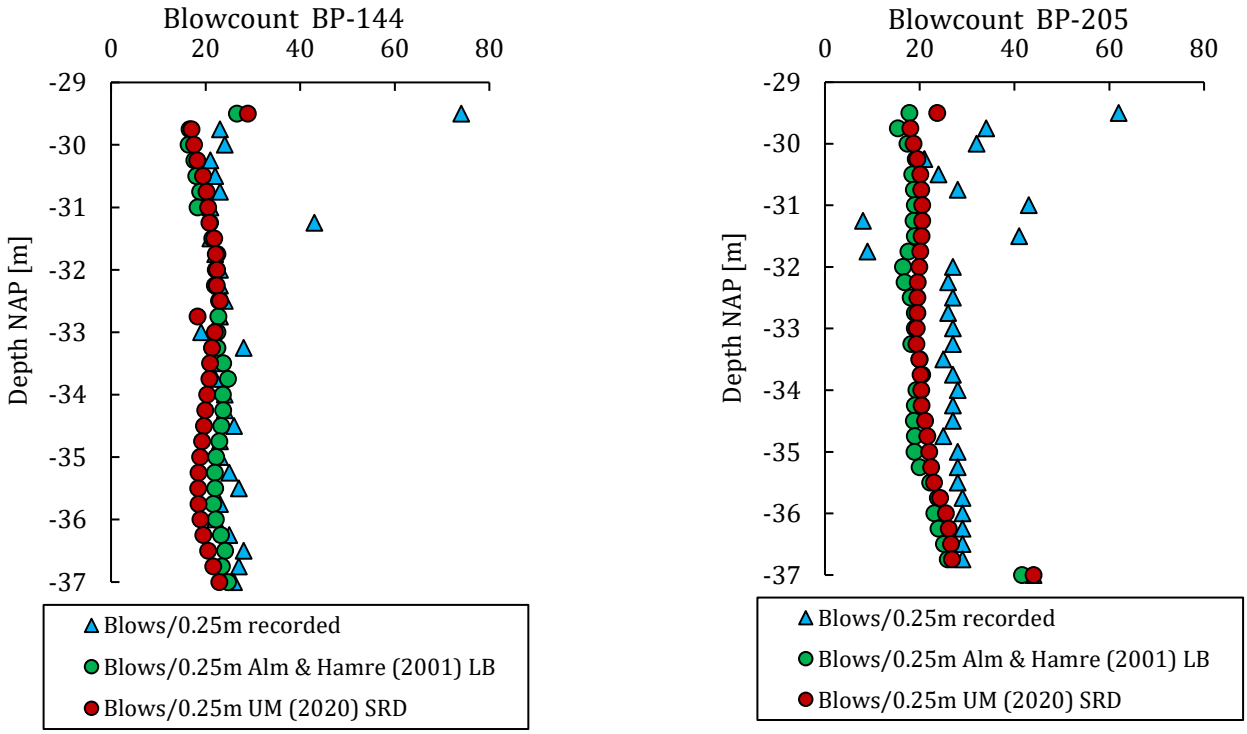

Figure 7.1-7: Blows/0.25 m for piles BP-144 and BP-205 of the HHTT project, produced by the Unified SRD Method and Alm & Hamre (2001) model.

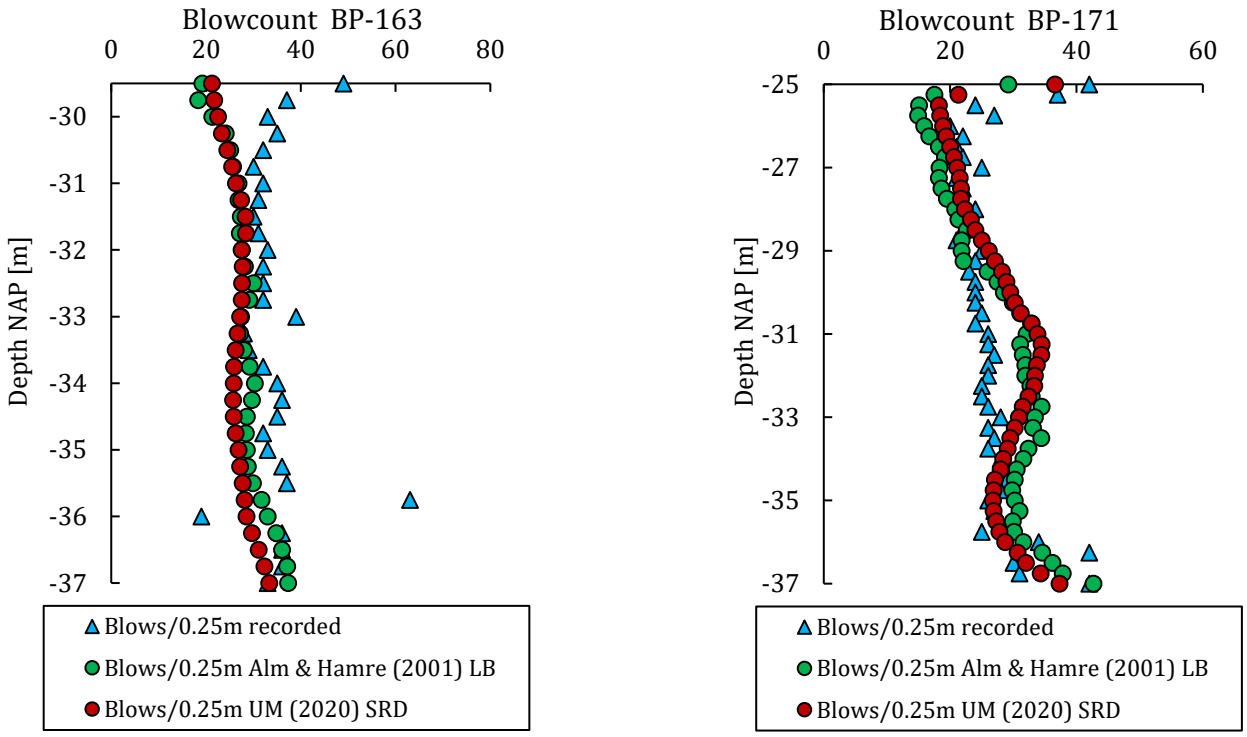

Figure 7.1-8: Blows/0.25 m for piles BP-163 and BP-171 of the HHTT project, produced by the Unified SRD Method and Alm & Hamre (2001) model.

As can be seen from Figure 7.1-7, and Figure 7.1-8, both methods produced an excellent post-prediction for the 4 piles of the HHTT project examined. It is mentioned that some slight overestimations or underestimations of the blow counts are observed without those being that significant.

Finally, the CPTs, as well as the results of the post-predictions of the Unified SRD Method and Alm & Hamre (2001) model for the Euripides project can be seen in Figure 7.1-9 and Figure 7.1-10. Transferred energies were also measured for this project.

In this case, the Unified SRD Method produced very satisfying results, while the Alm & Hamre (2001) model, generally underpredicted the blow counts. It is mentioned that for the Unified SRD Method, equation [6.2.10] leads to a $\frac{qb}{qb_{0.1,UM}}$ ratio of about 0.4 (including $0.1 * qb_{0.1,UM}$ residual loads as in the previous cases).

More details and comments, for all the post-predictions made in this Chapter are included in 7.2.

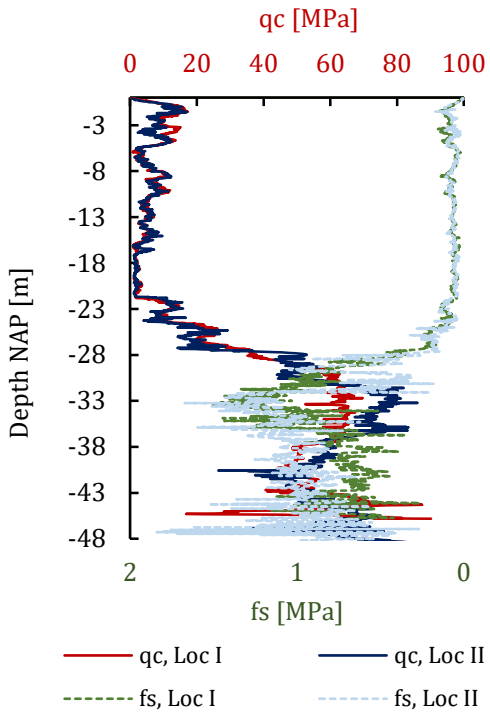

Figure 7.1-9: CPTs of the two locations of the Euripides project.

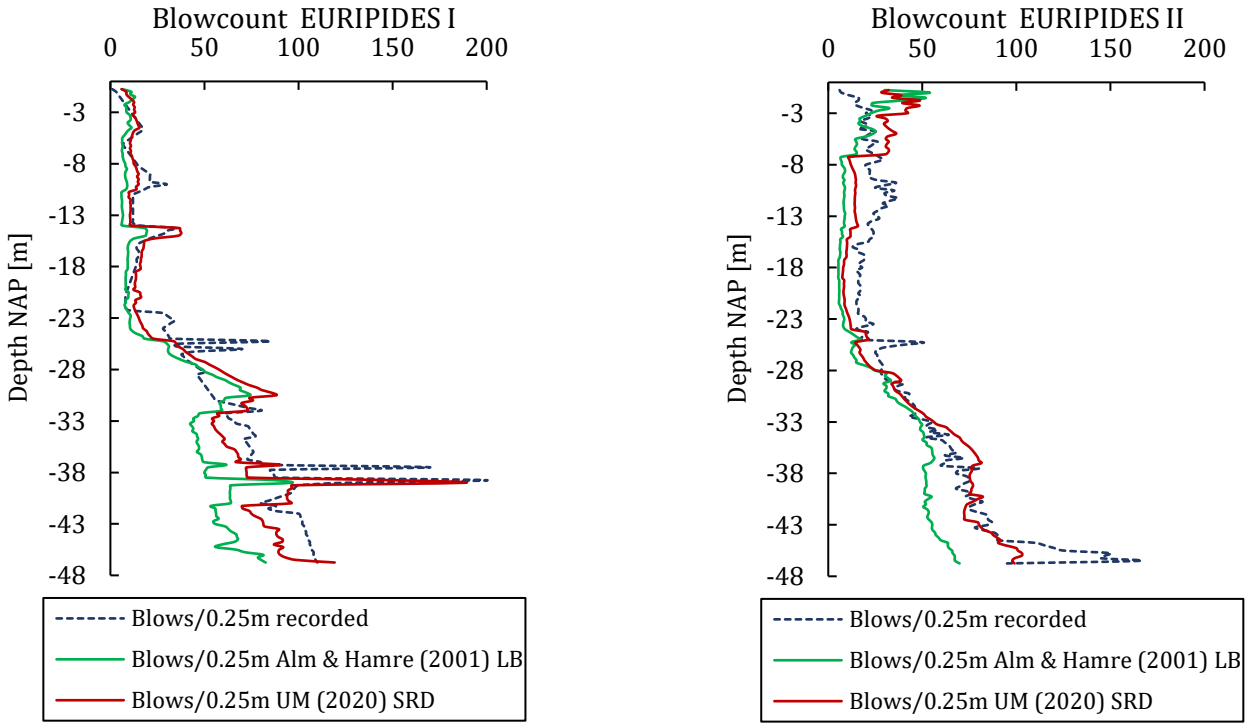

Figure 7.1-10: Blows/0.25 m for the Euripides pile which was driven in location I, extracted and red-driven in location II, utilizing the Unified SRD Method and Alm & Hamre (2001) model.

7.2 Evaluation of the Post-Predictions

Piles with diameters of 0.762 and $1.42\,m$ have been examined in this Chapter, installed in dense sand deposits. It was observed that both the Alm & Hamre (2001) model and the Unified SRD Method, resulted in some very reliable post-predictions for all projects. However, as in the case of the Amaliahaven project, the Unified SRD Method produced more reliable results meaning less average blow count error.

With respect to the SIF project, the post-predictions could be characterized as 'actual predictions', as only the pile properties were known, while the hammer energy was not recorded. Thus, an assumption has been made regarding the ratios of potential to rated energy and impact to potential energy, as mentioned. It is clearly observed in Figure 7.1-5 that assuming maximum energies the blows required to drive the piles reduce. Moreover, it can be said by observing Figure 7.1-4 that the Unified SRD Method resulted in an excellent prediction of blows/0.25 m, considering the uncertainties regarding the hammer energy. This uncertainty is also the cause of underestimation of the blows/0.25 m for pile BP-85 (Figure 7.1-4).

Considering the post-predictions made for the HHTT project, again both methods gave excellent estimation of the blows/0.25 m. For this project, as well as for the SIF and Amaliahaven projects, similar observations can be made. Specifically, with respect to the shaft resistances, the one estimated by the Unified SRD Method is less than the shaft resistance estimated by the Alm & Hamre (2001) model. That happens because, as mentioned in the previous sections, the latter model calculates the total shaft resistance, including the inner plug resistance, while the Unified SRD Method models only the friction developed at the outer shaft area. Moreover, the Unified SRD Method considers the inner plug resistance to the toe formulation, and therefore, it predicts higher toe resistances than the Alm & Hamre (2001) model (and lower shaft resistances). For fully coring piles, as the cases examined, the SRD profiles are eventually very similar.

On the other hand, for smaller diameter piles, (Euripides project), the Unified SRD Method has an advantage over the Alm & Hamre (2001) model, due to the fact that both shaft and toe resistances change based on the diameter and the PLR measurements. Specifically, for this project, an average FFR of 96% was recorded, which means that the pile is almost fully coring and that the shaft friction slightly increases (due to incorporation of the effective area factor, A_{re}). In addition, the $\Delta\sigma'_{rd}$ factor, which increases as the diameter of the pile decreases, leads to higher estimated shaft friction by the Unified SRD

Method. Therefore, by including, also the inner plug resistance to the toe model, (FFR of 96%), the post-predictions made for the Euripides project by this method are in excellent agreement with the records.

Below Figure 7.2-1, shows the shaft friction and toe resistance predicted by the two SRD models for the Location II of the Euripides project (the same trend can be observed for Location I). As can be seen, the difference between the two models is the mobilized shaft friction, while the toe resistances are almost the same. This is also in agreement with the second example case examined in Chapter 5.3. It is also mentioned that the Alm & Hamre (2001) model doesn't include (explicitly) the aforementioned influencing factors and has been calibrated using large offshore - fully coring piles, which explains the underprediction of the blow counts.

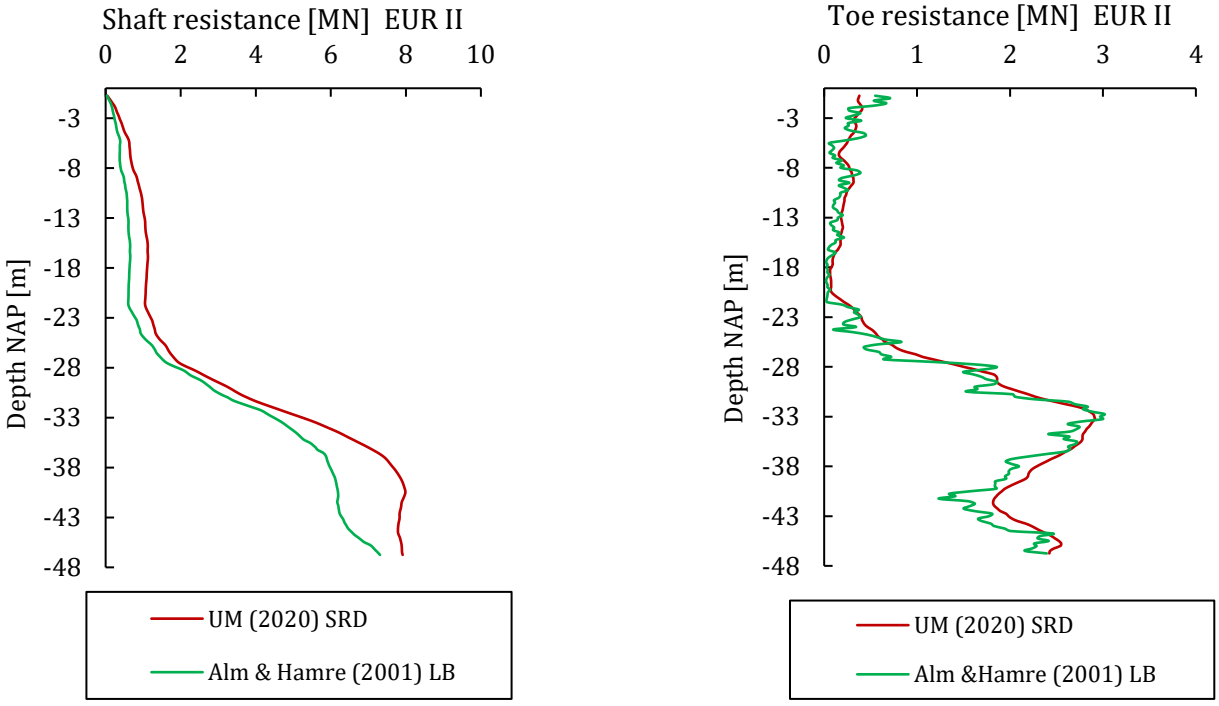

Figure 7.2-1: Shaft and toe resistance for the pile installed in Location II of the Euripides project. Post-predictions made by utilizing the Unified SRD Method and Alm & Hamre (2001) model.

8. Discussion & Conclusions

This Thesis is concluded with this final chapter, in which an overall discussion on the performance of the methods examined is presented. Moreover, an attempt is made to answer to the research questions stated in Chapter 1.3.

8.1 Discussion & Research Questions

Below a discussion is made on the overall performance of the SRD models examined, and answers are given to the research questions stated in Chapter 1.3.

First research question:

- *How reliable are the traditional SRD models in predicting the driveability of the steel open-ended tubular piles of the Amaliahaven project?*

To answer this question, three traditional SRD models have been examined, specifically the Toolan & Fox (1977), Stevens et al (1982), and the Alm & Hamre (2001) models, which estimate the soil Static Resistance during Driving (SRD). Blow counts required to drive 10 steel open-ended tubular piles ($D = 1.42m$) of the Amaliahaven project (APM and RWG sites) have been produced and compared to the actual recorded hammer blows. Most commonly, comparisons of blow count profiles are used to express driving resistance, since they are easy to read and understand. However, it is stated that the number of blows required to drive a pile should always be interpreted based on soil resistance and transferred to the pile hammer energy. The soil profile of the Amaliahaven project consists mainly of dense (silty) sand. In addition, impact hammer energy was also recorded and used in the analysis. More details can be found on Chapters 2 and 4.

From the post-predictions, some general observations regarding the performance of these three models are listed below, while a more detailed analysis follows.

General Observations

- The model suggested by Toolan & Fox (1977) (see also Chapter 4.2) highly overpredicted the blow counts required to drive the Amaliahaven piles (e.g., Figure 5.2-8), and even suggested (falsely) refusal. If this was a prediction, meaning that only the pile properties would have been known, this model would lead to much more expensive hammering equipment (heavier hammer), while the risks of damaging the piles during installation would greatly increase. On the other hand, it could also lead to a conservative re-design or selection of pile properties (e.g., increase thickness to avoid material damage caused by the heavier hammer), increasing as well the overall costs. Furthermore, by overestimating the soil resistance, this method would imply (falsely) that the desirable pile capacity can been achieved in shallower levels.

- On the contrary, Stevens et al (1982) (Lower Bound) model (see also Chapter 4.3), generally produced more reliable blow count profiles compared to the model suggested by Toolan & Fox (1977) (Figure 5.2-7). However, even when utilizing the Lower Bound formulations, an overestimation of the blow counts is evident, especially for the final few meters of penetration. This overprediction mainly occurs due to the fact that both the estimated shaft and toe resistances, which are mainly a function of the vertical effective pre-installation stresses, increase with depth (see equations [4.3.1] and [4.3.2]). Additionally, this model doesn't utilize CPT records of the cone or sleeve resistances.

- The Alm & Hamre (2001) model (see Chapter 4.4) is, in contrary to the other two models, the most frequently used in practice for driveability analysis, as it is based on a calibration procedure, for which, a large database of fully coring open-ended piles with diameters mainly in the range of about $1 - 2.7\,m$ was utilized. By correlating both shaft and toe resistances with the cone resistance from CPTs, and by incorporating the friction fatigue effect in the shaft formulation [4.4.1], it leads to the most reliable results between the methods examined.

Toolan & Fox (1977)

Shaft friction

The unit shaft friction mobilized during pile driving is estimated as the qc value from the CPT divided by a constant factor, specifically 300 [4.2.1] and it is applied both in the outer and inner shaft area. Issues with this approach are summarized below:

- This factor (300) is probably project specific, and keeping it constant might not be ideal for various soil conditions, e.g., silty sand, medium sand, dense sand, etc.

- This model does not take into account that the shaft friction does not remain constant during the pile installation process. On the contrary, it has been observed (Chapter 3.5) that the radial effective stresses that develop in any given soil horizon tend to reduce as the distance from the pile tip to that horizon increases (friction fatigue). This means that this model overestimates the shaft friction, and this is evident when inspecting the post-predictions of the Amaliahaven project (Figure 5.2-6).

- Furthermore, Gavin and Lehane (2003) have confirmed that τf varies with the degree of soil displacement during installation and that it is lowest for fully coring piles and largest for closed-ended piles (Chapter 4.5). However, partially plugging conditions (usually for $D < 0.76\,m$) are not taken into account in [4.2.1]. Therefore, the formula suggested by Toolan & Fox (1977) will probably not be suitable for smaller diameter piles that (partially) plug during driving.

- In addition, this method also suggests a limit of $120\,kPa$ for the unit shaft friction in sands, but this might also be an unconservative approach for a driveability study, in which the goal is to establish maximum resistances.

Toe Resistance

The toe resistance is calculated as a weighted average of the qc value over a number of pile diameters above and below the pile tip and is applied on the steel annulus. This is a reasonable approach despite the fact that there are suggestions for lower values (Alm & Hamre (2001), Schneider et al (2010)). However, this model doesn't consider the plug resistance mobilized at the pile's base area during installation of e.g., a smaller diameter plugged pile.

Overall, the overestimation of the driving resistance of the Amaliahaven piles is mainly attributed to the way shaft friction is calculated. An example was presented (Figure 5.2-9), in which 5.2.1 was utilized to reduce the total shaft resistance. It could be observed (Figure 5.2-9) that the blow counts produced, were much closer to the ones recorded, and the model had a very similar prediction to the one made by Stevens et al (1982). However, it is stated that 5.2.1 is not a suggestion, but it was simply used to prove that the overpredictions were a product of the shaft resistance.

Stevens et al (1982)

Shaft friction

The unit shaft friction is calculated with equation [4.3.1]. Some issues of this method are listed below:

- This model uses the pre-installation vertical effective stresses in order to estimate the shaft friction during driving. However, as mentioned in Chapter 3.2, during installation, the stresses on a soil element are not constant, due to for example displacements or grain crushing.

- The same applies for the lateral earth pressure coefficient, which is also assumed constant and equal to 0.7 for the entire driving process.

- This method doesn't consider friction fatigue or the degree of soil displacements during driving, as stated earlier for Toolan & Fox (1977) SRD model. This explains some overestimated blow counts produced by this method, even when using the Lower Bound.

- It is also highlighted that this model utilizes limits for the shaft friction (based on the soil density, friction angle, etc.), according to the API (2000) guidelines, which are suggestions for a conservative estimation of pile (mid-term) axial capacity. The interface friction angle is determined by the soil description and density (Figure 4.3-1). However, there are various formulas that can be used to determine the soil density (e.g., Lunne & Christoffersen (1983), Kulhawy et al (1990), Jamiolkowski et al (2001), Baldi et al (1986), Schmertmann (1978) etc.). Therefore, one may use different formulas or criteria to assess the relative soil density, which will lead to

different values of friction angle, and different limits for the shaft friction according to the API table (Figure 4.3-1).

Toe Resistance

The toe resistance is calculated by using equation [4.3.2],(bearing capacity factor times effective vertical stresses). Some issues that come with it are listed below:

- It can be seen from the post-predictions (e.g., Figure 5.2-4) that the toe resistance can't be greater than $1\,MN$. This happens due to limitations applied according to the API table (Figure 4.3-1). This however implies that for every pile with a diameter around $1 - 2\,m$ and a wall thickness around $20\,mm$, the maximum toe resistance that can be mobilized is between $0.7\,to\,1.5\,MN$.

- Utilizing pre-installation stresses to estimate the toe resistance doesn't account for soil displacements, grain crushing, re-orientation, etc., (see Chapter 3.2) and that the soil stresses are not constant during the installation process.

- Using a constant bearing capacity factor might not be ideal as well, in case for example of partially plugged piles. Specifically, Gudavalli et al (2013) suggested that Nq should be a function of PLR, which in turns is a function of internal diameter.

- Additionally, there is lack of agreement between published bearing capacity factors and furthermore, it is highly sensitive to even small variations of the friction angle or relative density (Figure 4.3-1).

Overall, this model (even when using the Lower Bound suggested) overestimates the blows required to drive the steel open-ended piles of the Amaliahaven project, without leading though to an unreasonable range or to refusal. Considering the aforementioned limitations and uncertainties regarding this model, its performance is satisfactory.

Alm & Hamre (1982)

Shaft friction

Equation [4.4.1] takes into account friction fatigue, while it incorporates the inner plug resistance (inner shaft friction) to the external shaft formulation. This results in generally high shaft resistances, which are slightly less than that suggested by Stevens et al (1982) (Figure 5.2-5). Due to the fact that this method has been calibrated for large fully coring piles, it may underpredict the shaft friction mobilized in smaller diameter (partially plugged) piles, as τf doesn't vary with the degree of soil displacements induced during driving (Euripides piles project is an example, Chapter 7.1).

Toe Resistance

Since the inner plug resistance for fully coring piles is incorporated to the external shaft formulation, Alm & Hamre (2001) suggest a toe resistance applied only on the steel annulus, in the range of $30-50\%$ of the qc value. This however, as mentioned before, will probably lead to underestimation of the toe resistance for plugged piles.

Overall, this model produced the most reliable post-predictions, due to the large (fully coring) pile database that was used for its calibration, and due to the fact that it considers the effect of friction fatigue, which doesn't lead, in contrast to the other two models, to overestimations of the shaft resistance.

Second research question:

- *How does the recently developed CPT based static capacity approach, namely the* Unified Method, *perform in SRD predictions (without modifications)?*

The equations for both the shaft and toe model in their 'raw' format (no modifications applied) of this method are presented in Chapter 4.5. It is mentioned here that the Unified Method is an axial capacity pile design method for driven piles in sand deposits, meaning that it is calibrated to estimate mid-term (around 2 weeks after installation) pile capacity. This design method will be included in the forthcoming 2022 edition of the ISO guidelines and will replace the four CPT based design methods (ICP, UWA, NGI, Fugro). Moreover, it was reported by Lehane et al (2020) that this method has produced more

reliable estimations of the total pile capacity than the aforementioned approaches for both open and closed-ended piles driven in sandy soils.

Post-predictions for the Amaliahaven piles (Figure 5.3-3) have proved that this method is not suitable for driveability analysis without modifications, as it highly overestimates the blows/0.25 m required to drive the steel open-ended tubular piles of the APM and RWG sites or even implies (falsely) refusal.

A detailed analysis (Chapter 5.3) that followed, revealed that the reason behind the overestimated driving resistance was, in contrast to the rest of the examined models, coming from the estimated toe resistance. Moreover, it was observed that without any modifications, the shaft resistance estimated by this method, although it is calibrated to estimate shaft capacities developed 2 weeks after installation (time effects), was very similar in shape and magnitude to that of the Alm & Hamre (2001) model (Figure 5.3-4). This observation was explained due to differences of the two models listed below:

1. Alm and Hamre (2001) mentioned the Lower Bound of their method was very close or slightly above the average back-calculated SRD profiles from various sites that they examined, meaning that the shaft resistance estimated by this method might be slightly higher than that observed. While on the other hand, Lehane et al (2020), examined measured to calculated shaft resistance ratios for open-ended piles (Qm/Qc) and concluded that the Unified Method might underestimate the shaft capacity by about 20%.
2. The Alm & Hamre (2001) model incorporates the inner shaft friction (plug resistance) to the external shaft formulation ([4.4.1]), while the Unified Method doesn't model explicitly the inner shaft resistance, but only the external shaft resistance. The plug resistance (inner friction) is incorporated to the base resistance formulation.
3. Furthermore, the Unified Method has been calibrated through static load tests using piles with diameter ranging from 300 to $800\,mm$, with 90% of the piles examined having a diameter less than $800\,mm$, while the Alm & Hamre (2001) model used driving data of piles with diameter ranging from 0.762 to $2.74\,m$. This scale difference might also be the cause for the Unified Method to produce less shaft resistance for large offshore piles even though it is calibrated with a median set up factor of 14 days after the installation.

Further analysis also revealed that the Unified Method for large offshore piles, e.g., diameters in the range of $1-2\,m$, and wall thickness around $40\,mm$, produces similar shaft resistances with the Alm & Hamre (2001) model (Figure 5.3-5), while for smaller diameter piles (Figure 5.3-7), with diameters in the range of $0.35\,m$, and wall thickness

around $12 - 14\,mm$, which have also a PLR around 40% (partially plugged piles) installed in Blessington's dense sand, Prendergast et al (2020)), the Unified Method estimates generally higher shaft resistances.

This can be attributed to two factors:

1. The effective area ratio [4.5.2] that is incorporated to the shaft formulation and allows τf to vary with the degree of soil displacement during installation, as was confirmed by Gavin and Lehane (2003). This means, that the Unified Method will produce higher shaft resistances for smaller diameter piles that may be driven under partially plugged conditions, and lower shaft resistances for large offshore piles that are mainly fully coring.
2. Moreover, for small diameter piles, this model allows for increase of the radial effective stresses during loading, due to constrain of dilation of the thin pile-soil interface zone by the surrounding soil mass (Chapter 4.5, $\Delta\sigma'_{rd}$).

With respect to the toe model, which is the main resistance factor that leads to high overestimations of the blows required to drive the Amaliahaven piles, this is calibrated to estimate the base resistance mobilized for toe displacements of $0.1 * D$. Therefore, for the Amaliahaven piles, with $D = 1.42\,m$, the estimated toe resistance according to this method, corresponds to tip displacement of about $14\,cm$. However, the pile tip displacement during each hammer blow is a few mm for normal driving conditions, meaning that less resistance will be mobilized.

Overall, the Unified Method can not be directly utilized in pile driveability analysis, and modifications are required so that this method can estimate resistances during driving, rather than mid-term pile capacities.

Third research question:

- *How can we utilize installation records of steel open-ended tubular piles in order to improve the SRD estimations of the* Unified Method, *and which key factors need to be considered in its modified form?*

It was proven previously that the Unified Method in its 'raw' format can not be utilized directly in pile driveability analysis. In addition, it was mentioned that the shaft and toe resistances correspond to pile shaft capacities developed around 2 weeks after the installation, and for pile tip displacements induced at failure ($0.1 * D$), respectively. This

means that both the shaft and toe models need to be modified, so that this method predicts resistances mobilized during driving.

In order to modify the Unified Method, driving records of highly instrumented piles need to be utilized. Specifically, the shaft model of this method, already incorporates 3 important factors that affect both the shaft driving resistance and mid-term shaft capacity:

1. Variation of τf with the degree of soil displacement during installation (factors A_{re}, PLR in [4.5.2]).
2. Friction fatigue as function of h and D, [4.5.2].
3. Increase of radial effective stresses during loading, due to constrain of dilation of the thin interface zone by the surrounding soil mass, [4.5.1].

This means that only a set up factor is mainly needed in order to convert the mid-term shaft resistance to resistance during driving. As part of the limitations of this Thesis, a set up factor has not been derived from the APM and RWG site. This could have been done by utilizing a PDA system to measure transferred energy, soil resistances and quake values during pile installation, and by taking the same measurements about 2 weeks later, by re-striking the same piles. This information could be used to:

1. Assess how much shaft capacity would have been regained over a period of two weeks.
2. Asses the driving resistance estimated by the examined models, and additionally,
3. Evaluate the shaft capacity estimated by the Unified Method.

Despite that, extensive research has been made regarding time effects (Chapter 3.4), for example by Jardine et al (2006), Gavin et al (2015), Lehane et al (2017) and eventually, equation [3.4.1] (derived from a large database of driving records) was used to establish a set up factor of about 0.7, which is also in agreement with the set up factors derived from other researchers, (Jardine et al (2006), Karlsrud et al (2014), and Gavin et al (2013)), and used to modify the shaft resistance of similar CPT based axial capacity methods (Byrne et al (2012), Byrne et al (2018), Prendergast et al (2020), ICP and UWA). In addition, a typical quake value of $2.5\,mm$ has been used for the shaft resistance, as suggested by the other methods examined (Toolan & Fox (1977), Stevens et al (1982), and Alm & Hamre (2001)).

With respect to the toe resistance, again a typical quake value of $2.5\,mm$ has been utilized. However, it is not known how much resistance will be mobilized at the pile base during each hammer blow. Inspecting [4.5.6], which is the general formulation of the toe resistance mobilized at $0.1 * D$ displacements, one should notice that:

1. It is applied on the entire pile base area.
2. It incorporates the plug resistance by utilizing the effective area ratio (similarly to assuming an equivalent closed-ended pile).
3. And for that reason, the same equation can be used for both open or closed-ended piles, for all plugging conditions, meaning fully or partially plugged or unplugged piles.

Therefore, it was decided to reduce the toe resistance corresponding to $0.1 * D$ displacement ([4.5.6]) to driving resistance mobilized at $2.5\ mm$ toe displacement (quake). To do so though, a base displacement model is needed that can estimate how much base resistance is mobilized with increasing pile base displacement.

For that reason, three base displacement models have been examined (API (2000), Gavin and Lehane (2007), Lehane et al (2020b)), utilizing records from a highly instrumented pile test performed by Han et al (2020), who specifically used a twin-walled instrumented $660\ mm$ diameter pile, with a wall thickness of $38\ mm$, and measured plug and steel annular resistances for various displacements to diameter ratios ($\frac{w_b}{D}$).

Specifically, the API (2000) approach, suggests ratios of mobilized base resistance to base resistance at failure ($\frac{q_{b_{mob}}}{q_{b0.1}}$) for various $\frac{w_b}{D}$ ratios. Therefore, equation [6.2.9] was developed, to approximate the $\frac{q_{b_{mob}}}{q_{b0.1}}$ recommended by the API (2000).

The aforementioned analysis (Q-z curves in Figure 6.2-2 of Chapter 6.2), showed that the API (2000) method, when it is slightly modified to calculate mobilized based resistance using the Unified Method, was in excellent agreement with the measured base displacement response for $\frac{w_b}{D}$ ratios of 0.05, 0.1 and 0.225. This analysis, does not only validate the applicability of this base displacement model, but it also validates the performance of the Unified Method in predicting the base resistance at failure ($0.1 * D$).

Therefore, with the developed equations, [6.2.9] and [6.2.10], one can predict the base resistance that will be mobilized for any pile type, meaning open or closed-ended, for every driving conditions, referring to plugged, partially plugged or fully coring piles, for any $\frac{w_b}{D}$ ratio (Figure 6.2-3). Thus, the base resistance mobilized during each hammer blow for a typical quake of $2.5\ mm$ can be estimated.

It is mentioned here that the blow counts, CPTs and driving energy of 33 piles across the entire Amaliahaven project have been examined, and the base resistance mobilized per hammer blow according to [6.2.10] was in the range of $[45\% - 50\%] * q_{b0.1}$. This also indicates an insignificant soil variability, as examined and highlighted at Chapter 5.1.

The new set of formulations suggested for the Unified SRD Method are listed under Table 6.3-1 (for both the shaft and toe model).

As part of the discussion, it is mentioned as well that in total 18 steel open-ended tubular piles (one was re-driven to a different location), with pile diameters $0.762\,m$ (Euripides project) and $1.42\,m$, were examined, from five different sites (APM and RWG terminals from the Amaliahaven project, SIF and HHTT terminals, and Euripides project). The % Match (average percentage of matching of predicted and actual blow counts) and % Under (percentage of the blow count curve that lies below the actual blow count curve), as were described in more detail at the end of Chapter 5.2, by utilizing the Alm and Hamre (2001) model and the Unified SRD Method, is presented in Table 8.1-1. The higher % Match, the greater the match between predicted and actual blow count curves, while (for example) 30% Under means that on average, only 30% of the predicted blow count curve lies below the actual one (underestimation of blow counts), whereas 70% of the same curve is above the recorded one (overestimation).

Table 8.1-1: Percentage of match (% Match) and underestimation (% Under) between recorded and predicted blow count curves using the Alm & Hamre (2001) LB model and the Unified SRD Method in five projects in the Netherlands.

		Alm & Hamre (2001) LB		Unified SRD Method	
		% Match	% Under	% Match	% Under
APM	BP-920	77 %	88 %	75 %	94
	BP-899	79 %	82 %	80 %	88
	BP-853	78 %	70 %	84 %	76
	BP-838	76 %	77 %	79 %	84
	BP-800	86 %	59 %	88 %	88
RWG	BP-02	77 %	21 %	82 %	21
	BP-33	83 %	38 %	87 %	30
	BP-48	87 %	56 %	87 %	56
	BP-64	83 %	43 %	86 %	36
	BP-80	87 %	45 %	91 %	45
SIF	BP-88	79 %	88 %	79 %	85
	BP-85	69 %	100 %	87 %	100
HHTT	BP-144	89 %	81 %	84 %	90
	BP-205	66 %	94 %	70 %	90
	BP-163	83 %	87 %	80 %	94
	BP-171	80 %	36 %	83 %	36
EURIPIDES	Location I	60 %	85 %	72 %	56
	Location II	51 %	89 %	60 %	61

It is clarified that the reader should always inspect first the blow count, shaft - toe resistances graphs produced from the driveability analysis, and not only the percentages shown in Table 8.1-1. These can only be used as an indication of the (average) performance of the models. Additionally, by observing both the graphs and the % Under of Table 8.1-1, both models show a tendency to underpredict the blow counts, irrespectively of the % Match.

It can be observed that in 2 out of 18 piles, both models had the same matching percentage, while the Unified SRD Method produced less average error, in 13 out of 18 piles. Specifically, for the Euripides piles ($D = 0.76\,m$, $PLR = 96\%$), the Alm and Hamre (2001) method had greater error, due to the fact that:

1. It doesn't incorporate variation of τf with the degree of soil displacement during installation, which is based on pile geometry and plug conditions.
2. It doesn't incorporate increase of radial effective stresses during loading, due to constrain of dilation of the thin interface zone by the surrounding soil mass.
3. It doesn't account for plug resistance developed at the pile base.
4. It is mainly calibrated for driveability predictions of larger diameter piles ($> 1m$).

The Unified SRD Method, not only incorporates the aforementioned factors, but based on this research study, at least for the range of diameters between $0.7 - 2m$, it estimates the most reliable SRD profiles. However, both the Alm and Hamre (2001) model and the Unified SRD Method generally underpredict the blows required to drive the examined piles (irrespectively of how good the prediction really is). Moreover, it is believed that the set of formulas suggested ([6.2.10]) can produce some reasonable SRD predictions for even larger or smaller pile diameters, and most probably, the same set of formulations can be used for pile driveability predictions of closed-ended piles.

Finally, it is mentioned here that the contribution of the shaft and toe resistances to the overall SRD was estimated, for both the Alm and Hamre (2001) model and the Unified SRD Method, for all projects examined in this research project. Specifically, for the Alm and Hamre (2001) model, for steel open - ended piles with diameter $1.42\,m$ and length in the range of about $32\,m - 37\,m$, installed in dense sand conditions (APM, RWG, HHTT, SIF), the average shaft contribution to the overall SRD was estimated to be in the range of $80\% - 85\%$. This means that a great part of the overall static resistance during driving is produced by shaft friction. On the contrary, utilizing the Unified SRD Method, the average shaft resistance contribution to the total SRD for the same piles - projects, was found to be in the range of $55\% - 64\%$. This difference is attributed to the fact that the Unified SRD Method estimates only the external shaft resistance [6.1.1], while the Alm and Hamre (2001) model takes into account both the internal and external friction with

equation [4.4.1]. However, in the Unified Method, the internal friction (plug resistance) is incorporated in the toe resistance formulation, which explains the higher toe resistance than that estimated by the Alm and Hamre (2001) model.

For the EURIPIDES project ($D = 0.762\,m$ and $L = 47\,m$), the average shaft resistance contribution to SRD was estimated to be around 75% and 77 % by the Alm and Hamre (2001) model and the Unified SRD Method, respectively. The reasons why the Alm and Hamre (2001) model generally leads to an underprediction (in this specific case) have been mentioned earlier. It is also stated here that due to the great length of the pile of the EURIPIDES project, it was expected to calculate a higher contribution from the shaft resistance.

Furthermore, it is believed that these percentages, of shaft and toe contribution to the overall resistance can vary when using the Unified SRD Method. This may happen due to the fact that this model takes into account the plugging conditions, meaning that for the same (sandy) soil conditions, if two piles with $D = 1.5\,m$ and $D = 0.3\,m$ are installed, the latter will probably be, if not fully plugged, partially plugged, while the first pile will be fully coring. In such a case (see also section 5.3), for the smaller diameter pile, the overall toe resistance contribution to the SRD (due to soil plugging) might be higher than that of the larger diameter pile. On the other hand, the Alm and Hamre (2001) model is suitable only for fully coring conditions.

8.2 Conclusions

This research study evaluated the performance of three traditional SRD models, suggested by Toolan & Fox (1977), Stevens et al (1982), and Alm & Hamre (2001). Among those, the one suggested by Alm & Hamre (2001), resulted in the most reliable post-predictions of the blow counts required to drive the steel open-ended tubular piles of the Amaliahaven project in dense sand conditions.

Moreover, it evaluated the applicability of a recent CPT based axial capacity design approach, namely the Unified Method. By suggesting modifications to this model and presenting a new set of formulas, it showed that overall, even better predictions than those made by the Alm & Hamre (2001) model can be produced, for 18 different piles examined from 5 different sites. In addition, the new set of formulas suggested in this research, is applicable to both open (and most probably) closed-ended piles, for various plugging

conditions (plugged - partially plugged - fully coring pile installations), and thus, for a greater range of pile diameters than the methods examined.

The overall contribution of this research study to the industry is summarized below:

- Amongst three SRD models, commonly used in practice, the Unified SRD Method resulted in the most reliable post-predictions for steel open-ended tubular piles installed in dense sand conditions.

- 16 out of 18 piles examined have been installed around the Maasvlakte, Rotterdam area. The Unified SRD Method produced blow count profiles that are in excellent agreement with the recorded ones. Therefore, at least for the Port of Rotterdam, a very reliable method for future pile driveability analysis is suggested.

- Having a high reliability SRD model:

    1. Minimization of installation risks with respect to under or over predictions of the soil resistance during driving is achieved.
    2. The most suitable and cost-efficient hammering equipment can be selected.
    3. Hammer, or pile material damage risks are reduced.
    4. Installation times are better predicted, which also leads to a reduction of costs from time delays.
    5. Reliable resistances at the end of driving are estimated, which cannot only be used to check if the desirable pile capacity has been achieved at a specific installation depth, but also to predict, in case of a pile that cannot further penetrate into the soil, if the capacity at that level is sufficient or not. This can greatly reduce the costs of a contractor if it is proven that he/she doesn't need to re-install the pile and time delays are avoided as well.

- As mentioned, one set of formulas can be used for different piles and plugging conditions.

- The Unified Method can be utilized both during the design phase, in which a pile geometry and installation depth need to be determined based on capacity requirements, but also, it can be used (Unified SRD Method) for driveability analysis as well. This leads to minimization of the engineering effort and confusion on which formulas - models - approaches to use for each case.

With respect to the limitations of this study (Chapter 1.5), suggestions are listed below for future research projects:

- Further investigation and verification on the pile diameter range, for which this method (Unified SRD Method) produces reliable estimations is needed. For example, this research study doesn't include very large offshore piles ($D \geq 4\,m$) or small plugged piles ($D \leq 0.7\,m$).
- The applicability of the Unified SRD Method to close-ended piles needs to be investigated and proved. Although the same set of formulas allows for estimation of toe and shaft resistances for any type of pile (open or closed-ended), it is not known for example, if the base displacement model that was suggested for this method [6.2.10], also leads to reliable estimations of $\frac{q_{b_{mob}}}{q_{b0.1}}$ ratios for the case of a closed-ended pile.
- Signal matching can reveal actual soil resistances which can be compared to predictions made by the Unified SRD Method, and new suggestions can be made based on the observations.
- Quake values are usually set to $2.5\,mm$, but signal matching may also indicate higher values. Assuming the same maximum mobilized resistance, a lower quake value will lead to lower blow counts than a higher value. A thorough analysis, using a large database of recorded quakes is therefore needed, in order to establish, for example, a correlation between maximum elastic soil displacement, with the qc value recorded from CPTs, pile diameters or plugging conditions, etc.
- A recent paper by Lehane et al (2022), suggests a set of formulas for the Unified Method that can be utilized to predict pile capacities installed in silt and clay layers. It would be important then, to examine the applicability of those in driveability analysis, as the model examined and the modifications suggested in this research are only for sand deposits.
- Finally, residual loads that might develop during driving of a small-diameter plugged pile and of a large offshore pile need to be further examined for various soil conditions.

References

- Alm, T., Hamre, L. (1998), Soil Model for Driveability Predictions. OTC 8835, Offshore Technology Conference, No. OTC 8835, 13.
- Alm, T., Hamre, L. (2001), Soil Model for Pile Driveability Predictions Based on CPT Interpretations. Proceedings of the 15th International Conf. on Soil Mechanics and Foundation Engineering, Istanbul, Vol. 2, pp. 1297–1302.
- API. (2000), API RP2A-WSD, Recommended Practice for Planning, Designing, and Constructing Fixed Offshore Platforms–working Stress Design. American Petroleum Institute, Washington, DC.
- API (2011), ANSI/API RP 2GEO: Geotechnical and foundation design considerations. ISO 19901-4:2003 (modified), Petroleum and natural gas industries-specific requirements for offshore structures, Part 4 − Geotechnical and foundation design considerations. 1st edn. Washington, DC, USA: API Publishing Services.
- Axelsson, G. (2000), Long term set-up of driven piles in sand. PhD thesis, Department of Civil and Environmental Engineering, Royal Institute of Technology, Stockholm, Sweden.
- Baldi, G., Bellotti, R., Ghionna, V.N., Jamiolkowski, M., Pasqualini, E. (1986), Interpretation of CPT and CPTU; 2nd part: drained penetration of sands. In Fourth International Geotechnical Seminar: 143–156. Singapore.
- Baldi, G., Belottini, R., Ghionna, V.N., Jamiolkowski, N.I., Lo Presti, D.L.F. (1989), Modulus of sands from CPTs and DMTs. Proc. 12th ICSMFE, Rio de Janeiro, Vol. I pp. 165-170.
- Boulanger, R.W.W., DeJong, J.T.T. 2018, Inverse filtering procedure to correct cone penetration data for thin-layer and transition effects. Cone Penetration Testing 2018: Proc 4th Int Symposium on Cone Penetration Testing (CPT'18), 21-22 June, 2018, Delft, The Netherlands: 25.
- Burland, J.B. (1990), On the compressibility and shear strength of natural clays. 30th Rankine Lecture, Géotechnique, Vol. 40, No. 3, pp. 327-378.
- Byrne, T., Doherty, P., Gavin, K., Overy, R. (2012), Comparison of pile driveability methods in North Sea sand. Proc. 7th Int. Conf. on Offshore Site Investigation and Geotechnics. SUT London, 481–488.
- Byrne, T., Gavin, K., Prendergast, L.J., Cachim, P., Doherty, P., Pulukul, S.C. (2018), Performance of CPT-based methods to assess monopile driveability in North Sea sands. Ocean Eng. 2018, 166, 76–91.

- Chow F.C., Jardine R.J., Nauroy J.F., and Brucy F. (1998), Effects of Time on Capacity of Pipe Piles in Dense Marine Sand. J. Geotech. and Geoenv. Engineering, ASCE, 124, 254–264.
- Clausen, C.J.F., Aas, P.M., and Karlsrud, K. 2005. Bearing capacity of driven piles in sand, the NGI approach. In Proceedings of the International Symposium on Frontiers in Offshore Geotechnics. Taylor & Francis, London. pp. 677–681.
- Das, B. M. (2011) Principles of Foundation Engineering. Seventh Ed. Cengage Learning, USA. Available at: https://tudelft.on.worldcat.org/oclc/840451377.
- Fahey, M., Lehane, B.M., Stewart, D. (2003), Soil stiffness for shallow foundation design in the Perth CBD. Australian Geomechanics Journal, 38:61-90.
- Fleming, K., Weltman, A., Randolph, M., & Elson, K. (2009), Piling Engineering (3rd ed.). CRC Press. https://doi-org.tudelft.idm.oclc.org/10.1201/b22272
- Flynn, K., McCabe, B. (2019), Driven cast-in-situ piles installed using hydraulic hammers: Installation energy transfer and driveability assessment. Soils and Foundations Journal, Vol 59, pp. 1946-1959.
- Gavin, K.G., and Lehane, B.M. (2003), The shaft capacity of pipe piles in sand. Canadian Geotechnical Journal, 40(1): 36–45.
- Gavin, K., Lehane, B. (2007), Base load–displacement response of piles in sand. Canadian Geotechnical Journal. 44(9):1053–1063.
- Gavin, K., Kirwan, L., Igoe, D. (2013), The effect of ageing on the axial capacity of piles in sand. Proc. Inst. Civ. Eng. Geotech. Eng, 166, 122–130.
- Gavin, K., Jardine, R.J., Karlsrud, K., Lehane, B.M. (2015), The effects of pile ageing on the shaft capacity of offshore piles in sand. In Proceedings of the International Symposium Frontiers in Offshore Geotechnics (ISFOG), Oslo, Norway, 10–12 June 2015.
- Gavin, K., Igoe, D. (2021), A field investigation into the mechanisms of pile ageing in sand. Geotechnique,71(2), 120-131.
- Gavin, K. G. (2021), Axial Resistance of Piles in Sand, Background Reading CIE 4362. Soil Structure Interaction lecture notes 2021, TU Delft.
- Gudavalli, S. R., Safaqah, O., Seo, H. (2013), Effect of soil plugging on axial capacity of open-ended pipe piles in sands. 1487-1490. Paper presented at 18th International Conference on Soil Mechanics and Geotechnical Engineering, ICSMGE 2013, Paris, France.
- Han, F., Ganju, E., Prezzi, M., Salgado, R., Zaheer, M. (2020), Axial resistance of open-ended pipe pile driven in gravelly sand. Géotechnique, 70(2), 138–152.
- Heerema, E.P. (1980). Predicting pile driveability: Heather as an illustration of friction fatigue. Ground Engng13. Apr.,15–37.

- Hirsch, T.J., Lowery, L.L., Coyle, H.M., Samson, C.H. (1970), Pile-Driving analysis by One-Dimensional Wave Theory: State of the Art. High Res. Rec., 1970.
- Hirsch, T.J., Carr, L., Lowery, L.L. (1976), Pile Driving Analyses-wave Equation User Manual. (TTI Prog. Implement. Packag. I-IV).
- IHC Merkwede. IHC Hydrohammer, Pile driving equipment. Available at: http://greenglobalgroup3g.com/images/sampledata/parks/landscape/IHCHydrohammerOffshore.pdf
- Jamiolkowski, M., LoPresti, D.C.F., Manassero, M. (2001), Evaluation of relative density and shear strength of sands from cone penetration test and flat dilatometer test. Soil Behavior and Soft Ground Construction (GSP 119), American Society of Civil Engineers, Reston, VA, 201 – 238.
- Jardine, R.J., Lehane, B.M., Everton, S.J. (1992), Friction coefficients for piles in sands and silts. Proc. Int. Conf. on Offshore Site Investigation and Foundation Behaviour, SUT, London,
- Kluwer (Dordrecht), pp. 661-677.
- Jardine, R., Chow, F., Overy, R., Standing, J. (2005), ICP design method for driven piles in sands and clays, Thomas Telford, London.
- Jardine, R., Standing, J., Chow, F. (2006), Some observations of the effects of time on the capacity of piles driven in sand. Geotechnique 55, 227–244.
- Jardine, R.J, Chow, F.C. (2007), Some recent developments in the design of offshore piles, London, 6th International Conference on Offshore Site Investigations and Geotechnics, Publisher: Society for Underwater Technology. Pages: 303-332.
- Karlsrud, K., Jensen, T.G., Lied, E.K.W., Nowacki, F., Simonsen, A.S. (2014), Significant ageing effects for axially loaded piles in sand and clay verified by new field load tests. In Proceedings of the Offshore Technology Conference, Houston, Texas, USA, 5–8 May 2014.
- Kirwan, L. (2015), Investigation of ageing mechanisms for axially loaded piles in sand. PhD thesis, University College Dublin, Dublin, Ireland.
- Kolk, H.J., Baaijens, A.E., and Sender, M. 2005a. Design criteria for pipe piles in silica sands. In Proceedings of the International Symposium on Frontiers in Offshore Geotechnics. Taylor & Francis, London. pp. 711–716.
- Kulhawy, F.H., Mayne, P.W. (1990), Estimating Soil Properties for Foundation Design. EPRI Report EL-6800, Electric Power Research Institute, Palo Alto.
- Lambe, T.W., Whitman, R.V. (1969), Soil Mechanics. John Wiley & Sons.
- Lehane, B.M., Jardine, R.J., Bond, A.J., and Frank, R. (1993), Mechanisms of shaft friction in sand from instrumented pile tests. Journal of Geotechnical Engineering, ASCE,119(1): 19–35.

- Lehane, B. M., Schneider, J. A., Xu, X. (2005), A Review of Design Methods for Offshore Driven Piles in Siliceous Sand, UWA Report, GEO: 05358.
- Lehane, B.M., Schneider, J.A., Xu, X. (2005a), Evaluation of design methods for displacement piles in sand. UWA Report, GEO: 05341.1.
- Lehane, B.M., Schneider, J.A., Xu, X. (2005b), CPT based design of driven piles in sand for offshore structures. UWA Report, GEO: 05345.
- Lehane, B.M., Schneider, J., Xu, X. (2007), Development of the UWA-05 Design Method for Open and Closed Ended Driven Piles in Siliceous Sand. Contemporary Issues In Deep Foundations, pp. 1–10.
- Lehane, B.M., Lim, J.K., Carotenuto, P., Nadim, F., Lacasse, S., Jardine, R., van Dijk, B.F.J. (2017), Characteristics of Unified Databases for Driven piles. In Proceedings of the 8th International Conference of Offshore Site Investigation and Geotechnics OSIG, London, UK, 12–14 September 2017.
- Lehane, B. M., Liu, Z., Bittar, E., Nadim, F., Lacasse, S., Jardine, R., Carotenuto, P., Rattley, M., Gavin, K., & More Authors. (2020), A New 'Unified' CPT-Based Axial Pile Capacity Design Method for Driven Piles in Sand. In Z. Westgate (Ed.), Proceedings Fourth International Symposium on Frontiers in Offshore Geotechnics (pp. 462-477). [3457].
- Lehane B., Li L. and Bittar E. (2020b), CPT-based load-transfer formulations for driven piles in sand. Geotechnique Letters, 10, 568–574.
- Lehane, B. M., Liu, Z., Bittar, E., Nadim, F., Lacasse, S. (2022), New CPT methods for evaluation of the axial capacity of driven piles. In Proceedings of the 5th International Symposium on Cone Penetration Testing (CPT'22), Bologna, Italy, 8-10 June 2022.
- Lim, J. K., Lehane, B. M. (2014), Characterisation of the effects of time on the shaft friction of displacement piles in sand. Géotechnique 64, No. 6, 476–485.
- Lunne, T., Christoffersen, H.P. (1983), Interpretation of Cone Penetrometer Data for Offshore Sands. Paper presented at the Offshore Technology Conference, Houston, Texas, May 1983. doi: https://doi-org.tudelft.idm.oclc.org/10.4043/4464-MS
- Lysmer, J., Richart, F. E. (1966), Dynamic response of footings to vertical loading. Journal of the Soil Mechanics and Foundations Division, 92(1), 65-91.
- van Mierloo, W., Koppejan, A. (1952), Lengte en draagvermogen van heipalen, vaststelling hiervan en enige daarbij verkregen ervaringen. Bouw 1952, no. 3.
- Middendorp, P., Verbeek, G. (2006), 30 Years of Experience with the Wave Equation Solution Based on the Method of Characteristics. GeoCongress 2006: Geotechnical Engineering in the Information Technology Age. 2006. 10.1061/40803(187)172.

- Niazi, F. S., Mayne, P. W. (2010), Evaluation of EURIPIDES Pile Load Tests Response from CPT Data. ISSMGE International Journal of Geoengineering Case Histories, Vol. 1, No. 4, 2010, pp. 367–386.
- Paik, K., Salgado, R., Lee, J., Kim, B. (2003), Behavior of open- and closed-ended piles driven into sands. J. Geotech.Geoenviron. Eng. 296–306.
- Prendergast, L.J., Gandina, P., Gavin, K. (2020), Factors Influencing the Prediction of Pile Driveability Using CPT-Based Approaches. Energies 2020, 13, 3128.
- Randolph, M.F. (2000), Pile-soil interaction for dynamic and static loading. Proceedings of the 6th International Conference on Application of Stress Wave Theory to Piles, Sao Paulo, Appendix, 3-11.
- Rausche, F., Goble, G.G, Likins, G. (1992), Investigation of dynamic soil resistance on piles using GRLWEAP. Application of Stress-Wave Theory to Piles, F.B.J. Barends (ed.), Balkema, Rotterdam, 1992.
- Saint-Venant, B.de. (1867), Memoire sur le doc longitudinal de deux barres elastiques, Journal de Mathematique, 2, ser XII, pp 237-376.
- Saldivar-Moguel, E.E. (2002), Investigation into the behaviour of displacement piles under cyclic and seismic loads. PhD Thesis, Imperial College, London.
- Schmertmann, J.H. (1978), Guidelines for cone test, performance and design. U.S. Federal Highway Administration, FHWATS-78209.
- Schneider, J.A., White, D.J., Lehane, B.M. (2007), Shaft Friction Of Piles Driven In Siliceous, Calcareous And Micaceous Sands. Paper presented at the Offshore Site Investigation and Geotechnics: Confronting New Challenges and Sharing Knowledge, London, UK, September 2007.
- Schneider, J., Harmon, I. (2010), Analyzing drivability of open ended piles in very dense sands. J. Deep. Found. Inst., 4, 32–44.
- Smith, A.E.L. (1960), Pile Driving Analysis by Wave Equation. Journal of SMFD ASCE 86(4) pp 35-61, 1960.
- Stevens, R., Wiltsie, E., Turton, T., 1982. Evaluating drivability for hard clay, very dense sand, and rock. In: Offshore Technology Conference. Houston, USA.
- The State of California, Department of Transportation, Division of Engineering Services. Foundation Manual. November 2008, Revision 2, October 2015.
- Toolan, F.E. and Fox, D.A. (1977). Geotechnical Planning of Piled Foundations for Offshore Platforms. Proc. Institution of Civil Engineers, London, Part 1, vol. 62.
- Voitus van Hamme, G.E.J.S.L., Jansz, J.W., Bomer, H., Arentsen, D. (1974), Hydroblok and Improved Pile Driving Analysis. De Ingenieur, Vol 86, no 8. pp 344-352, The Netherlands.
- White, D. J., Bolton, M. D. (2004), Displacement and strain paths during plane strain model pile installation in sand. Géotechnique. 54, (6):375–398.

- White, D. J. (2005), A general framework for shaft resistance on displacement piles in sand. Proceeding of the 1st International Symposium on Frontiers in Offshore Geotechnics (pp. 741-748). Taylor and Francis.
- Xu, X., Lehane, B., Schneider, J. (2005), Evaluation of end-bearing capacity of open-ended piles driven in sand from CPT data. In M. J. Cassidy, & S. Gourvenec (Eds.), Proceedings of the International Symposium on Frontiers in Offshore Geotechnics (Perth, Australia ed., Vol. n/a, pp. 725-731). CRC Press/Balkem.
- Xu, X., Schneider, J., Schneider, Lehane, B. (2008), Cone penetration test (CPT) methods for end-bearing assessment of open- and closed-ended driven piles in siliceous sand. Canadian Geotechnical Journal. 45(8): 1130-1141.
- Yang, Z.X., Jardine, R.J., Zhu, B.T., Foray, P., Tsuha, C.H.C. (2010), Sand grain crushing and interface shearing during displacement pile installation in sand. Geotechnique, 60(6), 469–482.

APPENDIX A

Figure A 1: Vibratory hammer (photo personally taken).

Figure A 2: Partial installation of combi-wall piles with the vibratory hammer (photo personally taken).

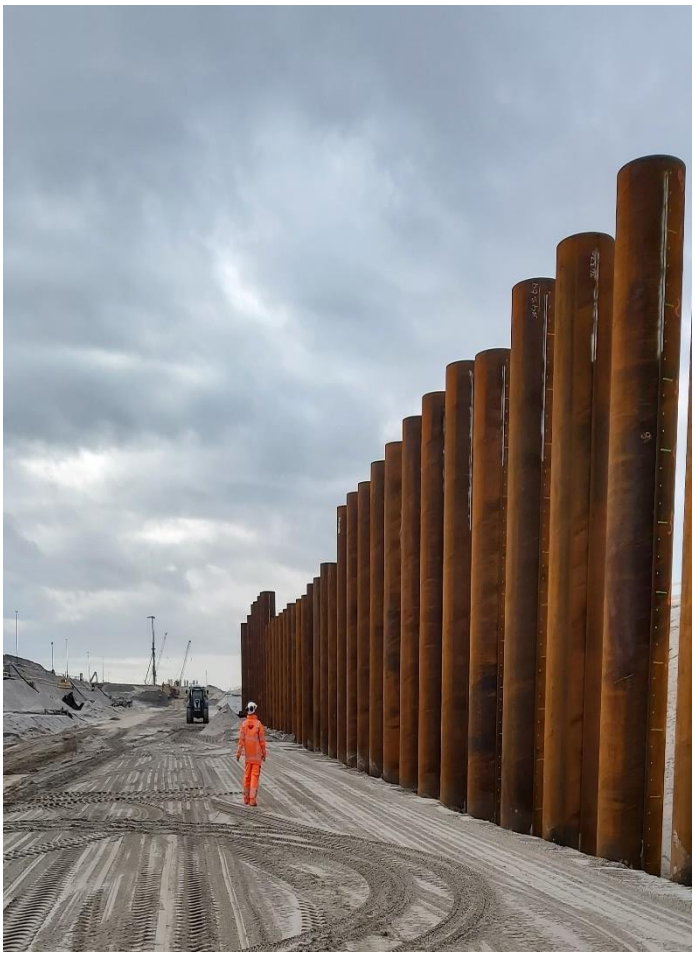

Figure A 3: Combi-wall piles after vibratory driving (photo personally taken).

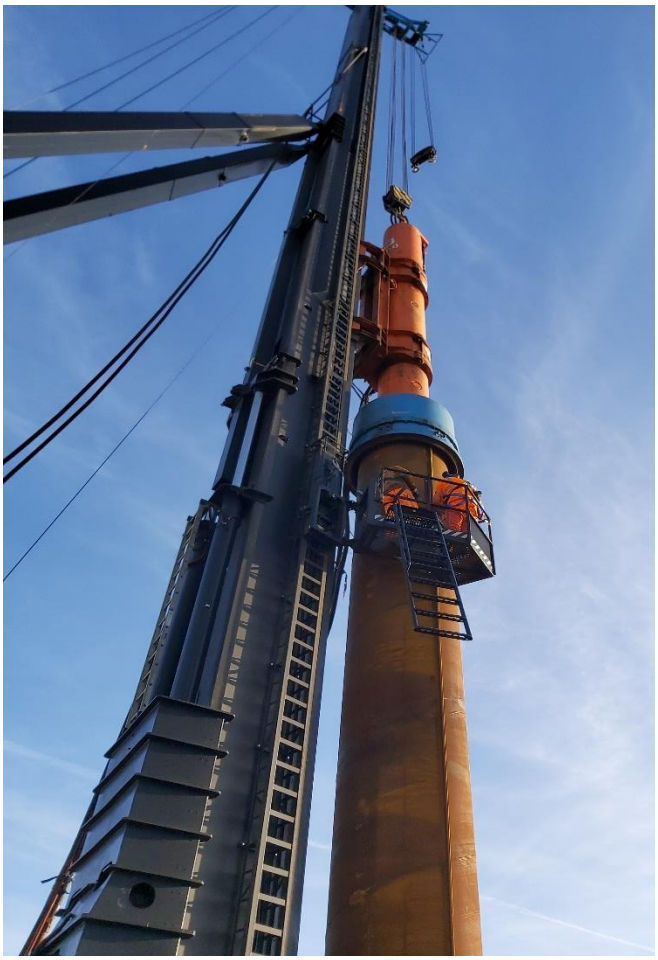

Figure A 4: Combi-wall pile installed to final depth using hydraulic hammer (photo personally taken).

Figure A 5: Combi-wall piles and sheet-pile wall installed to final depth (photo personally taken).

APPENDIX B

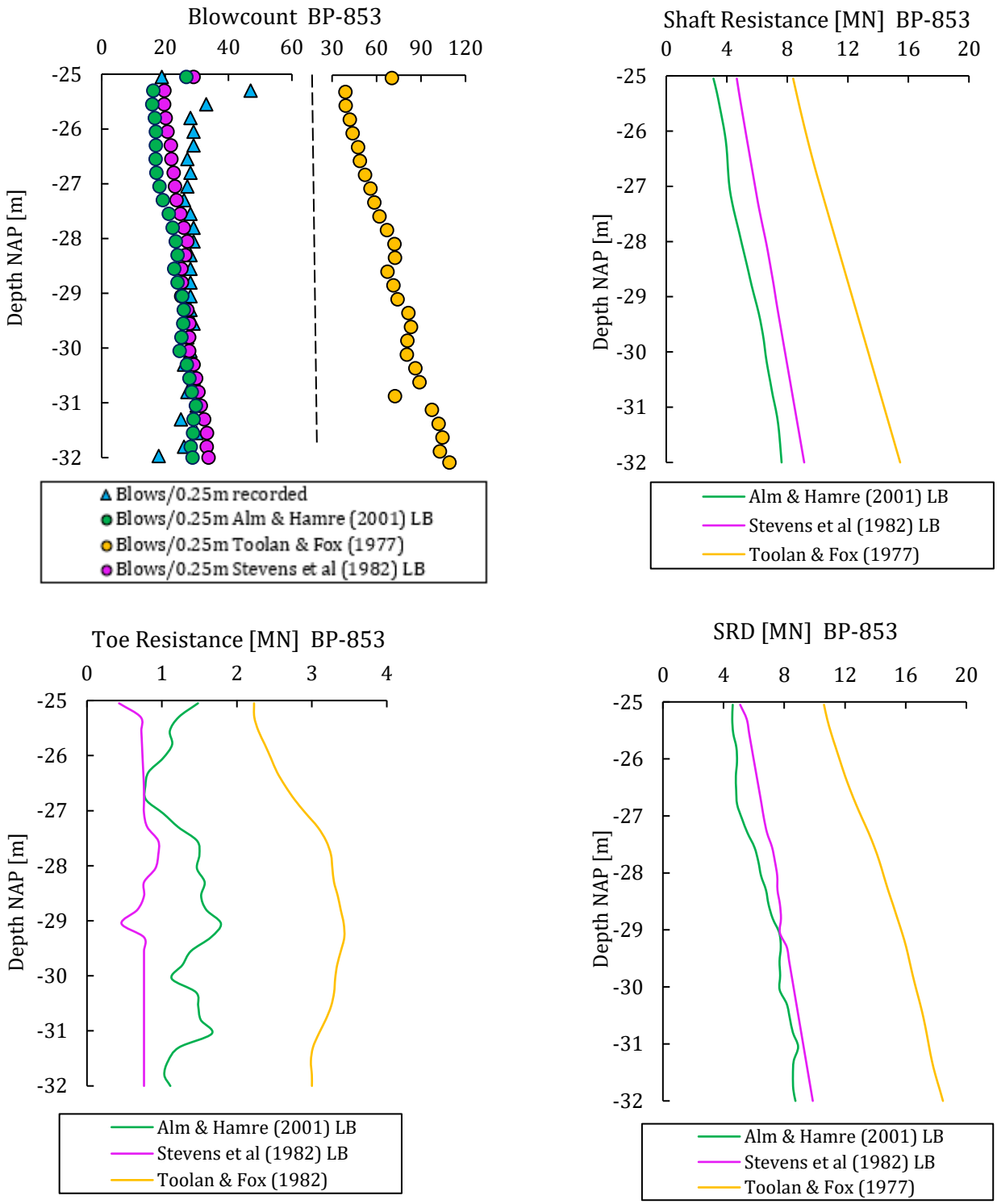

Figure B 1: Driveability post-prediction for combi-wall pile BP-853, using Alm & Hamre (2001), Toolan & Fox (1977), and Stevens et al (1982) SRD models. APM terminal.

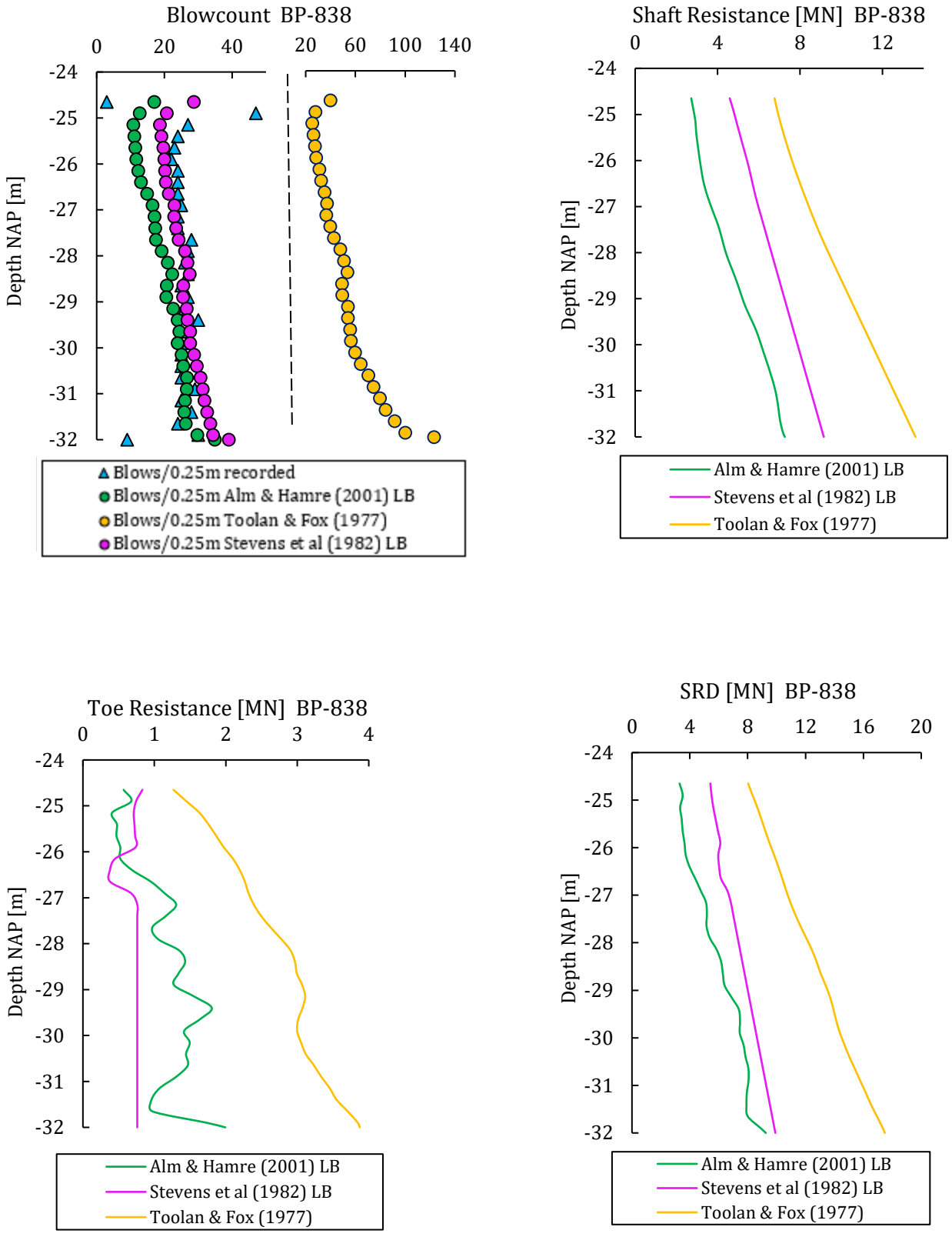

Figure B 2: Driveability post-prediction for combi-wall pile BP-838, using Alm & Hamre (2001), Toolan & Fox (1977), and Stevens et al (1982) SRD models. APM terminal.

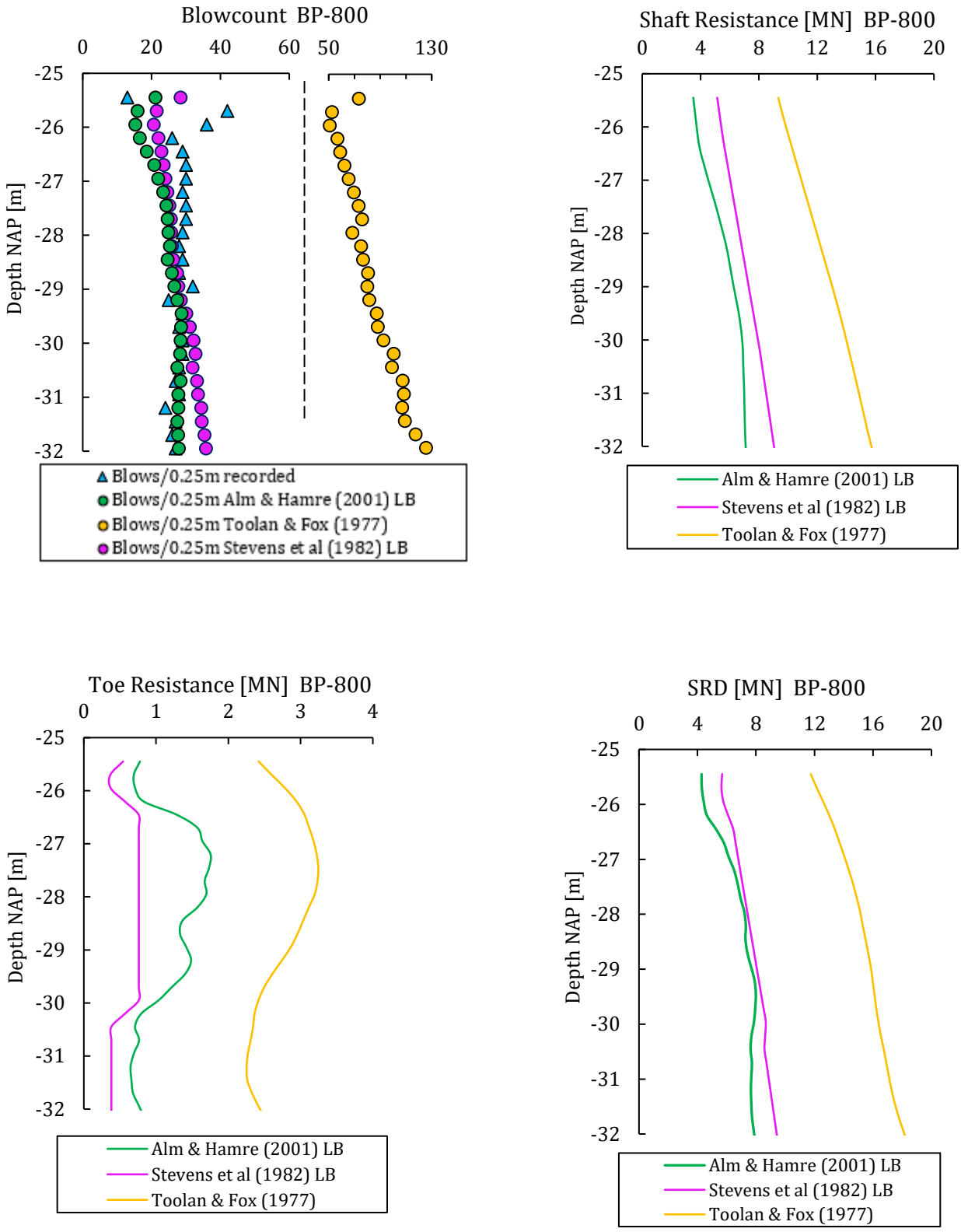

Figure B 3: Driveability post-prediction for combi-wall pile BP-800, using Alm & Hamre (2001), Toolan & Fox (1977), and Stevens et al (1982) SRD models. APM terminal.

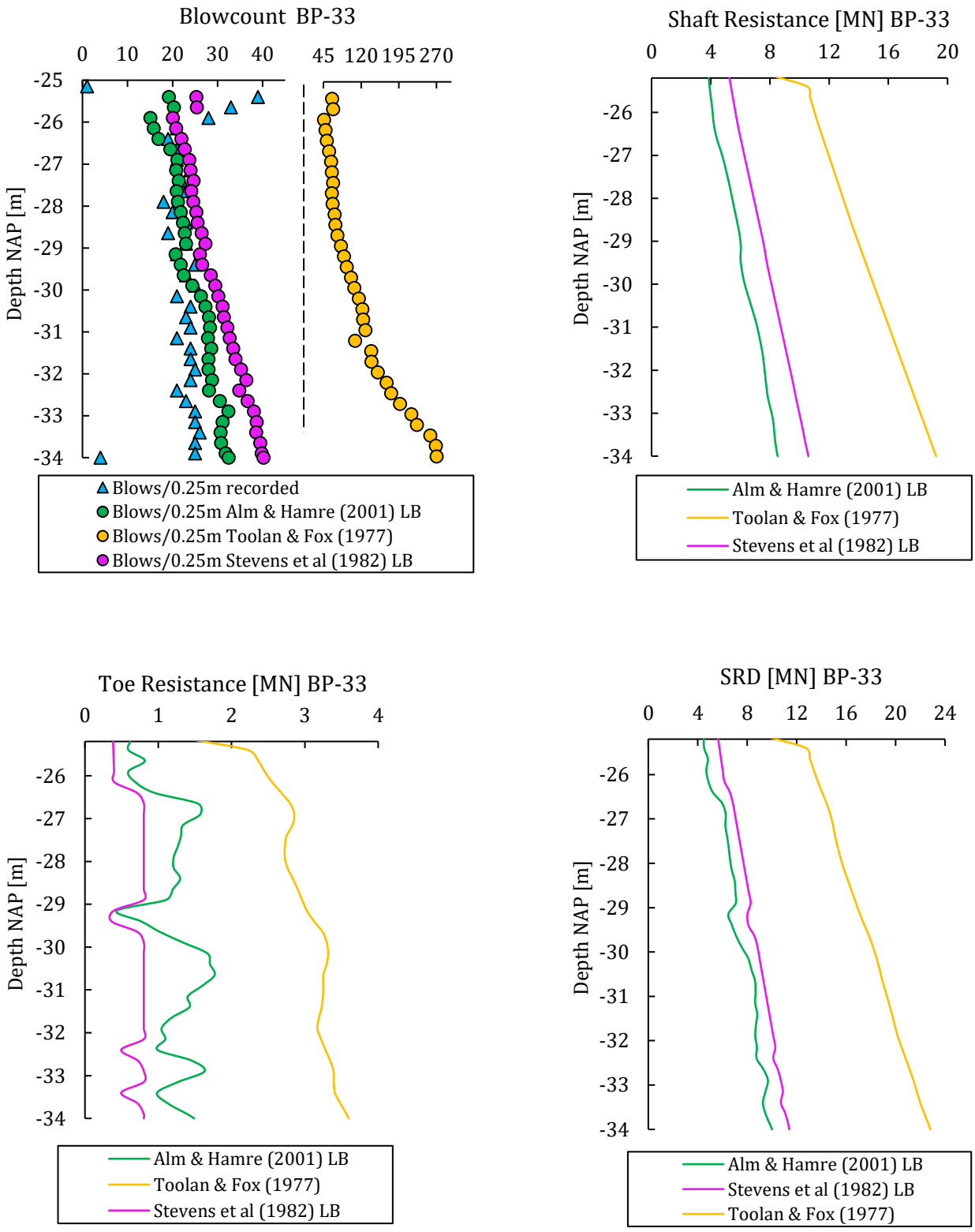

Figure B 4: Driveability post-prediction for combi-wall pile BP-33, using Alm & Hamre (2001), Toolan & Fox (1977), and Stevens et al (1982) SRD models. RWG terminal.

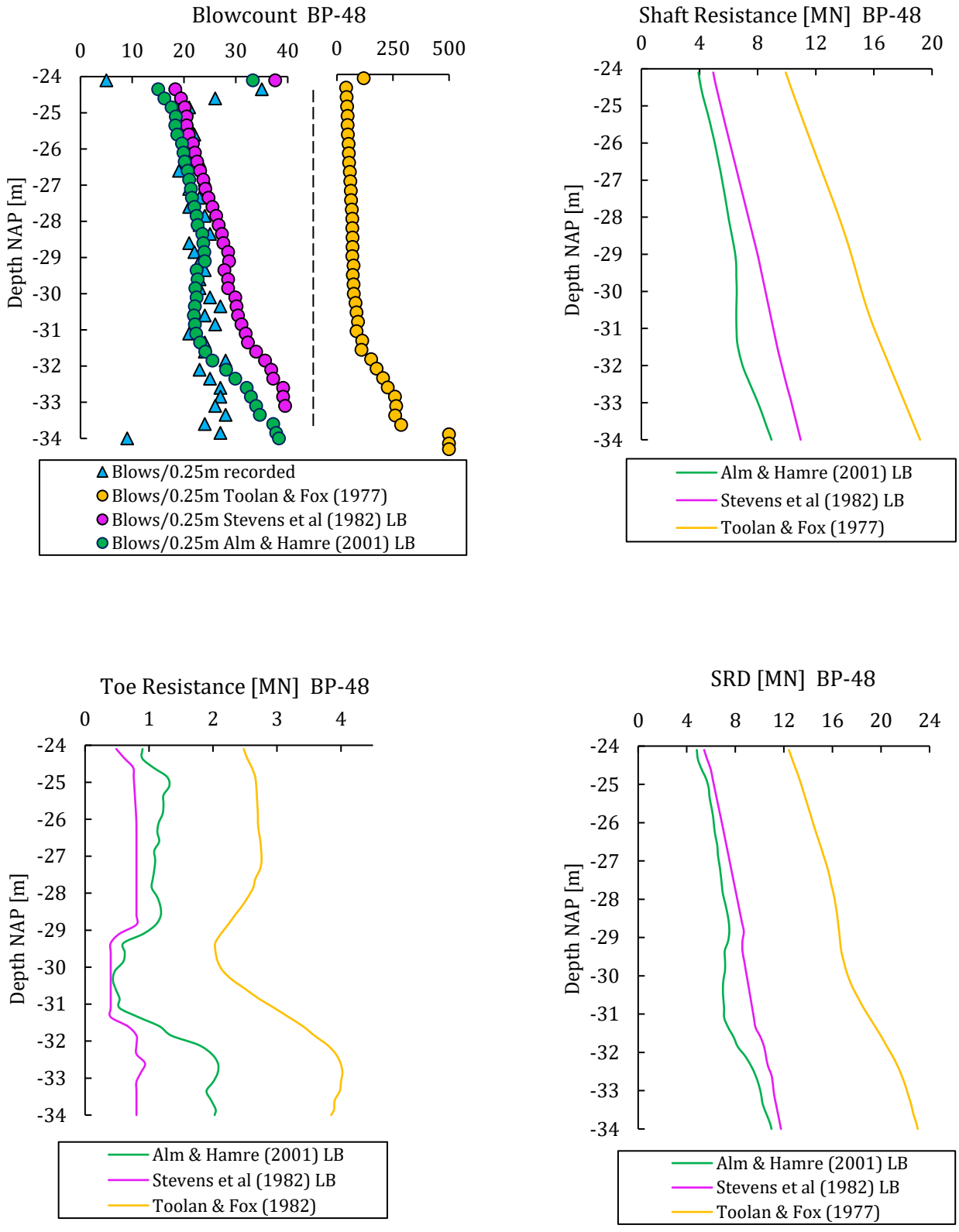

Figure B 5: Driveability post-prediction for combi-wall pile BP-48, using Alm & Hamre (2001), Toolan & Fox (1977), and Stevens et al (1982) SRD models. RWG terminal.

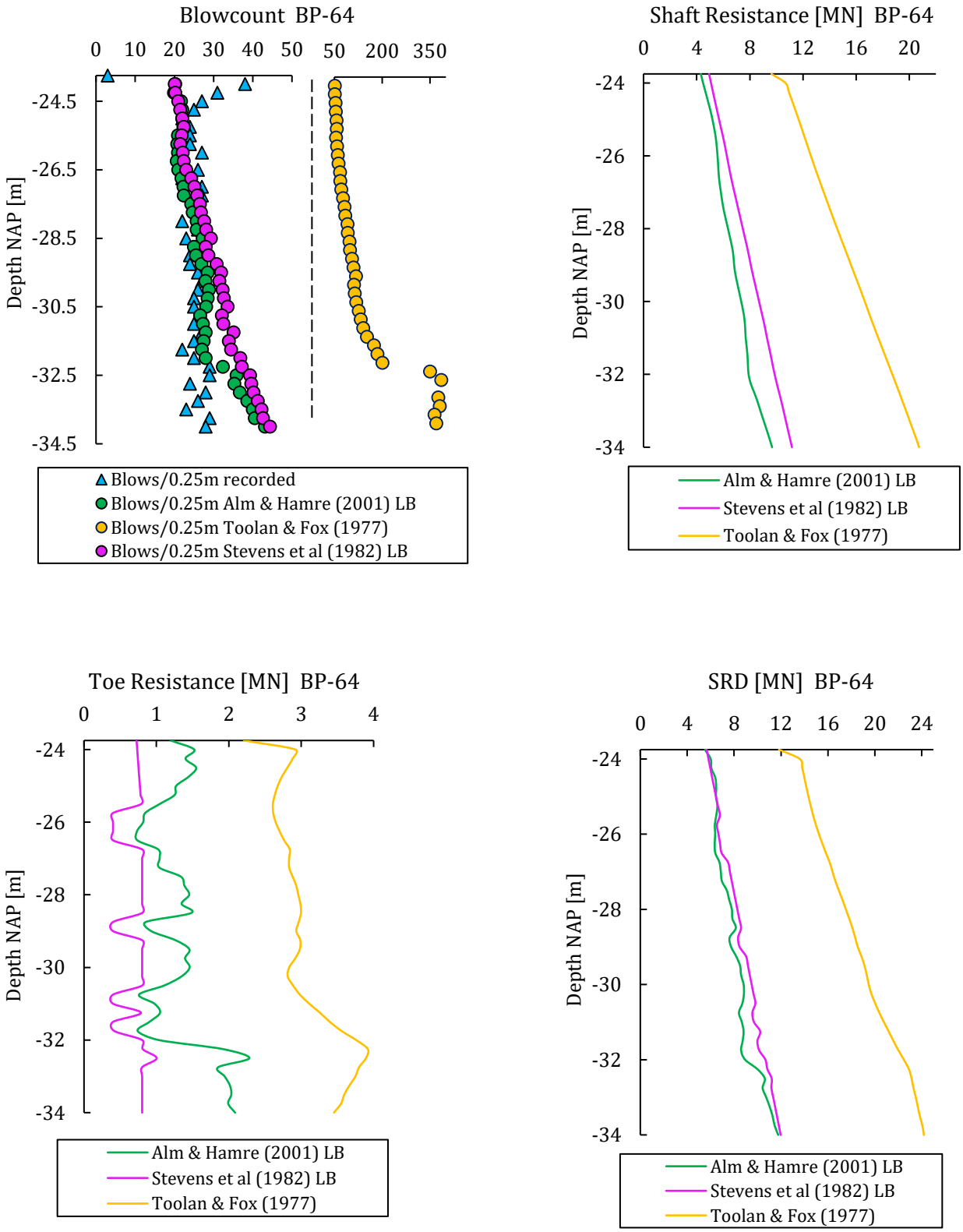

Figure B 6: Driveability post-prediction for combi-wall pile BP-64, using Alm & Hamre (2001), Toolan & Fox (1977), and Stevens et al (1982) SRD models. RWG terminal.

APPENDIX C

Table C 1: Normalized pile base-displacement response using the modified API equation: $\frac{qb}{qb_{0.1,UM}} = 2.23 \cdot (\frac{w}{D})^{0.347} + \frac{q_{res}}{qb_{0.1,UM}}$ $with \frac{w}{D} \leq 0.1$. Values presented below, have been calculated with $q_{res} = 0$. Table continues to the next pages.

Diamter [mm]		300		400		500		600		700	
Blows/0.25m	mm/Blow	w/D	qb/qb$_{01}$	w/D	qb/qb$_{01}$	w/D	qb/qb$_{01}$	w/D	qb/qb$_{01}$	w/D	qb/qb$_{01}$
10	25.0	0.0833	0.94	0.0625	0.85	0.0500	0.79	0.0417	0.74	0.0357	0.70
15	16.7	0.0556	0.82	0.0417	0.74	0.0333	0.69	0.0278	0.64	0.0238	0.61
20	12.5	0.0417	0.74	0.0313	0.67	0.0250	0.62	0.0208	0.58	0.0179	0.55
25	10.0	0.0333	0.69	0.0250	0.62	0.0200	0.57	0.0167	0.54	0.0143	0.51
30	8.3	0.0278	0.64	0.0208	0.58	0.0167	0.54	0.0139	0.51	0.0119	0.48
35	7.1	0.0238	0.61	0.0179	0.55	0.0143	0.51	0.0119	0.48	0.0102	0.45
40	6.3	0.0208	0.58	0.0156	0.53	0.0125	0.49	0.0104	0.46	0.0089	0.43
45	5.6	0.0185	0.56	0.0139	0.51	0.0111	0.47	0.0093	0.44	0.0079	0.42
50	5.0	0.0167	0.54	0.0125	0.49	0.0100	0.45	0.0083	0.42	0.0071	0.40
55	4.5	0.0152	0.52	0.0114	0.47	0.0091	0.44	0.0076	0.41	0.0065	0.39
60	4.2	0.0139	0.51	0.0104	0.46	0.0083	0.42	0.0069	0.40	0.0060	0.38
65	3.8	0.0128	0.49	0.0096	0.45	0.0077	0.41	0.0064	0.39	0.0055	0.37
70	3.6	0.0119	0.48	0.0089	0.43	0.0071	0.40	0.0060	0.38	0.0051	0.36
75	3.3	0.0111	0.47	0.0083	0.42	0.0067	0.39	0.0056	0.37	0.0048	0.35
80	3.1	0.0104	0.46	0.0078	0.41	0.0063	0.38	0.0052	0.36	0.0045	0.34
85	2.9	0.0098	0.45	0.0074	0.41	0.0059	0.38	0.0049	0.35	0.0042	0.33
90	2.8	0.0093	0.44	0.0069	0.40	0.0056	0.37	0.0046	0.35	0.0040	0.33
95	2.6	0.0088	0.43	0.0066	0.39	0.0053	0.36	0.0044	0.34	0.0038	0.32
100	2.5	0.0083	0.42	0.0063	0.38	0.0050	0.35	0.0042	0.33	0.0036	0.32
115	2.2	0.0072	0.40	0.0054	0.37	0.0043	0.34	0.0036	0.32	0.0031	0.30
120	2.1	0.0069	0.40	0.0052	0.36	0.0042	0.33	0.0035	0.31	0.0030	0.30
125	2.0	0.0067	0.39	0.0050	0.35	0.0040	0.33	0.0033	0.31	0.0029	0.29

Diamter [mm]		800		900		1000		1100		1200	
Blows/0.25m	mm/Blow	w/D	qb/qb_{01}	w/D	qb/qb_{01}	w/D	qb/qb_{01}	w/D	qb/qb_{01}	w/D	qb/qb_{01}
10	25.0	0.0313	0.67	0.0278	0.64	0.0250	0.62	0.0227	0.60	0.0208	0.58
15	16.7	0.0208	0.58	0.0185	0.56	0.0167	0.54	0.0152	0.52	0.0139	0.51
20	12.5	0.0156	0.53	0.0139	0.51	0.0125	0.49	0.0114	0.47	0.0104	0.46
25	10.0	0.0125	0.49	0.0111	0.47	0.0100	0.45	0.0091	0.44	0.0083	0.42
30	8.3	0.0104	0.46	0.0093	0.44	0.0083	0.42	0.0076	0.41	0.0069	0.40
35	7.1	0.0089	0.43	0.0079	0.42	0.0071	0.40	0.0065	0.39	0.0060	0.38
40	6.3	0.0078	0.41	0.0069	0.40	0.0063	0.38	0.0057	0.37	0.0052	0.36
45	5.6	0.0069	0.40	0.0062	0.38	0.0056	0.37	0.0051	0.36	0.0046	0.35
50	5.0	0.0063	0.38	0.0056	0.37	0.0050	0.35	0.0045	0.34	0.0042	0.33
55	4.5	0.0057	0.37	0.0051	0.36	0.0045	0.34	0.0041	0.33	0.0038	0.32
60	4.2	0.0052	0.36	0.0046	0.35	0.0042	0.33	0.0038	0.32	0.0035	0.31
65	3.8	0.0048	0.35	0.0043	0.34	0.0038	0.32	0.0035	0.31	0.0032	0.30
70	3.6	0.0045	0.34	0.0040	0.33	0.0036	0.32	0.0032	0.31	0.0030	0.30
75	3.3	0.0042	0.33	0.0037	0.32	0.0033	0.31	0.0030	0.30	0.0028	0.29
80	3.1	0.0039	0.33	0.0035	0.31	0.0031	0.30	0.0028	0.29	0.0026	0.28
85	2.9	0.0037	0.32	0.0033	0.31	0.0029	0.30	0.0027	0.29	0.0025	0.28
90	2.8	0.0035	0.31	0.0031	0.30	0.0028	0.29	0.0025	0.28	0.0023	0.27
95	2.6	0.0033	0.31	0.0029	0.29	0.0026	0.28	0.0024	0.27	0.0022	0.27
100	2.5	0.0031	0.30	0.0028	0.29	0.0025	0.28	0.0023	0.27	0.0021	0.26
115	2.2	0.0027	0.29	0.0024	0.28	0.0022	0.27	0.0020	0.26	0.0018	0.25
120	2.1	0.0026	0.28	0.0023	0.27	0.0021	0.26	0.0019	0.25	0.0017	0.25
125	2.0	0.0025	0.28	0.0022	0.27	0.0020	0.26	0.0018	0.25	0.0017	0.24

Diamter [mm]		1300		1400		1500		1600		1700	
Blows/0.25m	mm/Blow	w/D	qb/qb_{01}	w/D	qb/qb_{01}	w/D	qb/qb_{01}	w/D	qb/qb_{01}	w/D	qb/qb_{01}
10	25.0	0.0192	0.57	0.0179	0.55	0.0167	0.54	0.0156	0.53	0.0147	0.52
15	16.7	0.0128	0.49	0.0119	0.48	0.0111	0.47	0.0104	0.46	0.0098	0.45
20	12.5	0.0096	0.45	0.0089	0.43	0.0083	0.42	0.0078	0.41	0.0074	0.41
25	10.0	0.0077	0.41	0.0071	0.40	0.0067	0.39	0.0063	0.38	0.0059	0.38
30	8.3	0.0064	0.39	0.0060	0.38	0.0056	0.37	0.0052	0.36	0.0049	0.35
35	7.1	0.0055	0.37	0.0051	0.36	0.0048	0.35	0.0045	0.34	0.0042	0.33
40	6.3	0.0048	0.35	0.0045	0.34	0.0042	0.33	0.0039	0.33	0.0037	0.32
45	5.6	0.0043	0.34	0.0040	0.33	0.0037	0.32	0.0035	0.31	0.0033	0.31
50	5.0	0.0038	0.32	0.0036	0.32	0.0033	0.31	0.0031	0.30	0.0029	0.30
55	4.5	0.0035	0.31	0.0032	0.31	0.0030	0.30	0.0028	0.29	0.0027	0.29
60	4.2	0.0032	0.30	0.0030	0.30	0.0028	0.29	0.0026	0.28	0.0025	0.28
65	3.8	0.0030	0.30	0.0027	0.29	0.0026	0.28	0.0024	0.28	0.0023	0.27
70	3.6	0.0027	0.29	0.0026	0.28	0.0024	0.27	0.0022	0.27	0.0021	0.26
75	3.3	0.0026	0.28	0.0024	0.27	0.0022	0.27	0.0021	0.26	0.0020	0.26
80	3.1	0.0024	0.28	0.0022	0.27	0.0021	0.26	0.0020	0.26	0.0018	0.25
85	2.9	0.0023	0.27	0.0021	0.26	0.0020	0.26	0.0018	0.25	0.0017	0.25
90	2.8	0.0021	0.26	0.0020	0.26	0.0019	0.25	0.0017	0.25	0.0016	0.24
95	2.6	0.0020	0.26	0.0019	0.25	0.0018	0.25	0.0016	0.24	0.0015	0.24
100	2.5	0.0019	0.25	0.0018	0.25	0.0017	0.24	0.0016	0.24	0.0015	0.23
115	2.2	0.0017	0.24	0.0016	0.24	0.0014	0.23	0.0014	0.23	0.0013	0.22
120	2.1	0.0016	0.24	0.0015	0.23	0.0014	0.23	0.0013	0.22	0.0012	0.22
125	2.0	0.0015	0.24	0.0014	0.23	0.0013	0.22	0.0013	0.22	0.0012	0.21

Diamter [mm]		1800		1900		2000	
Blows/0.25m	mm/Blow	w/D	qb/qb_{01}	w/D	qb/qb_{01}	w/D	qb/qb_{01}
10	25.0	0.0139	0.51	0.0132	0.50	0.0125	0.49
15	16.7	0.0093	0.44	0.0088	0.43	0.0083	0.42
20	12.5	0.0069	0.40	0.0066	0.39	0.0063	0.38
25	10.0	0.0056	0.37	0.0053	0.36	0.0050	0.35
30	8.3	0.0046	0.35	0.0044	0.34	0.0042	0.33
35	7.1	0.0040	0.33	0.0038	0.32	0.0036	0.32
40	6.3	0.0035	0.31	0.0033	0.31	0.0031	0.30
45	5.6	0.0031	0.30	0.0029	0.29	0.0028	0.29
50	5.0	0.0028	0.29	0.0026	0.28	0.0025	0.28
55	4.5	0.0025	0.28	0.0024	0.27	0.0023	0.27
60	4.2	0.0023	0.27	0.0022	0.27	0.0021	0.26
65	3.8	0.0021	0.26	0.0020	0.26	0.0019	0.25
70	3.6	0.0020	0.26	0.0019	0.25	0.0018	0.25
75	3.3	0.0019	0.25	0.0018	0.25	0.0017	0.24
80	3.1	0.0017	0.25	0.0016	0.24	0.0016	0.24
85	2.9	0.0016	0.24	0.0015	0.24	0.0015	0.23
90	2.8	0.0015	0.24	0.0015	0.23	0.0014	0.23
95	2.6	0.0015	0.23	0.0014	0.23	0.0013	0.22
100	2.5	0.0014	0.23	0.0013	0.22	0.0013	0.22
115	2.2	0.0012	0.22	0.0011	0.21	0.0011	0.21
120	2.1	0.0012	0.21	0.0011	0.21	0.0010	0.21
125	2.0	0.0011	0.21	0.0011	0.21	0.0010	0.20

APPENDIX D

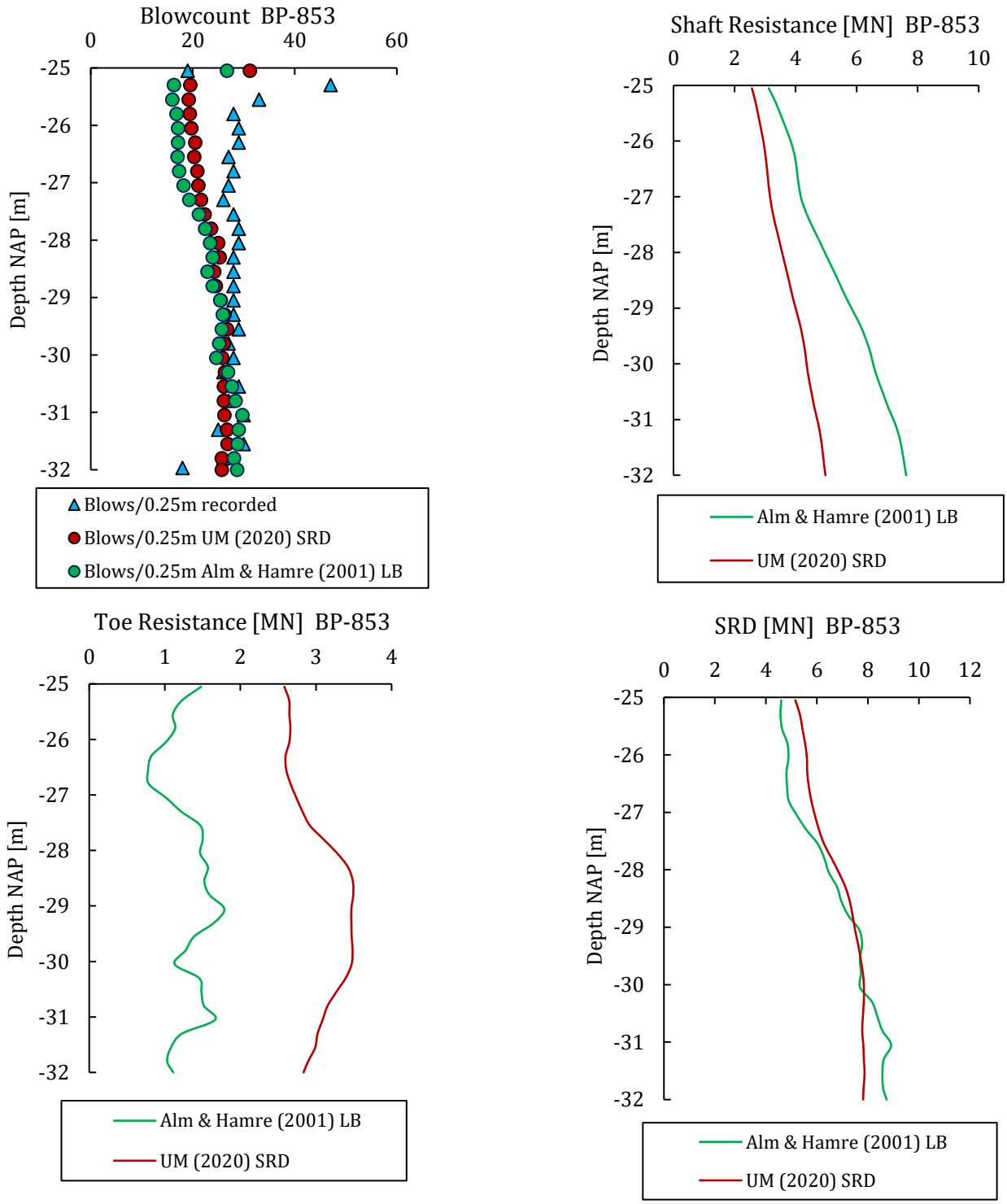

Figure D 1: Driveability post-prediction for combi-wall pile BP-853, using Alm & Hamre (2001) and the Unified SRD Method models. APM terminal.

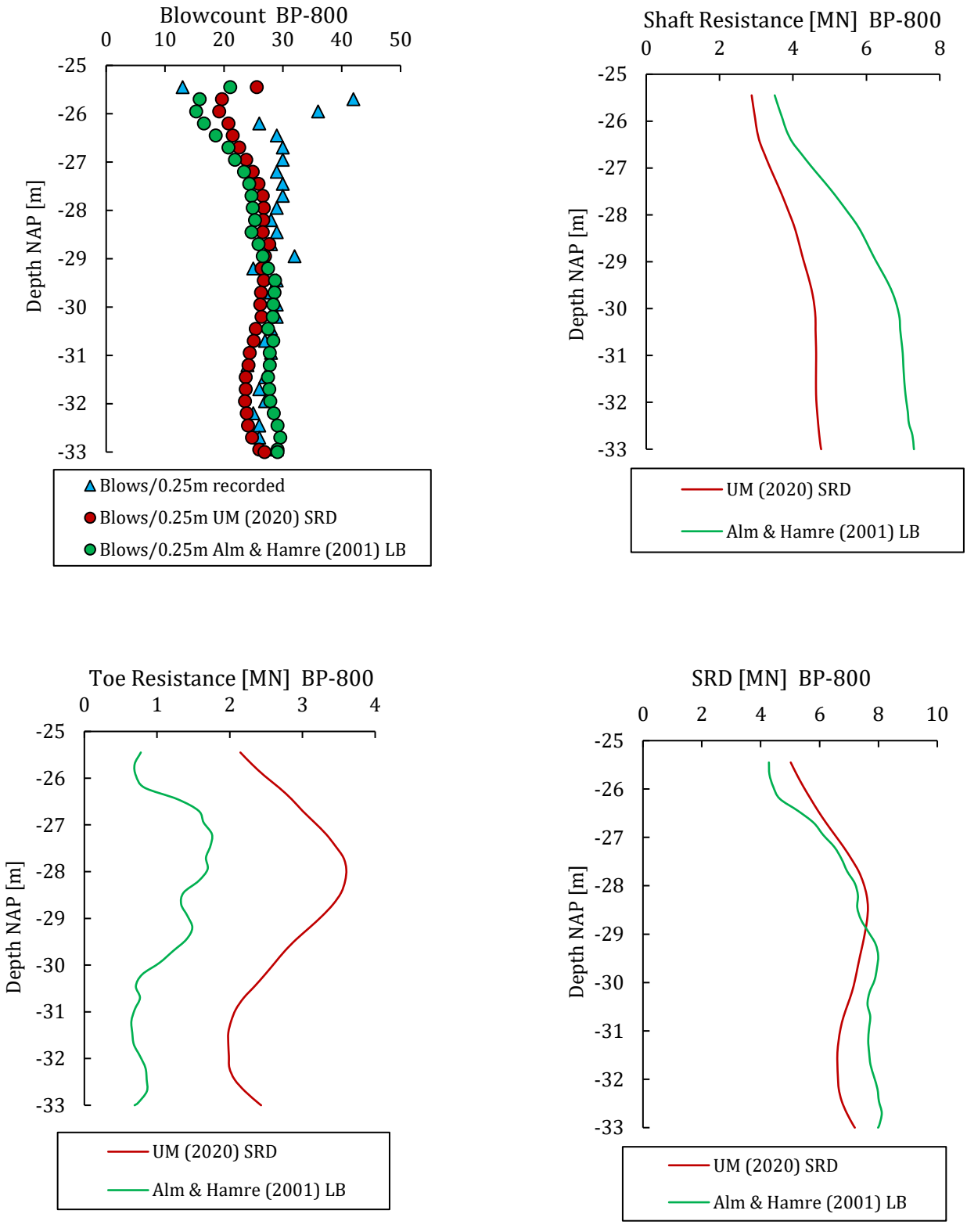

Figure D 2: Driveability post-prediction for combi-wall pile BP-800, using Alm & Hamre (2001) and the Unified SRD Method models. APM terminal.

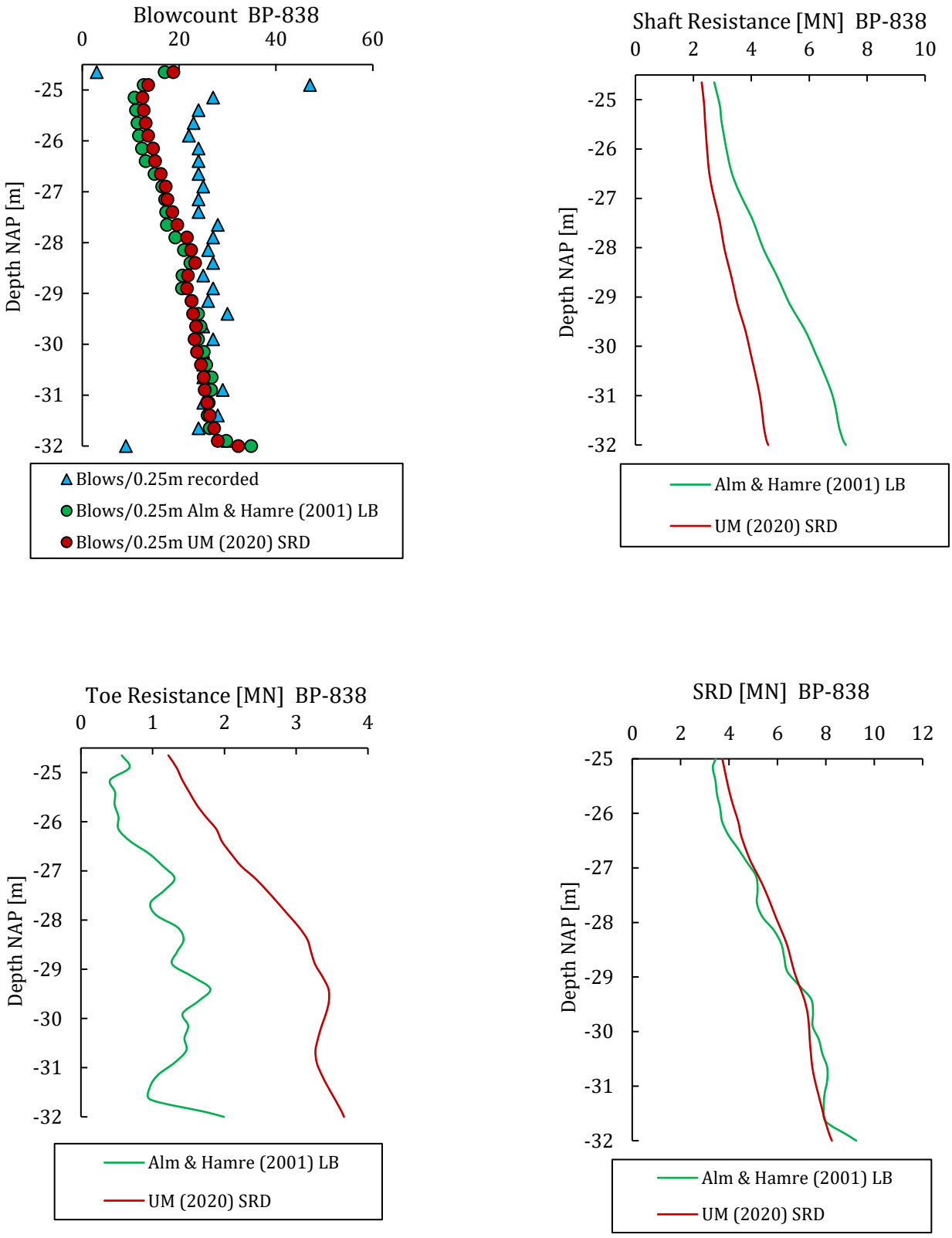

Figure D 3: Driveability post-prediction for combi-wall pile BP-838, using Alm & Hamre (2001) and the Unified SRD Method models. APM terminal.

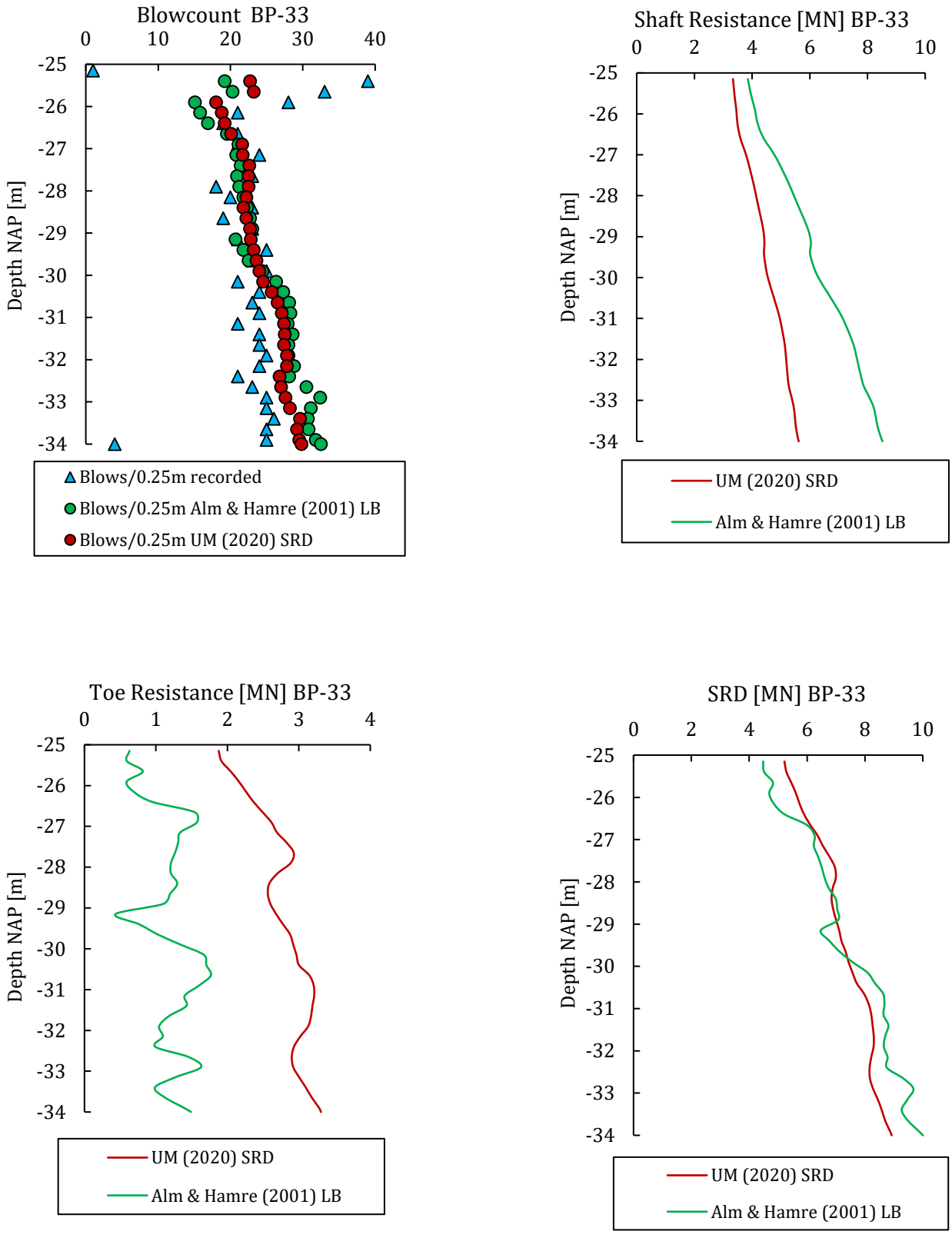

Figure D 4: Driveability post-prediction for combi-wall pile BP-33, using Alm & Hamre (2001) and the Unified SRD Method models. RWG terminal.

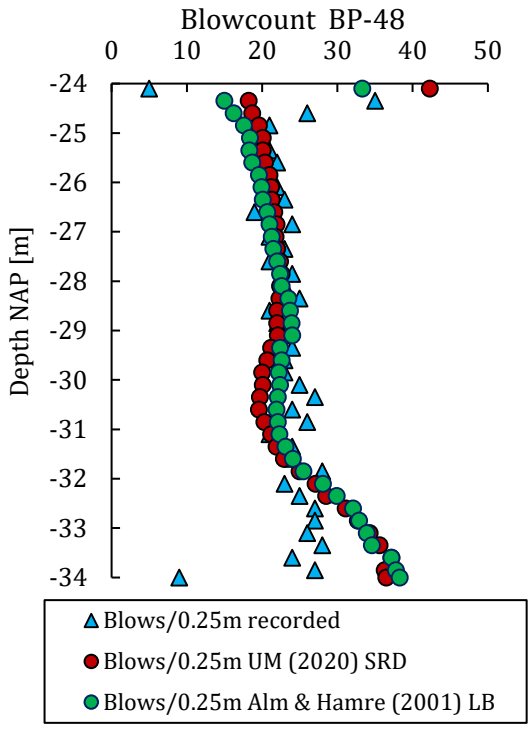

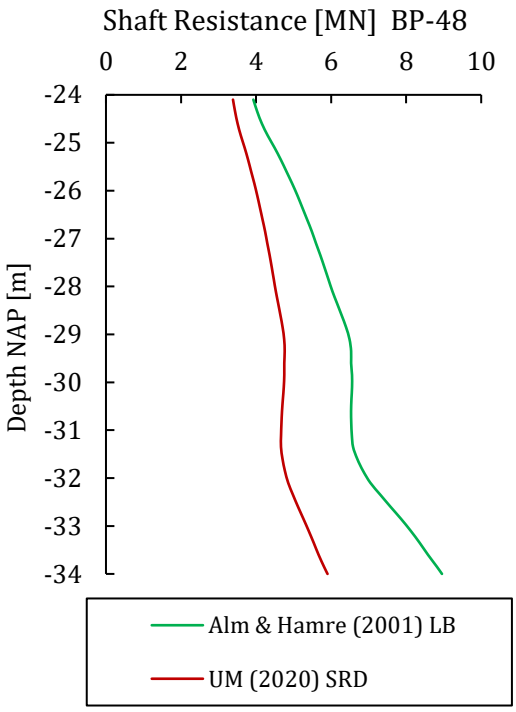

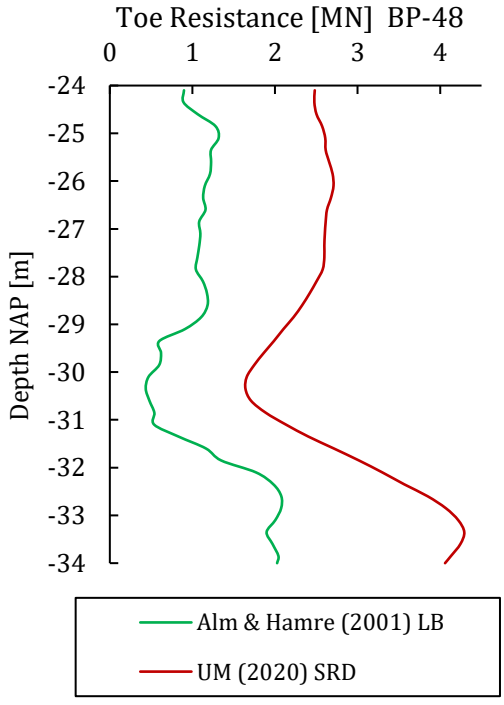

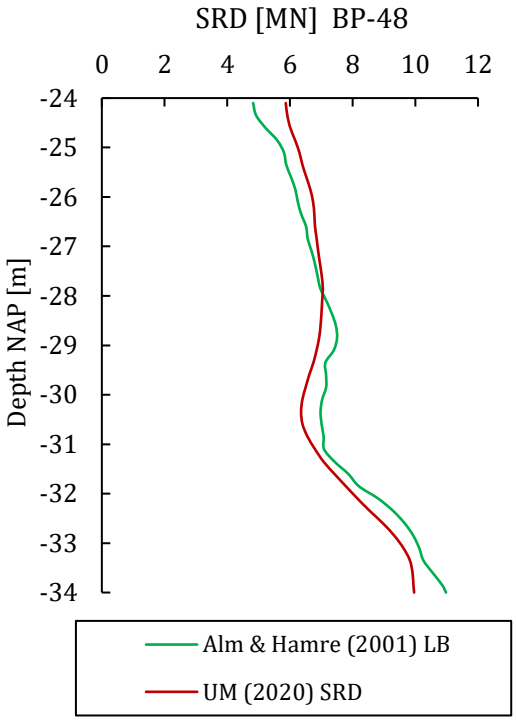

Figure D 5: Driveability post-prediction for combi-wall pile BP-48, using Alm & Hamre (2001) and the Unified SRD Method models. RWG terminal.

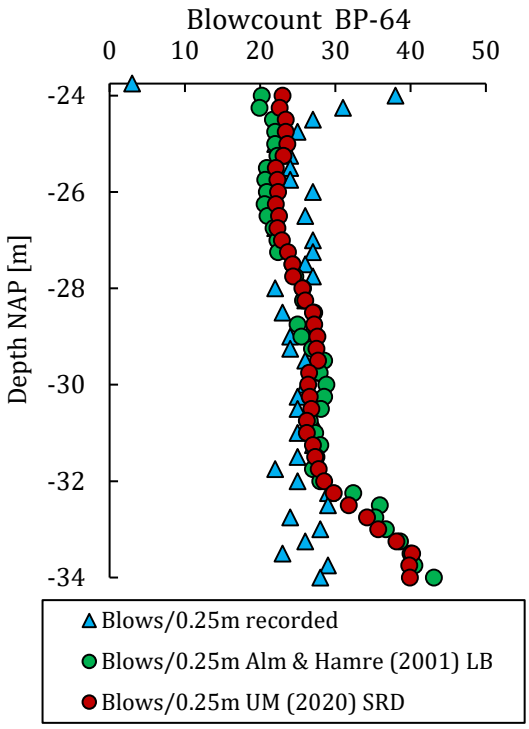

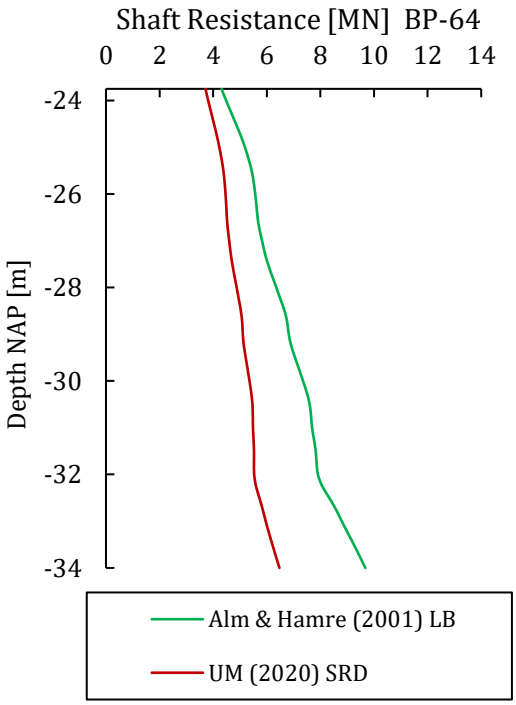

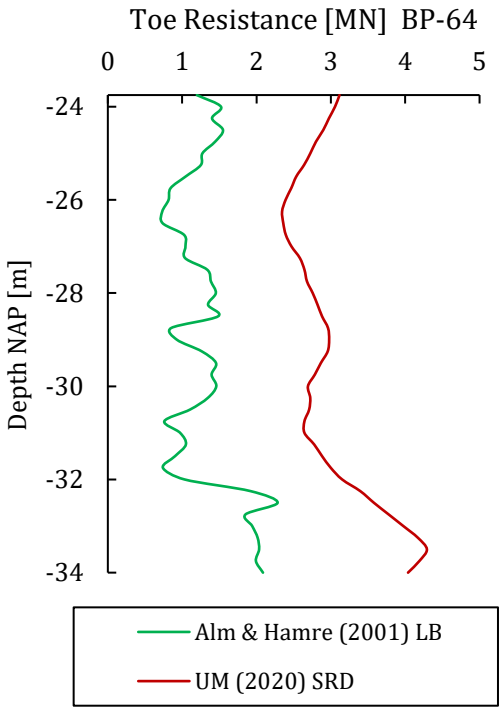

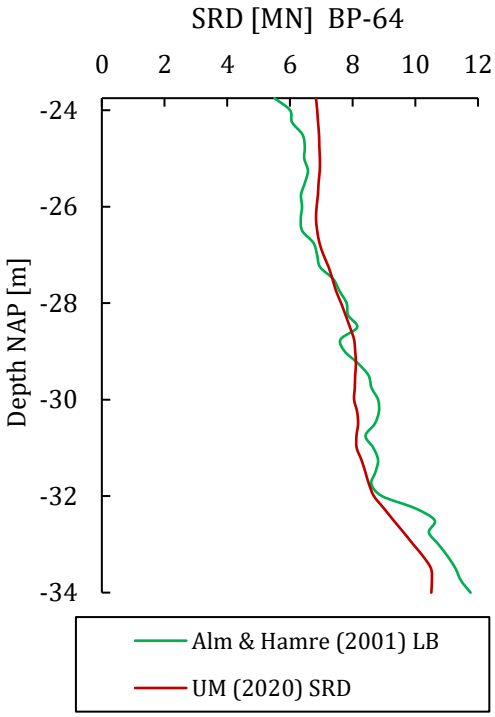

Figure D 6: Driveability post-prediction for combi-wall pile BP-64 using Alm & Hamre (2001) and the Unified SRD Method models. RWG terminal.